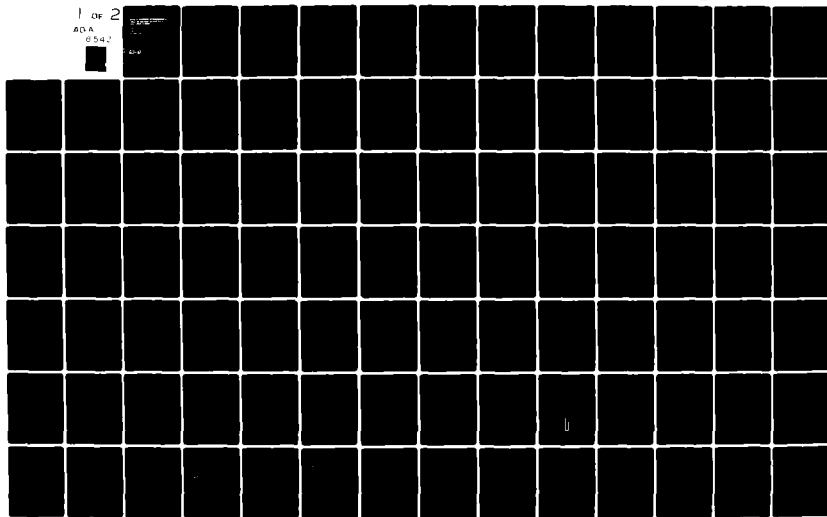


AD-A116 542 MCDONNELL DOUGLAS RESEARCH LABS ST LOUIS MO F/6 7/4
MAGNETIC RESONANCE DETERMINATIONS OF STRUCTURE AND REACTION KIN--ETC(U)
DEC 81 I M BROWN, A C LIND, T C SANDRECZKI N00019-80-C-0552
UNCLASSIFIED MDC-G0759 NL

1 of 2

ADA
0542



AD A116542

AD A116542
Contract No. DA19-60-0-0001

MAGNETIC RESONANCE DETERMINATIONS OF STRUCTURE AND REACTION KINETICS OF EPOXY/AMINE SYSTEMS

I. M. Dunn
A. C. Elm
T. C. Sandrock

McDonnell Douglas Research Laboratories
St. Louis, Missouri 63166

21 December 1961

Final Report for period 1 October 1960 to 31 December 1961

Approved for Public Release; Distribution Unlimited

MCDONNELL DOUGLAS RESEARCH LABORATORIES

MCDONNELL DOUGLAS



CORPORATION

UNCLASSIFIED

SECURITY CLASSIFICATION OF THIS PAGE (When Data Entered)

REPORT DOCUMENTATION PAGE		READ INSTRUCTIONS BEFORE COMPLETING FORM
1. REPORT NUMBER MDC Q0759	2. GOVT ACCESSION NO. AD-A116 542	3. RECIPIENT'S CATALOG NUMBER
4. TITLE (and Subtitle) MAGNETIC RESONANCE DETERMINATIONS OF STRUCTURE AND REACTION KINETICS OF EPOXY/AMINE SYSTEMS		5. TYPE OF REPORT & PERIOD COVERED Final Report 1 Oct 80 - 31 Dec 81
		6. PERFORMING ORG. REPORT NUMBER
7. AUTHOR(s) I. M. Brown A. C. Lind T. C. Sandreczki		8. CONTRACT OR GRANT NUMBER(s) N00019-80-C-0552
9. PERFORMING ORGANIZATION NAME AND ADDRESS McDonnell Douglas Research Laboratories McDonnell Douglas Corporation St. Louis, Missouri 63166		10. PROGRAM ELEMENT, PROJECT, TASK AREA & WORK UNIT NUMBERS
11. CONTROLLING OFFICE NAME AND ADDRESS Department of the Navy Naval Air Systems Command Washington, DC 20361		12. REPORT DATE 31 December 1981
		13. NUMBER OF PAGES 104
14. MONITORING AGENCY NAME & ADDRESS (if different from Controlling Office)		15. SECURITY CLASS. (of this report) Unclassified
		15a. DECLASSIFICATION/DOWNGRADING SCHEDULE
16. DISTRIBUTION STATEMENT (of this Report) Approved for public release; distribution unlimited.		
17. DISTRIBUTION STATEMENT (of the abstract entered in Block 20, if different from Report)		
18. SUPPLEMENTARY NOTES		
19. KEY WORDS (Continue on reverse side if necessary and identify by block number)		
Amines	Electron paramagnetic resonance	Plasticizer
Epoxy resins	Nuclear magnetic resonance	Quaternary amines
Spin probes	Glass transition temperature	Relaxation times
Spin labels	Correlation time	Swelling
Reaction kinetics	Crosslink network	Microstructure
20. ABSTRACT (Continue on reverse side if necessary and identify by block number)		
<p>Electron paramagnetic resonance (EPR) and nuclear magnetic resonance (NMR) were used to investigate (1) the kinetics of the reactions between amines and epoxies using model compounds and (2) the microstructure present in amine-cured epoxies. The cured resins were studied close to the glass transition as a function of temperature and as a function of solvent content (methylene chloride).</p>		

DD FORM 1 JAN 73 1473

EDITION OF 1 NOV 65 IS OBSOLETE

UNCLASSIFIED

SECURITY CLASSIFICATION OF THIS PAGE (When Data Entered)

UNCLASSIFIED

SECURITY CLASSIFICATION OF THIS PAGE(When Data Entered)

In the EPR experiments, stable nitroxide free radicals were used as spin labels and spin probes. The lineshapes were used to investigate the kinetics of the initial addition reactions between the epoxy diglycidyl ether of bisphenol A (DGEBA), and two model compounds, a secondary amine nitroxide and a tertiary amine nitroxide. The rate constants for both reactions (k_1 , k_2) showed the same temperature dependence, viz., $k_{1,2} = k_0 \exp - \Delta E/RT$, where $k_0 = 7.8 \times 10^2 \text{ s}^{-1}$ and $\Delta E = 41.5 \text{ kJ mole}^{-1}$. The equality of the rate is tentatively explained in terms of solvation effects which reduce any differences in reaction rates arising from either differences of nucleophilic character of the amine or differences in steric factors of the transition states.

In dry, cured epoxy samples, the EPR lineshape of the spin probe could be characterized by one value of the motional correlation time. The values of the motional correlation time depended on the average crosslink density and obeyed a modified form of the WLF equation. On the other hand, at some solvent contents, the EPR lineshapes could be resolved into two spectra associated with a slow phase and a fast phase indicating a bimodal distribution of motional correlation times. The amount of fast phase was found to depend linearly on solvent content but only slightly on crosslink density. The two phases were identified with nitroxides located in regions of different crosslink density, i.e., regions of high crosslink density (the slow phase) embedded in and bound to regions of low crosslink density (the fast phase).

The methodology of using nitroxide amines to determine the number of unreacted epoxy groups in an amine-cured epoxy sample is described.

^{13}C NMR was used to investigate the kinetics of the reaction between 1,2-epoxy-3-phenoxypropane (EPOP) and N-methylbutylamine (MBA). The reaction was found to be third order with the third component being both the hydrogen-bond donors present as impurities in the initial reactants and the hydrogen-bond donor (OH) created as a result of the reaction. The rate constant at 300 K for the third-order reaction involving the hydrogen-bond donor created during the reaction was $8 \times 10^{-6} \text{ L}^2 \text{ mole}^{-2} \text{ s}^{-1}$.

The hydrogen spin-spin relaxation times of cured epoxy polymers at high temperature or saturated with methylene chloride were found to be related to the molecular weight between crosslinks (crosslink density). Both mobile and rigid components were observed, and the amount of mobile component increased with increasing temperature, solvent content, and molecular weight between crosslinks.

UNCLASSIFIED

SECURITY CLASSIFICATION OF THIS PAGE(When Data Entered)

PREFACE

This report is an account of the work performed by the McDonnell Douglas Research Laboratories on the Magnetic Resonance Determination of Structure and Reaction Kinetics of Epoxy/Amine Systems for the Naval Air Systems Command, Contract No. N00019-80-C-0552, from 1 October 1980 to 31 December 1981. The work was performed in the Chemical Physics Department, managed by Dr. D. P. Ames. The principal investigators were Dr. I. M. Brown and Dr. A. C. Lind; Dr. T. C. Sandreczki was a co-investigator. The project monitor was Mr. R. Dempsey, Naval Air Systems Command, Washington, DC.



A

TABLE OF CONTENTS

	<u>Page</u>
1. INTRODUCTION.....	1
2. EPR EXPERIMENTS ON EPOXY RESINS.....	4
2.1 Nitroxide-DGEBA Kinetics.....	4
2.2 Investigation of the Microstructure in Cured Epoxies.....	22
2.3 Determination of the Number of Unreacted Epoxide Groups.....	41
2.4 Discussion of EPR Results.....	42
3. NMR EXPERIMENTS ON EPOXY RESINS.....	45
3.1 Epoxy/Amine Reaction Kinetics.....	45
3.1.1 Liquid Studies.....	45
3.1.2 Solid Studies.....	59
3.2 Crosslink Structure Studies.....	59
3.2.1 NMR Sample Preparation.....	60
3.2.2 NMR Measurements.....	60
3.2.3 Characteristics of NMR Signals from Crosslinked Epoxies.....	61
3.2.4 Temperature-Dependent Studies.....	62
3.2.5 Solvent-Dependent Studies.....	67
3.2.6 Crosslink Density Determinations.....	78
4. SUMMARY OF CONCLUSIONS.....	84
4.1 EPR Conclusions.....	84
4.2 NMR Conclusions.....	85
APPENDIX A: Pseudo-first-order reaction rates in spin-label formation...	87
REFERENCES.....	88
DISTRIBUTION LIST.....	91

PRECEDING PAGE BLANK-NOT FILMED

LIST OF ILLUSTRATIONS

<u>Figure</u>	<u>Page</u>
1. Epoxy resin and curing agents used in the EPR experiments.....	2
2. Spin probes and spin labels used.....	3
3. EPR spectra observed at 295 K for different times into reaction of end-label formation (reaction temperature = 295 K).....	7
4. Definitions of spectral line amplitude parameters.....	7
5. Typical lineshapes observed in the EPR kinetics experiments.....	8
6. Time dependence of the normalized spin-probe concentration in end-label formation (reaction temperature = 295 K).....	9
7. Time dependence of the normalized spin-probe concentration in end-label formation (reaction temperature = 318 K).....	10
8. Time dependence of the normalized spin-probe concentration in end-label formation (reaction temperature = 333 K).....	11
9. Time dependence of the normalized spin-probe concentration in end-label formation (reaction temperature = 343 K).....	12
10. Temperature dependence of the rate constants for METAMIN and DIMETAMIN reactions with DGEBA.....	14
11. EPR spectra observed at 299 K for different times into reaction of spin-labeled quaternary-base formation (reaction temperature = 299 K).....	15
12. EPR spectra observed at 318 K for different times into formation of spin-labeled quaternary base (reaction temperature = 318 K).....	15
13. Time dependence of the normalized spin-probe concentration in the formation of spin-labeled quaternary base (reaction temperature = 299 K).....	16
14. Time dependence of the normalized spin-probe concentration in formation of spin-labeled quaternary base (reaction temperature = 318 K).....	17
15. Time dependence of the normalized spin-probe concentration in formation of spin-labeled quaternary base (reaction temperature = 388 K).....	18
16. Time dependence of the normalized spin-probe concentration in formation of spin-labeled quaternary base (reaction temperature = 363 K).....	19
17. Time dependence of the normalized spin-probe concentration in the formation of spin-labeled quaternary base formation (reaction temperature = 373 K).....	20
18. Temperature dependence of extrema splitting for samples of DIMETAMIN in DGEBA.....	21

LIST OF ILLUSTRATIONS (continued)

<u>Figure</u>	<u>Page</u>
19. Spectrum observed in reaction of DIMETAMIN with DGEBA.....	22
20. Reaction scheme for formation of different spin-labeled quaternary bases in homopolymerization of DGEBA with DIMETAMIN as the initiator.....	23
21. Temperature dependence of EPR spectra of TANOL in sample of DDH/DGEBA.....	24
22. EPR spectra of TANOL in amine-cured samples of DGEBA with different crosslink densities.....	25
23. Temperature dependence of motional correlation time for TANOL in samples of amine-cured DGEBA with different crosslink densities.....	26
24. Shear moduli and $\tan \delta$ as function of temperature for sample with stoichiometry DAB:DDH:DGEBA = 3:2:5.....	27
25. Shear modulus as function of temperature for amine-cured samples of DGEBA.....	28
26. Motional correlation time at selected temperatures for TANOL in amine-cured DGEBA samples with different molecular weights between crosslinks.....	28
27. Experimental crosslink densities as a function of theoretical normalized crosslink density.....	29
28. WLF plot for TANOL in amine-cured sample with stoichiometry DAB:DDH:DGEBA = 2:3:5.....	30
29. WLF plot for TANOL in amine-cured epoxy sample with stoichiometry DAB:DGEBA = 1:1.....	31
30. Plot of solvent content as a function of exposure time.....	33
31. Crosslink density as a function of Flory-Huggins parameter.....	34
32. Crosslink density from swelling data as a function of theoretical normalized crosslink density.....	35
33. EPR spectra of TANOL in samples of DGEBA/DDH containing different amounts of methylene chloride.....	38
34. EPR spectra of TANOL in samples of DGEBA/DAB containing different amounts of methylene chloride.....	38
35. EPR spectra of TANOL in samples of DGEBA/DDH and DGEBA/DAB containing the same amounts of methylene chloride.....	39
36. EPR spectra of TANOL in DGEBA/DDH sample as a function of benzene content.....	39
37. Typical examples of spectra observed in plasticizing experiments....	40
38. Plot of mobile fraction for TANOL in amine-cured samples of DGEBA...	40

LIST OF ILLUSTRATIONS (continued)

<u>Figure</u>	<u>Page</u>
39. Proposed transition states involved in amine-epoxy reactions.....	43
40. Epoxy and amine compounds used in the ^{13}C NMR kinetics study.....	46
41. ^{13}C NMR spectra of the epoxy/amine reaction.....	47
42. Aromatic ^{13}C spectra of epoxy/amine reaction.....	49
43. Kinetics for the reaction of approximately 1:9.8 mole neat mixtures of EPOP:MBA.....	50
44. Kinetics for the reaction of a 1:9.3 mole neat mixture of EPOP:MBA.....	51
45. Smith mechanism involving hydrogen bonding to the epoxy.....	52
46. Mika and Tanaka mechanism involving hydrogen bonding to the amine...	53
47. Kinetics for the reaction of a 1:5.3 mole neat mixture of EPOP:MBA..	54
48. Kinetics for the reaction of a 1:9.3 mole neat mixture of EPOP:MBA..	55
49. Kinetics for the reaction of a 1:7.04 mole neat mixture of EPOP:MBA.....	55
50. Kinetics for the reaction of a 1:9.9 mole neat mixture of EPOP:MBA diluted with C_6D_{12} to 0.29 of the neat concentration.....	56
51. Kinetics for the reaction of a 1:9.5 mole mixture of EPOP:MBA diluted with C_6D_{12} to 0.15 of the neat concentration.....	56
52. Identification of the sources of the hydrogen-bond donors.....	58
53. ^{13}C NMR spectrum of a solid 5:0:5 DAB:DDH:DGEBA sample.....	59
54. Hydrogen NMR free-induction decay signal.....	61
55. Temperature dependence of Lorentzian spin-spin relaxation time for DAB:DDH:DGEBA samples.....	62
56. Temperature dependence of spin-spin relaxation times for DAB:DDH:DGEBA samples.....	63
57. Temperature dependence of the Lorentzian fraction for DAB:DDH:DGEBA samples.....	64
58. Temperature dependence of the spin-lattice relaxation time for DAB:DDH:DGEBA samples.....	67
59. Apparatus for determining the relation between the methylene chloride vapor pressure and the density of the methylene-chloride/paraffin-oil mixture.....	68
60. Normalized pressure of methylene chloride vapor in equilibrium with a methylene-chloride/paraffin-oil mixture.....	70
61. Vapor pump for rapidly introducing methylene chloride vapor to the epoxy sample.....	71

LIST OF ILLUSTRATIONS (continued)

<u>Figure</u>	<u>Page</u>
62. Room-temperature sorption isotherms for DAB:DDH:DGEBA samples exposed to methylene chloride.....	72
63. Lorentzian fraction of DAB:DDH:DGEBA samples as a function of sorbed methylene chloride.....	73
64. Gaussian spin-spin relaxation times of DAB:DDH:DGEBA samples exposed to methylene chloride vapor.....	74
65. Gaussian spin-spin relaxation times of DAB:DDH:DGEBA samples as a function of sorbed methylene chloride.....	75
66. Lorentzian spin-spin relaxation times of DAB:DDH:DGEBA samples as a function of sorbed methylene chloride.....	76
67. Spin-lattice relaxation times of DAB:DDH:DGEBA samples as a function of sorbed methylene chloride.....	78
68. Calculated equilibrium epoxy volume fractions as a function of methylene chloride vapor pressure.....	79
69. Comparison of molecular weight between crosslinks of DAB:DDH:DGEBA epoxy samples as predicted from stoichiometry and as determined from swelling measurements.....	81
70. Plateau values of spin-spin relaxation times of DAB:DDH:DGEBA epoxy samples.....	82

LIST OF TABLES

<u>Table</u>	<u>Page</u>
1. Reaction Rates of Nitroxide Amines with DGEBA.....	13
2. Crosslink Densities Calculated for Amine-Cured DGEBA Samples.....	36
3. Amount of Unreacted Epoxy Groups in a Cured Sample with Stoichiometry DGEBA:DDH = 1:1.....	41
4. Verification of the Source of the Hydrogen-Bond Donors.....	58
5. Comparison Between Different Transition Temperatures.....	65
6. High-Temperature Plateau Values of the Lorentzian Spin-Spin Relaxation Times.....	66
7. Lorentzian Spin-Spin Relaxation Times of Samples Saturated With Methylene Chloride Vapor.....	76
8. Calculated Crosslink Parameters for the DAB:DDH:DGEBA Samples.....	80

INTRODUCTION

Amine-cured epoxy resin systems are widely employed as the matrix materials for fibrous composite structural components in the aerospace industry. In some of these cured epoxy resins, the crosslink density is nonuniform to such an extent that the polymer network can be considered as rigid regions of high crosslink density dispersed in and bound to a surrounding matrix of lower crosslink density.¹⁻⁷ The exact nature of this heterogeneous network may depend on the relative rates of the chemical reactions that play a role in crosslinking before and after the gel formation. In particular, unreacted epoxy and amine groups may be trapped in the rigid network.

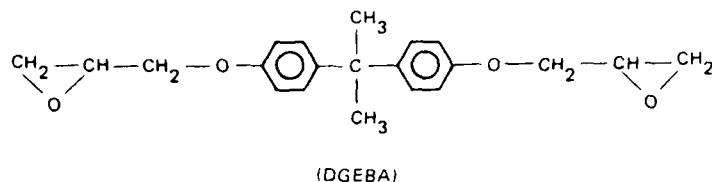
In this study we used the magnetic resonance spectrometric techniques, electron paramagnetic resonance (EPR) and nuclear magnetic resonance (NMR), to obtain information about the microstructure present in amine-cured epoxy networks and the rates of some of the reactions relevant to the cure. In the EPR part of this work, nitroxide free radicals⁸ were used to monitor their dynamic environments in the polymer. The nitroxide was employed either as a spin label⁸ where it was covalently bound at a known site on the epoxy or as a spin probe where it was randomly distributed throughout the polymer.

The epoxy resin studied was the diglycidyl ether of bisphenol A (DGEBA) in the form of the commercial resin DER 332 obtained from the Dow Chemical Company. The curing agents used were the bifunctional aliphatic amine, N,N'-dimethyl-1,6-diaminohexane (DDH), or the tetrafunctional amine, 1,4-diaminobutane (DAB). Both amines were used without further purification. The molecular structures for these compounds are shown in Figure 1.

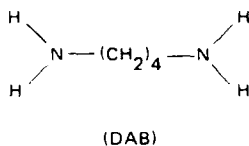
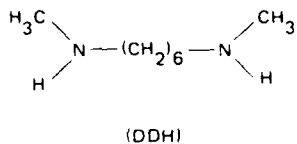
The following three specific EPR tasks were undertaken in this study:

- (1) Investigate and measure the kinetics of the reactions between nitroxide amines and DGEBA.
- (2) Investigate the nature of the microstructure present in the polymer network of amine-cured samples of DGEBA.
- (3) Determine the amount of unreacted epoxy groups in cured samples of DGEBA using nitroxide amines.

Epoxy resin:



Curing agents



GP11 1200 6

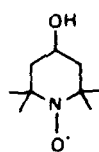
Figure 1. Epoxy resin and curing agents used in the EPR experiments.

The nitroxide amines used to label DGEBA in the kinetics experiments were 4-methylamino-2,2,6,6-tetramethylpiperidine-1-oxyl (METAMIN) and 4-dimethylamino-2,2,6,6-tetramethylpiperidine-1-oxyl (DIMETAMIN). The nitroxide, 2,2,6,6-tetramethyl(1,2,3,6-tetrahydropyridine)-1-oxyl (TEMPENE), appeared as a by-product in the labeling experiments. The nitroxide, 4-hydroxy-2,2,6,6-tetramethylpiperidine-1-oxyl (TANOL), was used as a spin probe in the microstructural investigations. The molecular structures of these nitroxides are shown in Figure 2.

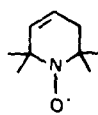
The following two NMR tasks were undertaken in this study:

- (1) Use ^{13}C NMR to investigate and measure the kinetics of the reaction of a monofunctional epoxy with a monofunctional amine.
- (2) Use ^1H NMR to investigate the relationship between the nuclear relaxation times and the crosslink density of amine-cured DGEBA.

Spin probes:

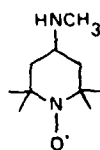


(TANOL)

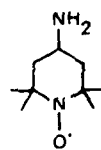


(TEMPENE)

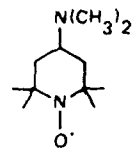
Spin labels:



(METAMIN)



(TAMIN)



(DIMETAMIN)

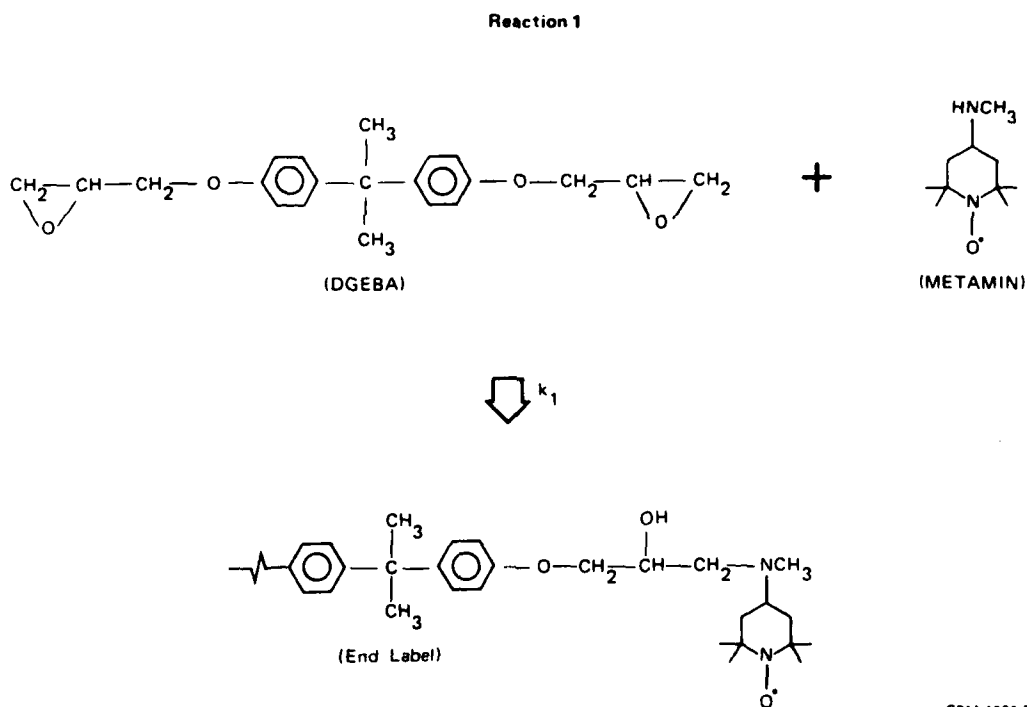
GP11 1200-7

Figure 2. Spin probes and spin labels used.

2. EPR EXPERIMENTS ON EPOXY RESINS

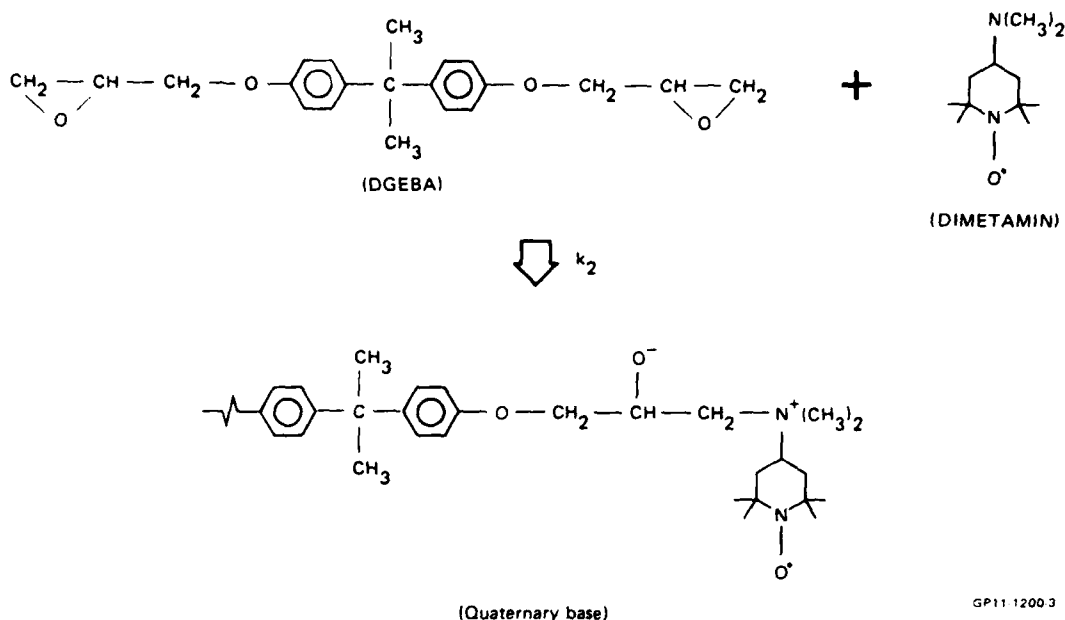
2.1 Nitroxide-DGEBA Kinetics

EPR methods were used to measure the rates of reaction of two nitroxide amines with the epoxy resin DGEBA. These reactions were: (1) the binding of METAMIN to the DGEBA monomer to form the end label⁹ (see reaction (1)), and (2) the binding of the tertiary amine DIMETAMIN to the DGEBA monomer to form the spin-labeled quaternary base⁹ (see reaction (2)), viz.,



and

Reaction 2



GP11 1200.3

Reaction (1) can be considered as a model for the initial step in the reactions involved in the curing of an epoxy resin with a conventional amine curing agent. Similarly, reaction (2) can be considered as a model for the initial step in the reactions involved in the catalytic cure of an epoxy resin with a conventional tertiary amine curing agent.

In both reactions (1) and (2), the samples were prepared in the following manner. An amount of DGEBA resin was heated at ~ 328 K until all visible monomer crystals had melted. All samples contained only small amounts of nitroxide ($\lesssim 0.08$ wt%). The latter was added to the resin at room temperature and was stirred thoroughly until all nitroxide dissolved. The sample was degassed in a vacuum oven at room temperature for ~ 5 min before an amount (≈ 0.25 mL) was transferred into a 3 mm i.d. tube.

The EPR spectra obtained at 296 K after certain times into reaction (1) were stored on magnetic tape using a data acquisition system (Varian E-900). These spectra can be field-shifted, scaled, subtracted, added, and integrated.

In a typical sequence of spectra recorded at different times into reaction (1) (Figure 3 is an example), it is assumed that the spectrum recorded initially (i.e., approximately 16 min after mixing) is that of the METAMIN spin probe, whereas the spectrum obtained at the end of the reaction (2660 min), is that of the end label. As can be seen from Figure 3, when the METAMIN spin probe binds to the epoxy to form the end label, the initial spin probe spectrum is replaced with one having a longer motional correlation time, i.e., a slower tumbling nitroxide is formed. The problem is to measure accurately and reliably the areas under the spectra associated with the spin probe and the end label as the composite spectrum develops in time.

The following method was found to be both accurate and reliable. The height of each recorded spectrum was measured at the two field values near the low-field derivative peak shown in Figure 4, viz., A, B for the end label, A', B' for the spin probe, and A'', B'' for the composite spectrum. The following relations hold

$$xA + yA' = A'' \quad (1)$$

$$xB + yB' = B'' , \quad (2)$$

where x and y are the relative amounts of end label and spin probe present respectively. The value of y (or $x = 1 - y$) was evaluated for each composite spectrum, and the value obtained was used to scale the spin-probe spectrum. This scaled spin-probe spectrum was subtracted from each composite spectrum to obtain a difference spectrum which corresponds to the amount of spin label present. Figure 5 illustrates the typical results of such a procedure. The areas under the absorption lineshape (first integral of the experimentally determined derivative lineshape) for the scaled spectrum and the difference spectrum were taken as the amount of spin probe and end label present, respectively.

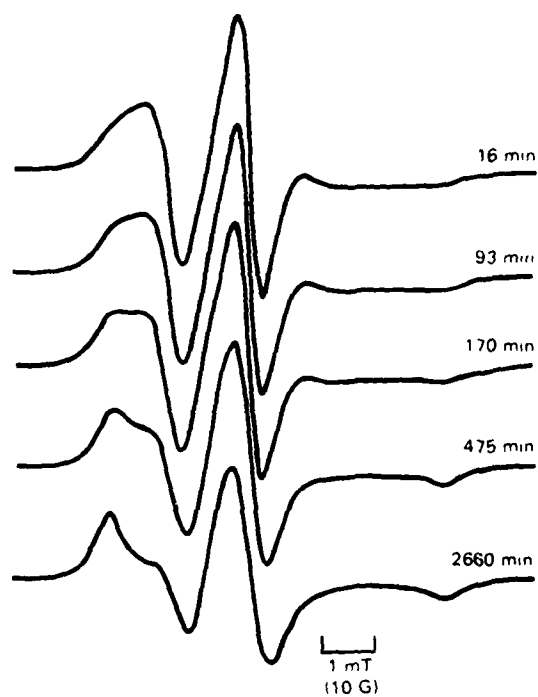


Figure 3. EPR spectra observed at 295 K for different times into reaction of end-label formation (reaction temperature = 295 K).

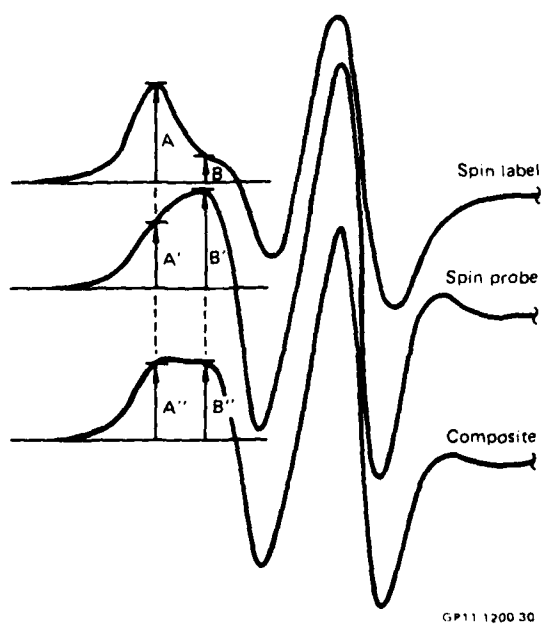


Figure 4. Definitions of spectral line amplitude parameters.

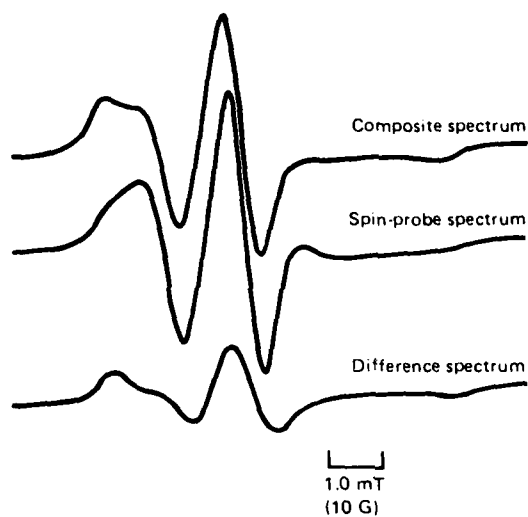


Figure 5. Typical lineshapes observed from the composite spectrum, the spin-probe spectrum, and the difference spectrum (i.e., spin-label spectrum) in the EPR kinetics experiment.

The actual data analysis was performed with a program written for the calculator (HP 9825) used in the data acquisition system. This program uses horizontal and vertical cursors in the oscilloscope to measure the height of each spectrum at the two designated field values. The scaling factor is calculated from the values of the parameters A'' , B'' in each spectrum. The area under each spectrum is normalized to the same value (i.e., that of the initial spectrum). The latter procedure was necessary since the total area under each spectrum varied as much as $\pm 10\%$ because of variations in filling factor when the sample was repositioned in the EPR microwave cavity after different times into the reaction. The normalized amounts of spin probe (P/P_0) and end label ($1-(P/P_0)$) were printed by the calculator, where P_0, P are the concentrations of spin probe initially and at time t , respectively.

Reaction (1) was carried out at different temperatures from 295 K to 366 K in a temperature-controlled convection oven (Imperial III, Lab-line Instrument Company). The sample tube was removed from the oven at different times into the reaction, and all EPR spectra were measured at 296 K. The normalized amounts of spin probe, P/P_0 , plotted as a function of time for reaction (1) carried out at 295 K, 318 K, 333 K, and 343 K are shown in Figures 6, 7, 8, and 9 respectively.

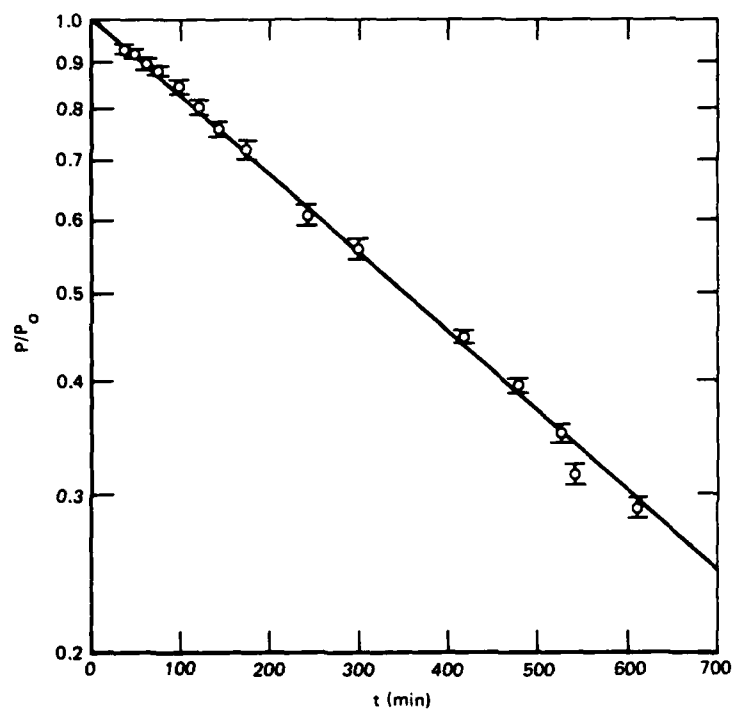
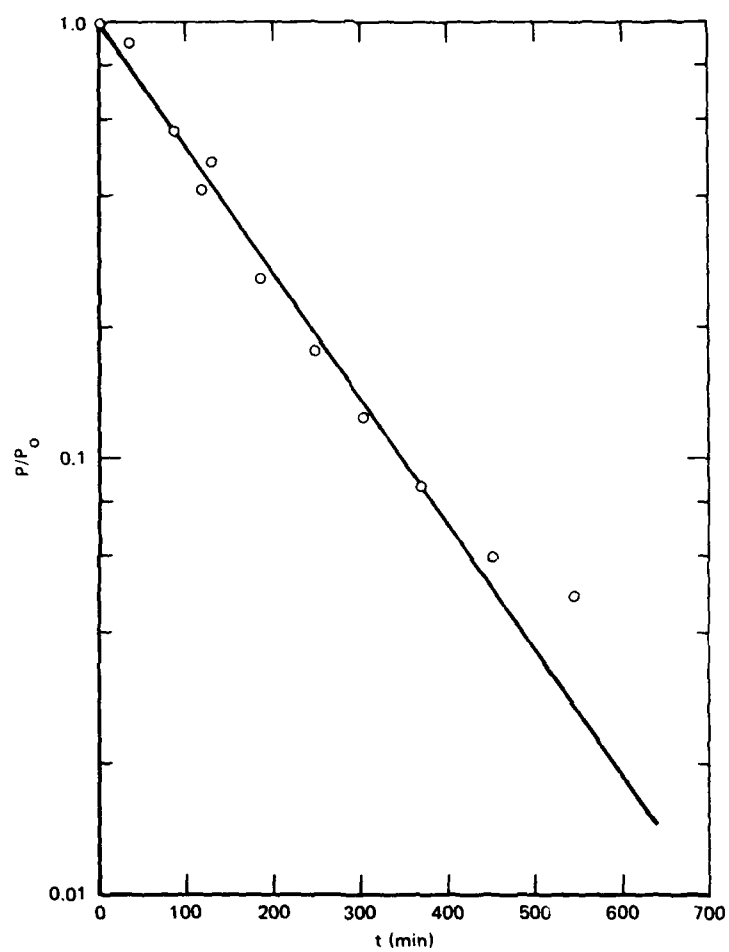


Figure 6. Time dependence of the normalized spin-probe concentration, P/P_0 , in end-label formation (reaction temperature = 295 K).



GP11.1200.12

Figure 7. Time dependence of the normalized spin-probe concentration, P/P_0 , in end-label formation (reaction temperature = 318 K).

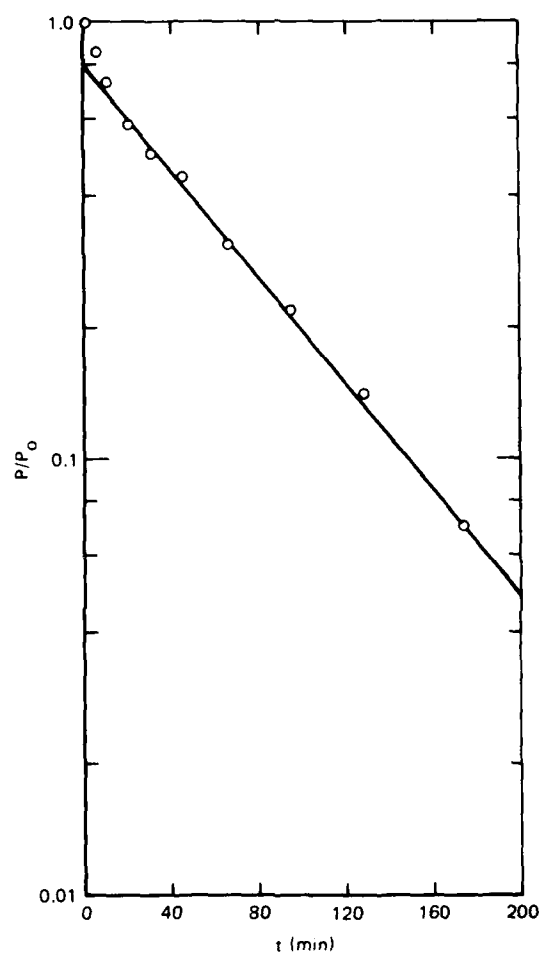
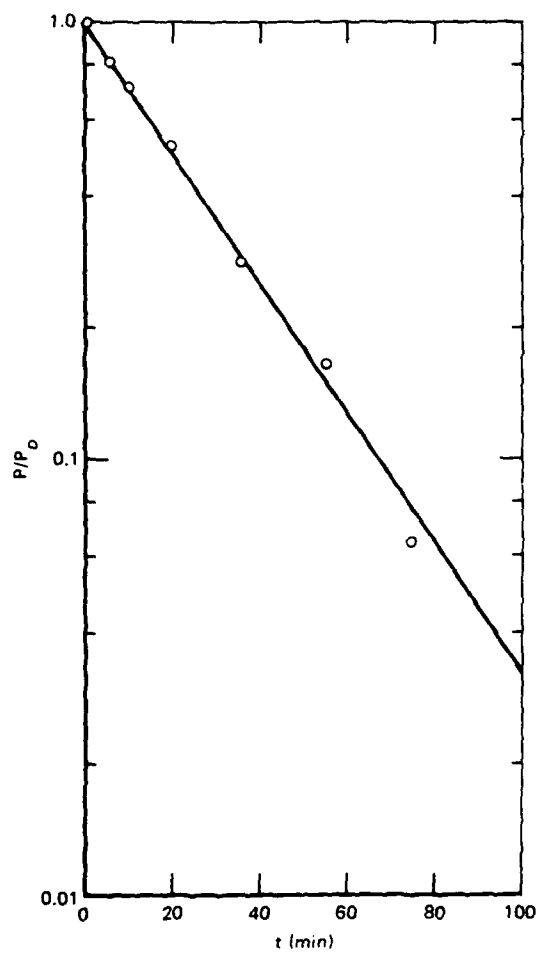


Figure 8. Time dependence of the normalized spin-probe concentration, P/P_0 , in end-label formation (reaction temperature = 333 K).



GP11 1200 9

Figure 9. Time dependence of the normalized spin-probe concentration, P/P_0 , in end-label formation (reaction temperature $\approx 343 \text{ K}$).

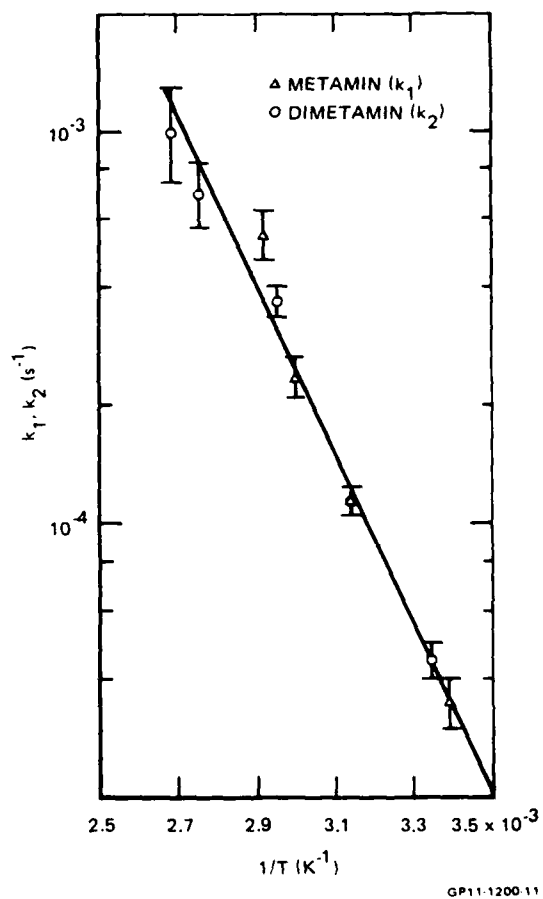
The agreement with a single exponential time dependence in Figures 6, 7, 8, and 9 implies a pseudo-first-order reaction with the values of the rate constant k_1 for the different temperatures shown in Table 1 (see Appendix A). These values of the rate constant are plotted as a function of $1/T$ in Figure 10 where the data show that $k_1 = k_0 \exp - \Delta E/RT$, where ΔE is the activation energy and K_0 is the frequency factor. From the data in Figure 10, one obtains $\Delta E = 41.5 \pm 5 \text{ kJ mole}^{-1}$ and $k_0 = 7.8 \times 10^2 \text{ s}^{-1}$.

The rates of the reaction of the tertiary amine DIMETAMIN with the epoxy resin DGEBA to form the spin-labeled quaternary base were also measured at several temperatures between 299 K and 373 K. When the reaction was carried out at 299 K, the EPR spectra were recorded at 299 K for the most accurate results. Figure 11 shows the sequence of spectra observed at the times shown. However, when the reaction was carried out at 318 K, 338 K, 363 K, and 373 K, the EPR spectral measurements were made at 318 K to enhance the discrimination between the spectrum from the DIMETAMIN spin probe and that from the spin-labeled quaternary base. Figure 12 shows the typical sequence of spectra observed at 318 K. The spectra were analyzed in the same manner as those described above for the end label.

TABLE 1. REACTION RATES OF NITROXIDE AMINES WITH DGEBA.

Nitroxide	Rate constant (k_1, k_2) (s^{-1})	Temperature (K)
METAMIN	3.5×10^{-5}	295
	1.15×10^{-4}	318
	2.35×10^{-4}	333
	5.5×10^{-4}	343
DIMETAMIN	4.5×10^{-5}	299
	1.15×10^{-4}	318
	3.7×10^{-4}	339
	7.0×10^{-4}	363
	1.0×10^{-3}	373

GP11 1200 1



GP11-1200.11

Figure 10. Temperature dependence of the rate constants k_1 , k_2 for METAMIN and DIMETAMIN reactions with DGEBA.

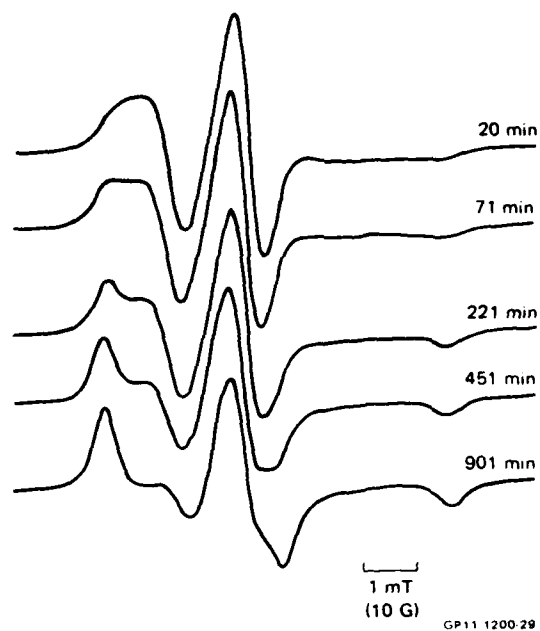


Figure 11. EPR spectra observed at 299 K for different times into reaction of spin-labeled quaternary-base formation (reaction temperature = 299 K).

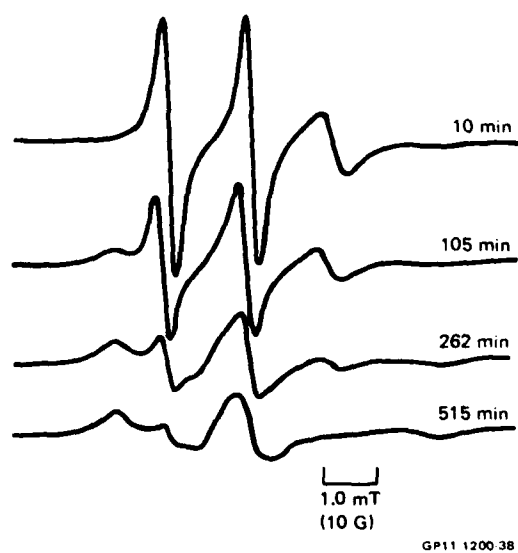


Figure 12. EPR spectra observed at 318 K for different times into formation of spin-labeled quaternary base (reaction temperature = 318 K).

The time dependence for the normalized spin-probe concentration, P/P_0 , at the reaction temperatures 299 K, 318 K, and 338 K are shown in Figures 13, 14, and 15. As can be seen in these data, the decay of P/P_0 shows a good fit to a single exponential. This result implies that reaction (2) also obeys pseudo-first-order kinetics since all measurable spin probe was converted to the quaternary base before appearance of the Hofmann elimination product^{9,10} TEMPENE. On the other hand, in Figures 16 and 17, where the data show plots of the normalized amount of fast-phase component as a function of time, the decays are not simple single exponentials. The reason for this difference is

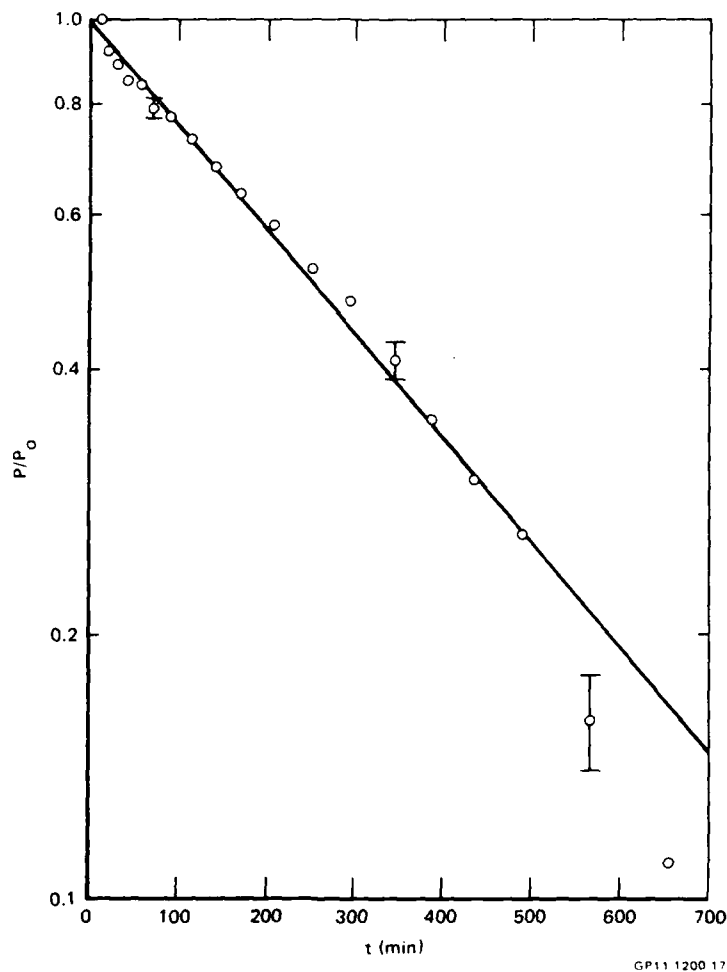


Figure 13. Time dependence of the normalized spin probe concentration, P/P_0 , in the formation of spin-labeled quaternary base (reaction temperature = 299 K).

that the TEMPENE spectrum appeared before the complete disappearance of the DIMETAMIN spin-probe signal. Since the TEMPENE spectrum is similar to that of DIMETAMIN, the presence of TEMPENE makes it appear as though the spin-probe concentration increases again in time. The initial slopes of the decays in Figures 16 and 17 are assumed to give the reaction rate k_2 .

The values of k_2 obtained for the reaction carried out at 299 K, 318 K, 338 K, 363 K, and 373 K are listed in Table 1 and plotted in Figure 10. These values show that $k_2 = k_0 \exp - \Delta E/RT$ with the values $\Delta E = 41.5 \pm 5 \text{ kJ mole}^{-1}$ and $k_0 = 7.8 \times 10^2 \text{ s}^{-1}$, i.e., $k_1 \approx k_2$.

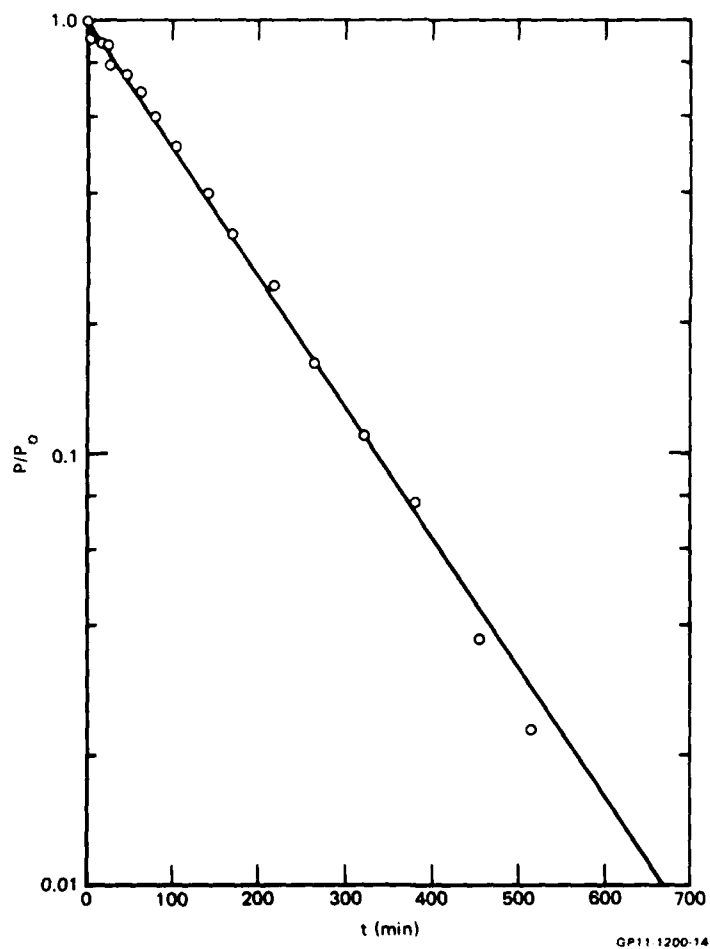


Figure 14. Time dependence of normalized spin-probe concentration, P/P_0 , in formation of spin-labeled quaternary base (reaction temperature = 318 K).

The rates of the Hofmann elimination reaction⁹⁻¹¹ were investigated at different temperatures, but it was impossible to measure them reliably because of the presence of parallel reactions. These reactions are of the type shown below involving charge separation caused by the stepwise addition of DGEBA molecules following oxirane ring opening by the O^- groups.

The evidence presented for the existence of these different quaternary bases with different degrees of charge separation is contained in the temperature dependence of the EPR spectra. Figure 18 shows the temperature dependence of the collapse of the extrema splitting for two samples of DGEBA con-

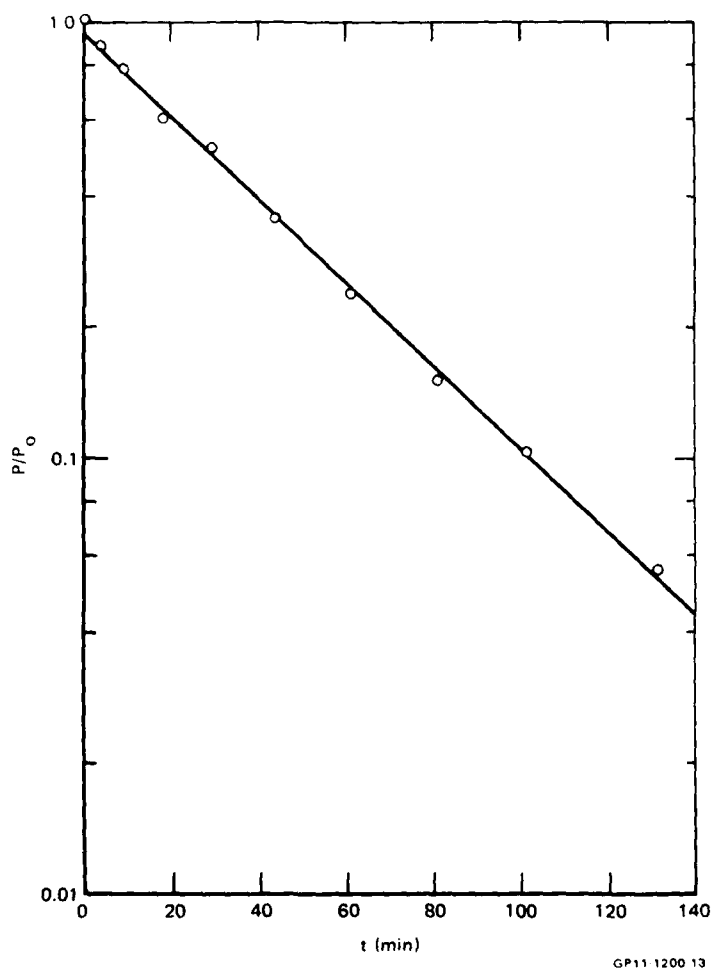


Figure 15. Time dependence of the normalized spin-probe concentration, P/P_0 , in formation of spin-labeled quaternary base (reaction temperature = 338 K).

taining DIMETAMIN. One sample, (a), which had been heated at 363 K for 6 h, contained the spin-labeled quaternary base only; the other sample, (b), which had been heated at 363 K for 4 days, contained the spin-labeled quaternary base and a large amount of TEMPENE (the area under the TEMPENE spectrum was ~ 18% of the area under the total spectrum). As shown in Figure 18, the collapse of the extrema splitting for the spin-labeled quaternary base in sample (b) occurred at a higher temperature than that for the quaternary base in sample (a). This result implies that the motional correlation time for the quaternary base in sample (b) is slower than that in sample (a). The reason is either an increase in the molecular size of the quaternary base or an

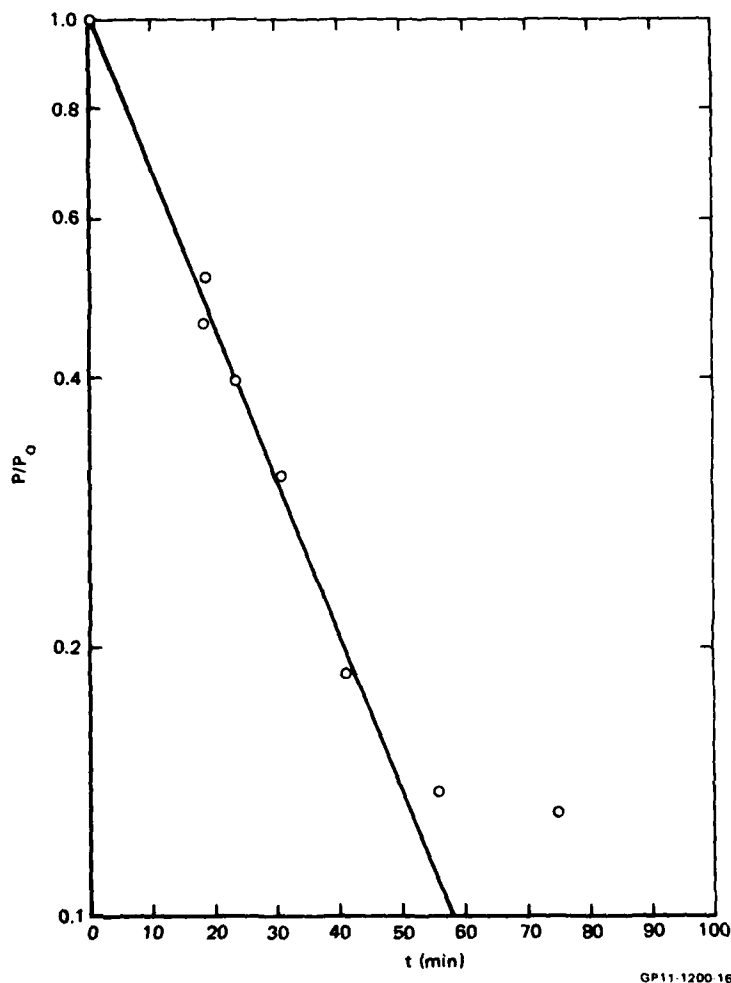


Figure 16. Time dependence of the normalized spin-probe concentration, P/P_0 , in the formation of spin-labeled quaternary base (reaction temperature = 363 K).

increase in the viscosity of the resin because of extensive crosslinking resulting from catalytic homopolymerization. The latter effect was shown to be negligible since only small amounts of DIMETAMIN were used (these samples contained < 0.08 wt% DIMETAMIN). Thus, a sample of DGEBA containing only TEMPENE exhibited a three-line spectrum with the same relative intensities as the spectrum exhibited by TEMPENE produced in the DIMETAMIN reaction with DGEBA (see Figures 19 a, b). The identical spectra indicate the same value of the motional correlation time for TEMPENE in both samples, thus proving that the resin viscosity was unaffected by the presence of the quaternary base.

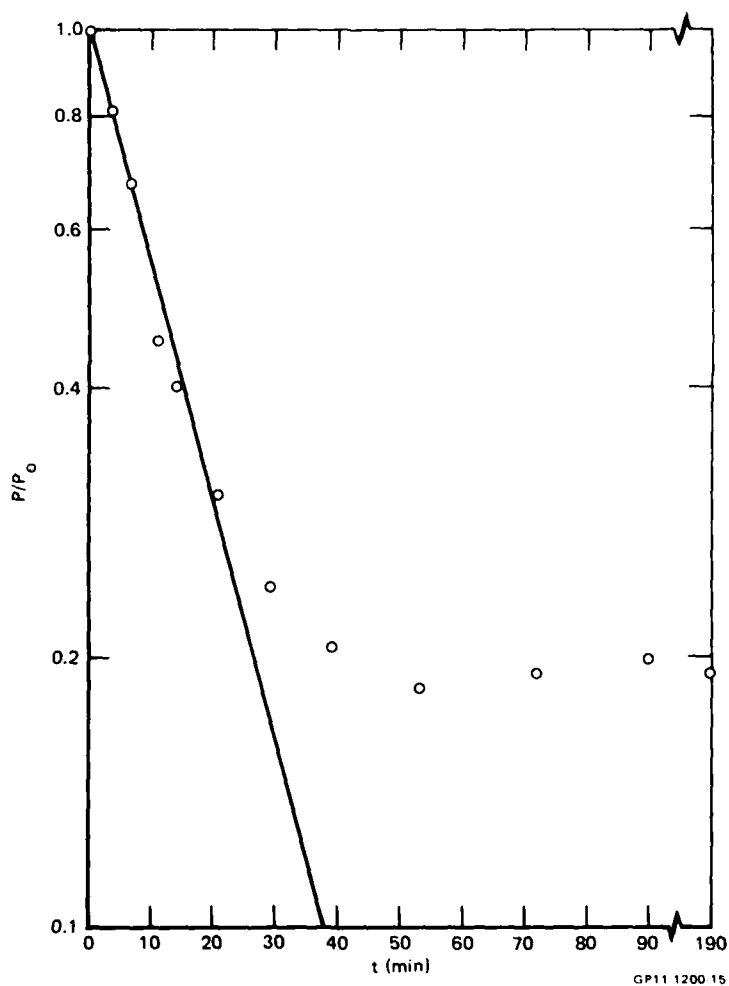


Figure 17. Time dependence of the normalized spin-probe concentration, P/P_0 , in formation of spin-labeled quaternary base (reaction temperature = 373 K).

Hence the data in Figure 18 imply that there is an increase in the molecular size of the quaternary base with time, presumably because of reactions of the type shown in Figure 20.

If there is enough DIMETAMIN present, quaternary base reactions of the type shown in Figure 20 can lead to catalytic homopolymerization of the DGEBA. This reaction is evidenced by our preparation of a rigid sample of DGEBA catalytically cured with the addition of only ~ 5 wt% DIMETAMIN.

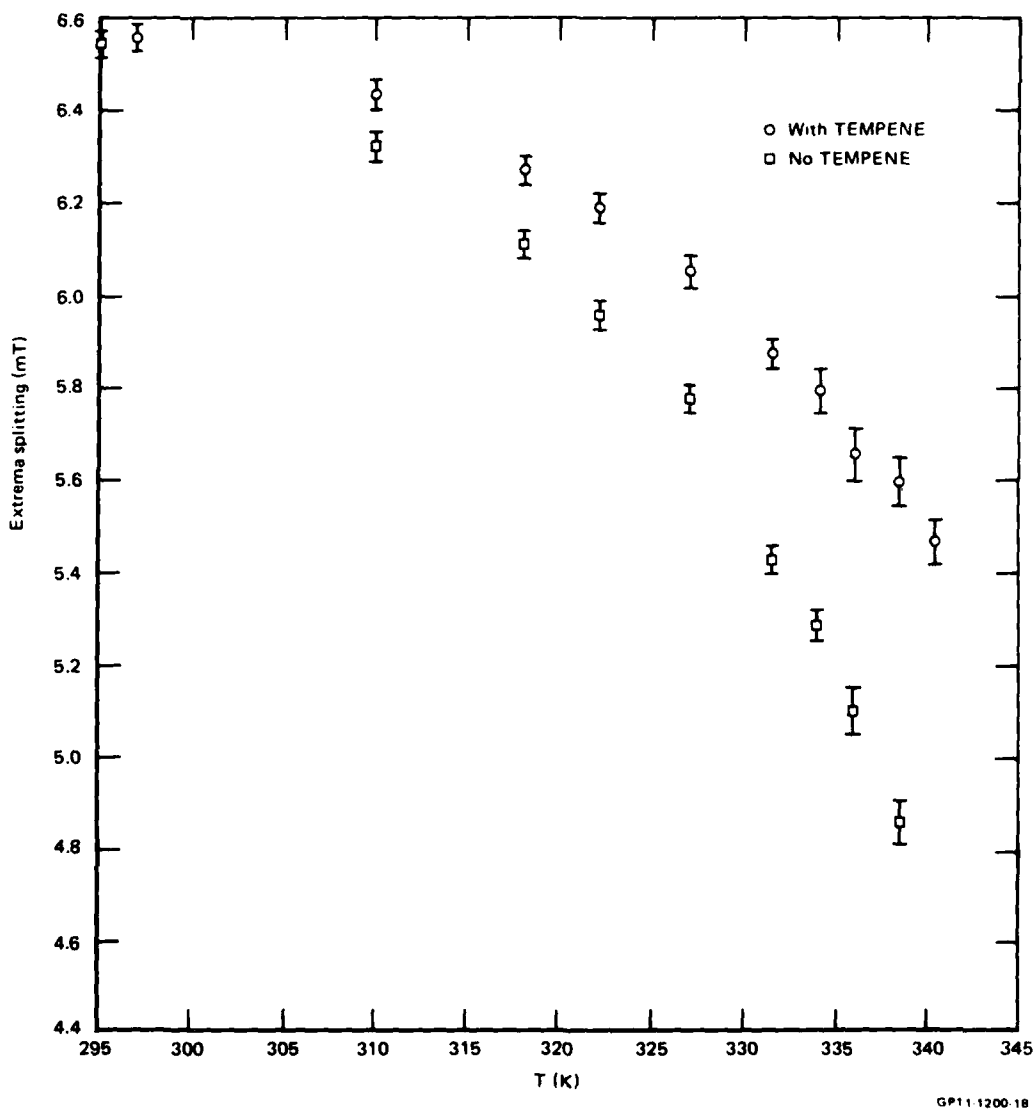
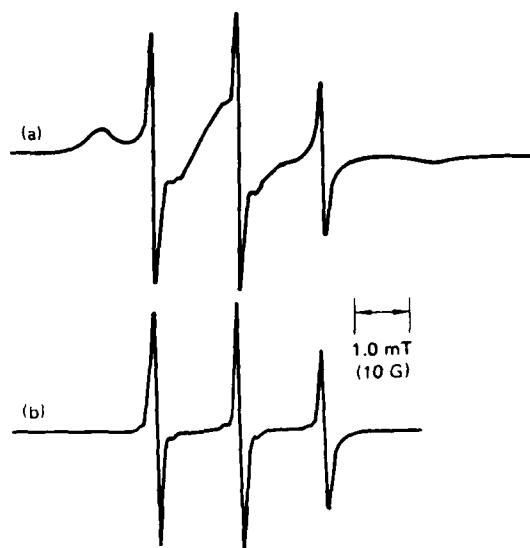


Figure 18. Temperature dependence of extrema splitting for sample of DIMETAMIN in DGEBA which had been heated for 4 days at 363 K (with TEMPENE) and also a sample which had been heated for 6 h at 363 K (no TEMPENE).



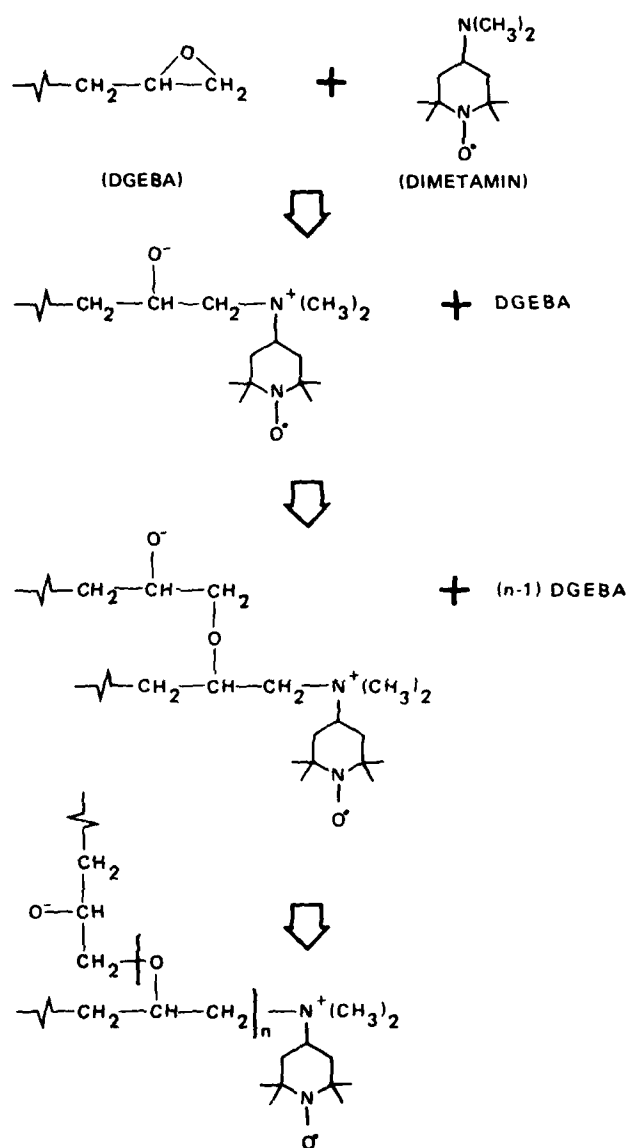
GP11 1200 78

Figure 19. (a) Spectrum observed in the reaction of DIMETAMIN with DGEBA and (b) spectra observed from TEMPENE in DGEBA.

2.2 Investigation of the Microstructure in Cured Epoxies

The main objective in this task was to investigate the nature of the microstructure in amine-cured epoxy samples with different average crosslink densities.^{9,10} The average crosslink density was varied by curing with stoichiometric amounts of mixtures of amine curing agents with different amine functionalities.

Samples of DGEBA containing the nitroxide spin probe TANOL were cured with stoichiometric amounts of the bifunctional amine, N,N'-dimethyl-1,6-diaminohexane (DDH), and the tetrafunctional amine, 1,4-diaminobutane (DAB), and also with mixtures of DDH and DAB. The samples prepared from these mixtures contained 1:4:5, 2:3:5, and 3:2:5 equivalent ratios of DAB:DDH:DGEBA. The DGEBA/DDH samples, which were composed of lightly crosslinked linear chains, were soft and flexible, whereas the DGEBA/DAB samples composed of a highly crosslinked three-dimensional network were hard and brittle.



GP11-1200-19

Figure 20. Reaction scheme for the formation of the different spin-labeled quaternary bases involved in the homopolymerization of DGEBA with DIMETAMIN as the initiator.

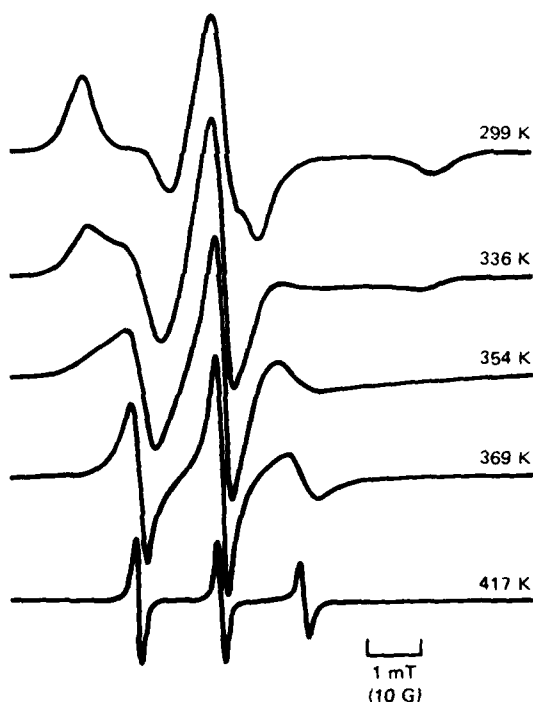
The temperature dependences of the EPR spectra of TANOL in each of these samples indicate that at each temperature, the spectrum can be characterized by essentially one value of the motional correlation time, τ_c . Figure 21 is an example of how the EPR spectra of TANOL in one of these epoxy samples change with temperature, whereas Figure 22 illustrates how the spectra of TANOL differ in the four epoxy samples at a given temperature (385 K).

The correlation times were evaluated for $\tau_c < 3 \times 10^{-9}$ s from the EPR lineshapes using the theory of Kivelson.¹² The equation used was

$$\tau_c = 4 \left[\left(\frac{Y(0)}{Y(1)} \right)^{1/2} + \left(\frac{Y(0)}{Y(-1)} \right)^{1/2} - 2 \right] b^{-2} W(0)^{-1} \quad (3a)$$

with

$$b = \frac{4\pi}{3} \left[A_{zz} - \frac{1}{2} (A_{xx} + A_{yy}) \right] \quad (3b)$$



GP11 1200 33

Figure 21. Temperature dependence of EPR spectra of TANOL in sample of DGEBA cured with DDH.

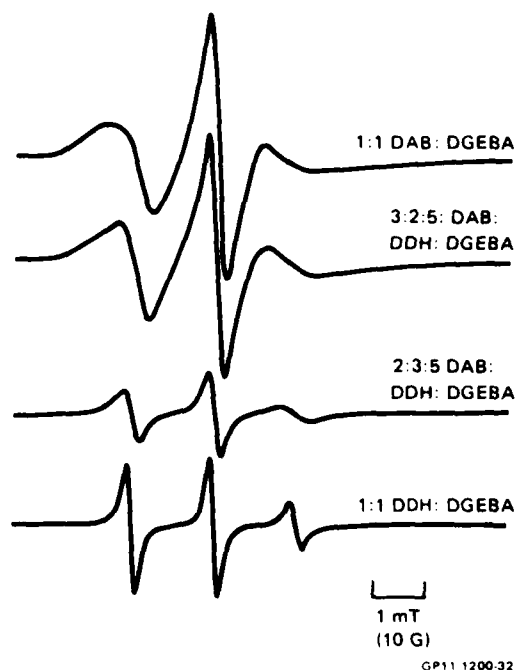


Figure 22. EPR spectra of TANOL in amine-cured samples of DGEBA with different crosslink densities at a temperature of 385 K.

where $Y(1)$, $Y(0)$, and $Y(-1)$ are the intensities of the low, middle, and high field lines, A_{xx} , A_{yy} , and A_{zz} are the principal values of the nitrogen hyperfine interaction tensor, and $W(0)$ is the width of the center line. The values $A_{zz} = 3.45$ mT and $A_{xx} = A_{yy} = 0.6$ mT were used for TANOL.

The measured values of τ_c for TANOL in the cured epoxy resin samples are shown as a function of $(\text{temperature})^{-1}$ in Figure 23. The lightly crosslinked samples show the shortest τ_c values. Moreover, lightly crosslinked samples show a straight-line dependence of $\ln \tau_c$ on $(\text{temperature})^{-1}$, whereas the more heavily crosslinked samples show a slight curvature.

The crosslink density was calculated from the value of the shear modulus above T_g using the expression,¹³

$$G' = \frac{\rho RT}{\alpha M}, \quad (4)$$

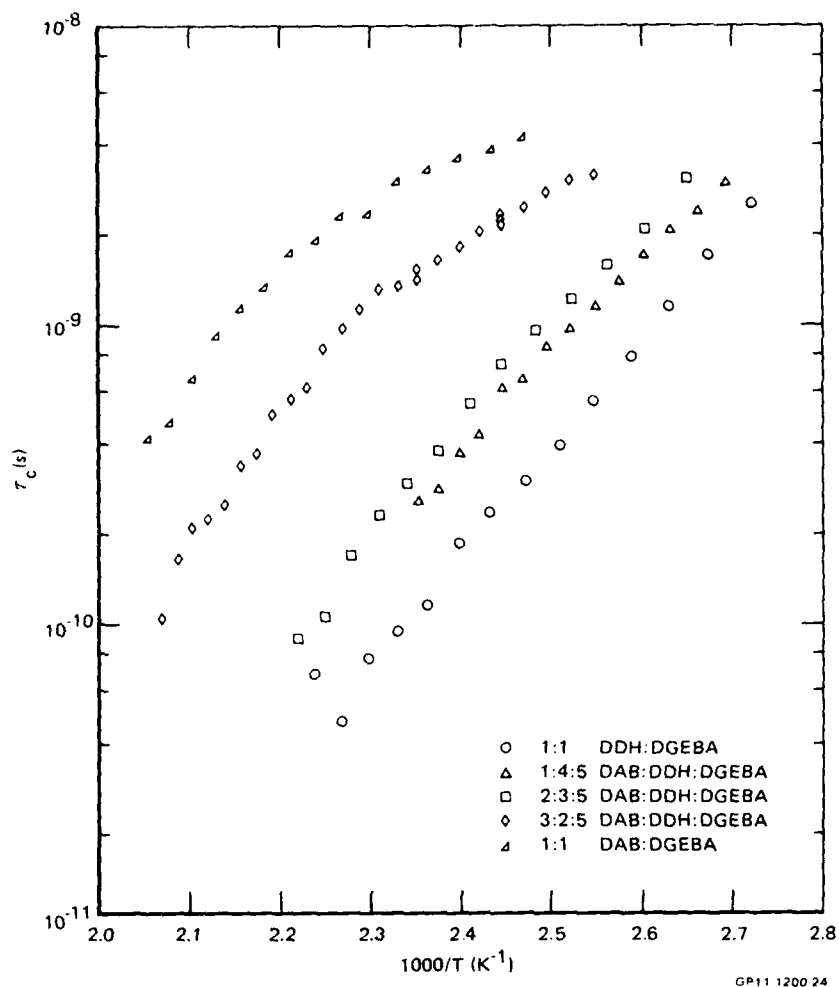


Figure 23. Temperature dependence of motional correlation time for TANOL in samples of amine-cured DGEBA with different crosslink densities.

where G' is the real part of the dynamic shear modulus above T_g , ρ is the density of the cured epoxy, M is the molecular weight between crosslinks, R is the gas constant, and α is a constant with a value between 1 (from theory of rubber elasticity) and 0.53 (see Tobalsky¹³).

The shear moduli of the four epoxy samples were measured using a dynamic mechanical spectrometer (Rheometrics model RDS 7700). The typical temperature dependence of G' , G'' , and $\tan \delta = G''/G'$ obtained in the four epoxy samples for a heating rate of $2^\circ/\text{min}$ is shown in Figure 24. The value of T_g was taken at the maximum of the $\tan \delta$ peak. The temperature dependence of G' for the four epoxy samples is shown in Figure 25. These four samples had been postcured at 413 K for 2 h.

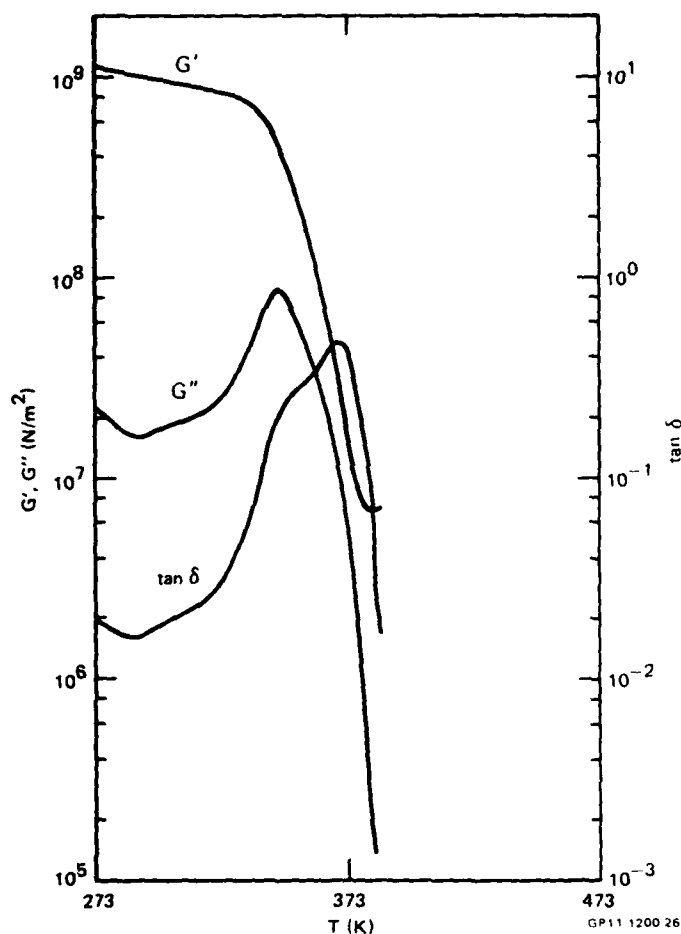


Figure 24. Shear moduli, G' and G'' , and $\tan \delta$ as a function of temperature for 3:2:5 DAB:DDH:DGEBA.

The values of τ_c obtained from Figure 23 at a chosen temperature are plotted against the values of M^{-1} obtained from Equation (4) for the four epoxy samples. The results are shown in Figure 26 for four different temperatures. Figure 26 shows that at all four temperatures, the logarithm of the motional correlation time is approximately linearly dependent on the crosslink density (M^{-1}) over the range of crosslink densities studied. Theoretical crosslink densities were also calculated¹⁴ from the known stoichiometric amounts of the amines with known functionality used in the cure. The expression used was

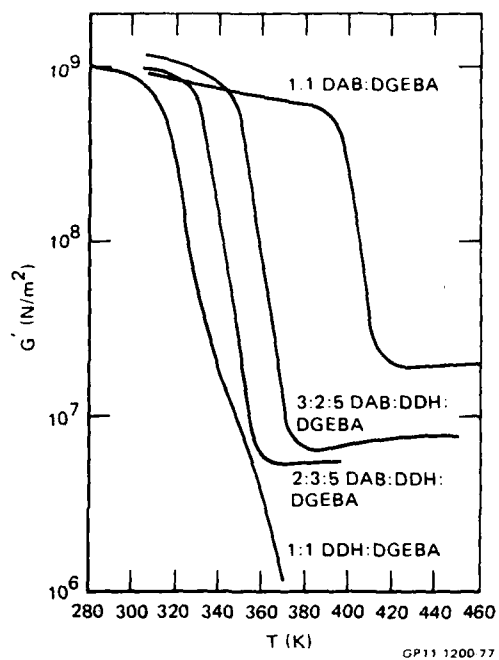


Figure 25. Shear modulus G' as a function of temperature for the amine-cured samples of DGEBA with the stoichiometries indicated.

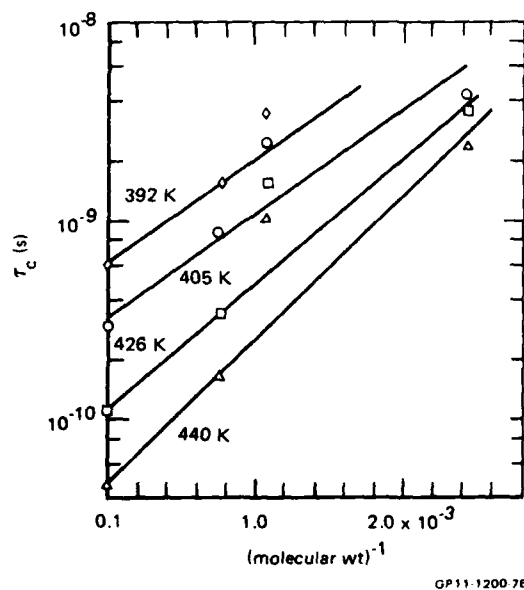


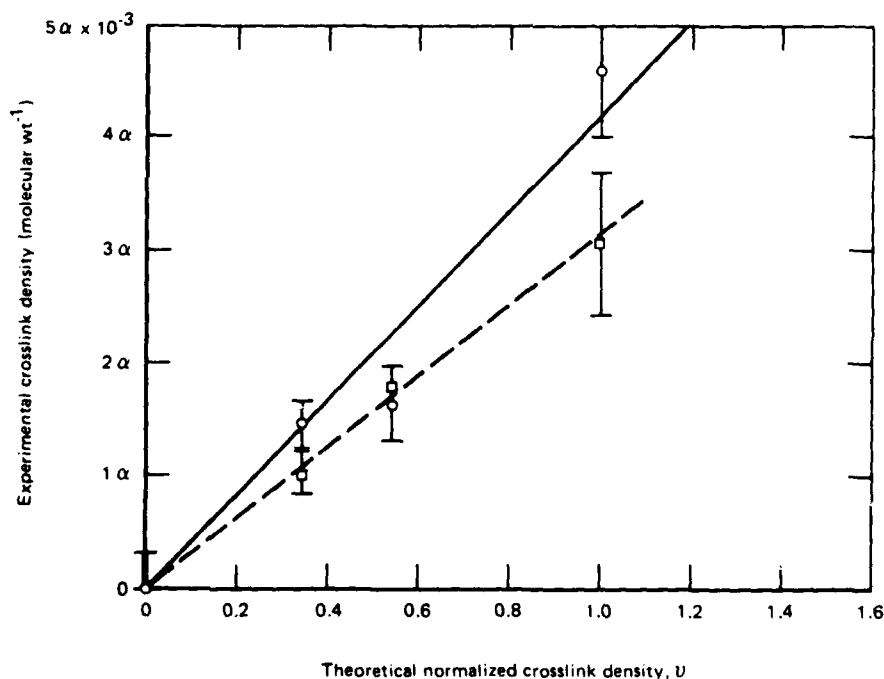
Figure 26. Motional correlation time at the selected temperatures shown for TANOL in amine-cured DGEBA samples having different molecular weights between crosslinks.

$$\nu = \left(\frac{f}{2}\right) \left(\frac{m}{w}\right) \rho, \quad (5)$$

where ν is the crosslink density, f is the functionality of the amine used (e.g., $f = 4$ for DAB), m is the number of moles of DAB in the sample, w is the weight of the sample, and ρ is the density of the sample.

A plot of the experimentally obtained crosslink densities (M^{-1}) as a function of the normalized values of theoretically derived crosslink densities (ν) is shown in Figure 27 (the values of ν are normalized such that in the sample DAB:DGEBA = 1:1, $\nu \approx 1$). The data for the four postcured samples and the four samples which were not postcured are shown. The linearity of the agreement supports the use of the (M^{-1}) values obtained from Equation (4) as a measure of the crosslink densities.

In drawing conclusions from the results depicted in Figure 23, it is important to remember that the Kivelson theory which was used to obtain the



GP11-1200-75

Figure 27. Experimental crosslink density from dynamic mechanical data as a function of theoretical values calculated from sample stoichiometry. $\alpha = 1.0$, scale factor for ideal sample; $\alpha = 0.53$, Tobolsky. \circ = samples postcured two hours at 413K, \square = samples not postcured.

τ_c values from the lineshapes is valid for $\tau_c \lesssim 3 \times 10^{-9}$ s. Although this limitation may explain some of the curvature in the $\ln \tau_c$ plots for τ_c values $> 3 \times 10^{-9}$ s in Figure 23, some curvature remains in the DAB/DGEBA data even for $\tau_c < 3 \times 10^{-9}$ s, whereas the data for DDH/DGEBA samples show a linear dependence of $\ln \tau_c$ on $(\text{temperature})^{-1}$. Thus the DGEBA/DAB data do not follow an Arrhenius temperature dependence. On the other hand, as shown in Figures 28 and 29, the data from both the DAB/DGEBA and DAB:DDH:DGEBA = 2:3:5 samples show excellent agreement with the following modified form for the WLF equation.^{9,15}

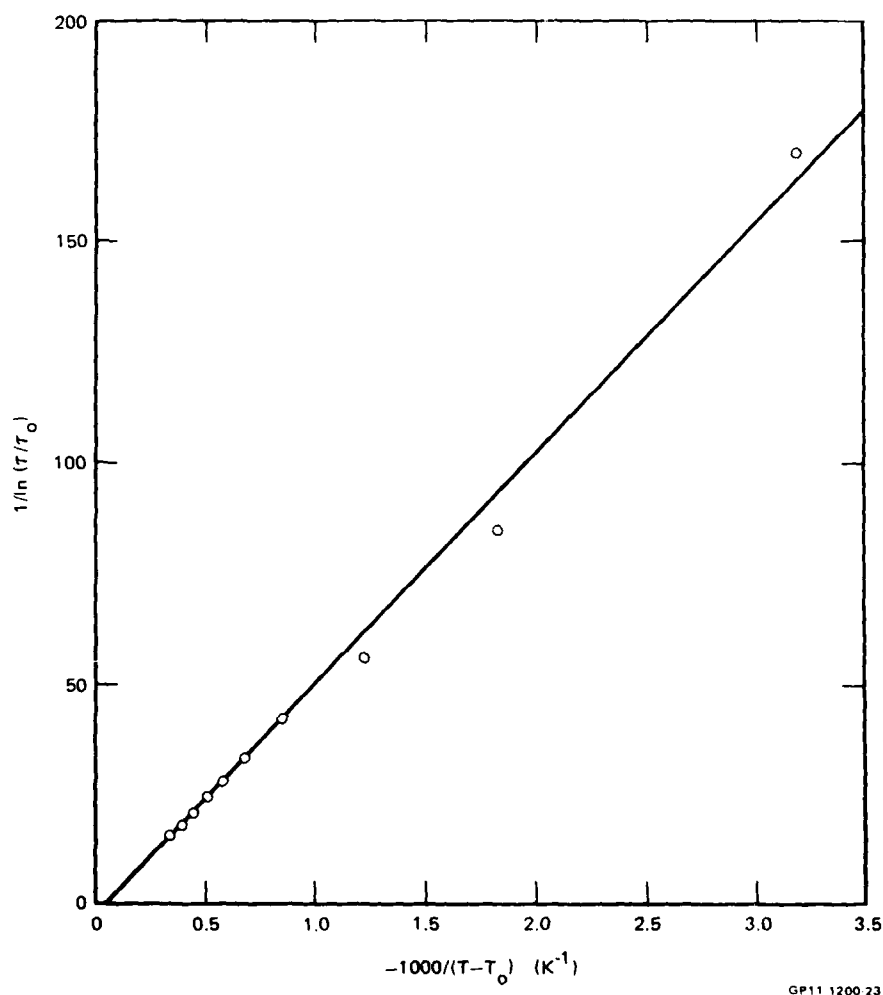


Figure 28. WLF plot for TANOL in amine-cured epoxy sample with stoichiometry DAB:DDH:DGEBA = 2:3:5.

$$1/\ln(\tau_c/\tau_{cR}) = f_R^2/[B\epsilon \beta (T-T_R)] + \alpha f_R/B, \quad (6)$$

where τ_c , τ_{cR} are the spin-probe motional correlation times at temperature T and reference temperature T_R ; f_R is the free-volume fraction at reference temperature T_R ; $B(=1)$ is the coefficient that appears in the Doolittle equation¹⁵; β is the difference in the thermal expansion coefficients above and below T_g ; and ϵ and α are empirical constants which account for the sensitivity of the spin-probe rotational motions to changes in the free volume. The plots in Figures 28 and 29 show that $1/\ln(\tau_c/\tau_{cR}) \propto 1/(T-T_R)$. If the typical conventional values $B = 1$, $\beta = 5 \times 10^{-4}$, and $f_R = 0.025$ are substi-

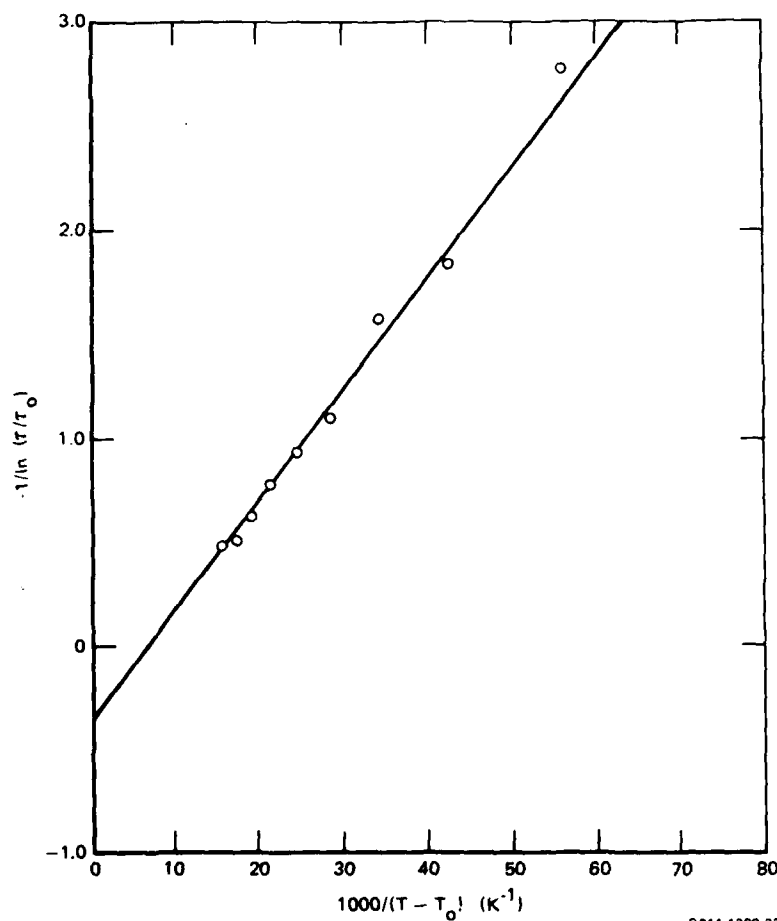


Figure 29. WLF plot for TANOL in amine-cured epoxy sample with stoichiometry DAB:DGEBA = 1:1.

tuted into Equation (6), one obtains $\epsilon \approx 0.1$. This is a reasonable value for ϵ for the case of rotational diffusion, since one would expect this value to be smaller than the values of $\epsilon = 0.6$ to 1.0 typical for translational diffusion.¹³

The following swelling experiments were performed prior to investigating the EPR behavior of nitroxides in plasticized epoxy samples. The six samples that were cured (but not postcured) with stoichiometric amounts of DDH and DAB mixtures were immersed in the solvents, methylene chloride and benzene. Subsequent weight gains measured following different solvent exposure times were assumed to be proportional to the sample swelling, i.e., the volumes of polymer and sorbed solvent were assumed to be additive. Figure 30 is a plot of weight percent solvent uptake as a function of time for these samples. As can be seen from Figure 30, the degree of swelling depends on the solvent used and the sample crosslink density. For each solvent, the weight of sorbed solvent increased with decreasing crosslink density in agreement with the Flory-Rehner equation,¹⁶ viz.,

$$\nu = - \frac{\ln(1 - v_2) + v_2 + \chi v_2^2}{V(v_2^{1/3} - v_2/2)} \quad (7a)$$

where ν is the number of moles of crosslink strands per liter, v_2 is the volume fraction of polymer in the swelled samples, V is the molar volume of the solvent, and χ is the Flory-Huggins solvent-polymer interaction parameter related to the enthalpy of mixing. Typical values of χ range from less than 0 for a solvent having great affinity for the polymer to over 0.5 for a solvent with little affinity for the polymer. For each sample stoichiometry, methylene chloride swells the samples to a larger extent than benzene, indicating that methylene chloride has a greater affinity for the epoxy samples, i.e., $\chi_{\text{benzene/epoxy}} > \chi_{\text{methylene chloride/epoxy}}$. It is possible to calculate crosslink densities, ν , from Equation (7a) if V , v_2 , and χ are known. From the swelling data of Figure 30, v_2 can be calculated, and for methylene chloride, V is equal to $6.41 \times 10^{-2} \text{ L} \cdot \text{mole}^{-1}$. Equation (7a) thus can be reduced to the following form:

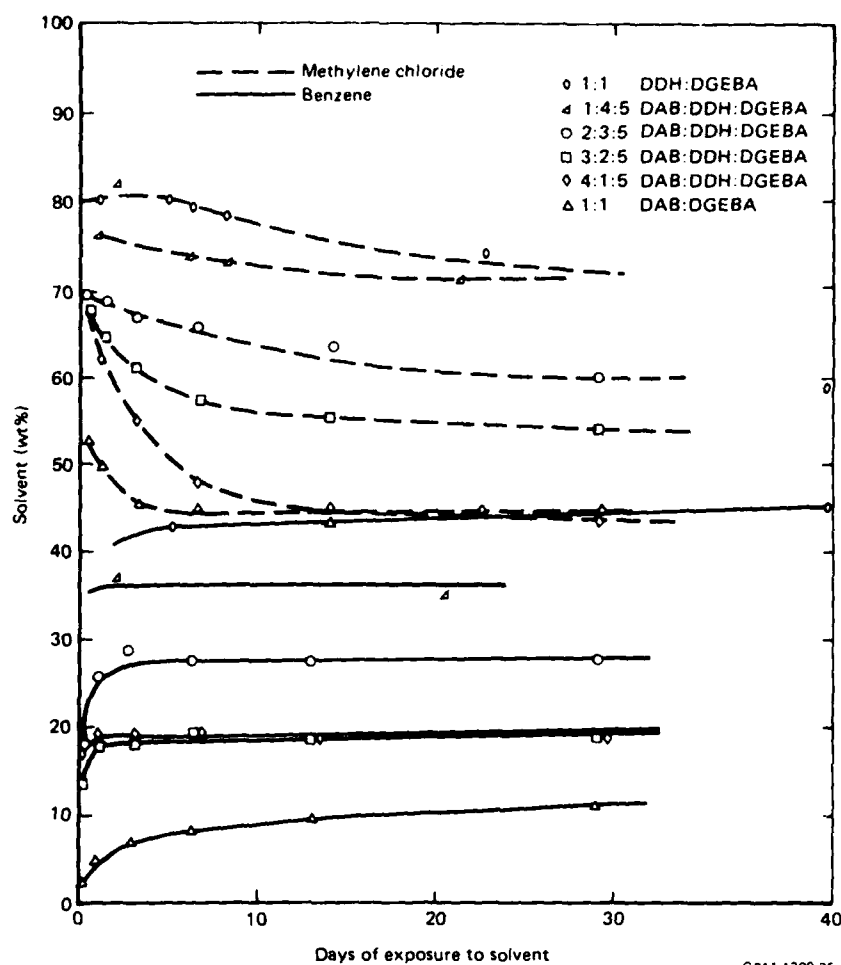


Figure 30. Plot of solvent (benzene, methylene chloride) content as a function of exposure time of sample to solvent for the sample stoichiometries shown.

$$v = a + bx, \quad (7b)$$

where

$$a = - \frac{\ln(1 - v_2) + v_2}{v(v_2^{1/3} - v_2/2)} \quad (7c)$$

and

$$b = \frac{-v_2^2}{v(v_2^{1/3} - v_2/2)} \quad (7d)$$

Plots of v as a function of χ for samples having different DDH:DAB ratios are shown in Figure 31. The values of v_2 substituted into Equations (7c) and (7d) for a and b were calculated from asymptotic values of the curves in Figure 30 corresponding to a 40-day immersion in methylene chloride. With the assumptions that χ was the same for all samples (i.e., the samples were all chemically similar) and the relative values of the crosslink densities among the different samples were the same as the relative values anticipated theoretically using Equation (5), χ was calculated using a linear least-squares routine to be 0.49 (see Figure 32). This value of χ is indicated by the

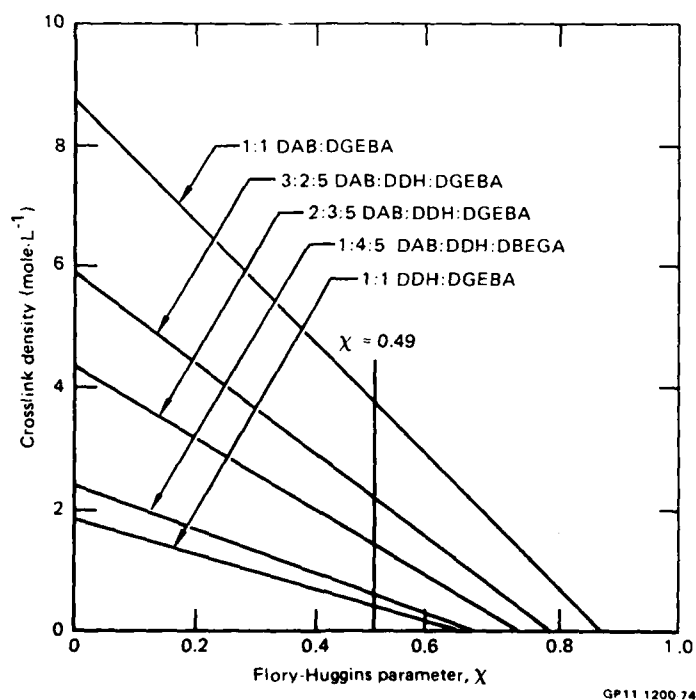


Figure 31. Crosslink density as a function of χ using data shown in Figure 30. Vertical line is value of χ determined by least squares calculation.

vertical line in Figure 31. The intersections of this line with the $v(\chi)$ lines yield values of v for each sample. These values are shown along with the average molecular weight between crosslinks in Table 2b.

Values of v were recalculated using the solvent content corresponding to less than a one day exposure to methylene chloride. Swelling of the samples was a maximum at this time, resulting in the lower crosslink densities reported in Table 2a. The corresponding value of χ was calculated to be 0.52.

The crosslink density values listed in Table 2b are about 25% higher than those predicted theoretically using Equation (5). In addition, considering the observed affinity of methylene chloride for the epoxy solids, one would expect a value $\chi < 0.5$. These results may be due to a breakdown in the applicability of the Flory-Rehner equation to highly crosslinked polymers such as epoxy resins. The situation where the experimentally determined crosslink density is greater than the theoretical value is similar to that encountered in the dynamic mechanical determination of crosslink densities, where α was necessarily assigned a value 0.53 rather than 1.0 in Equation (4).

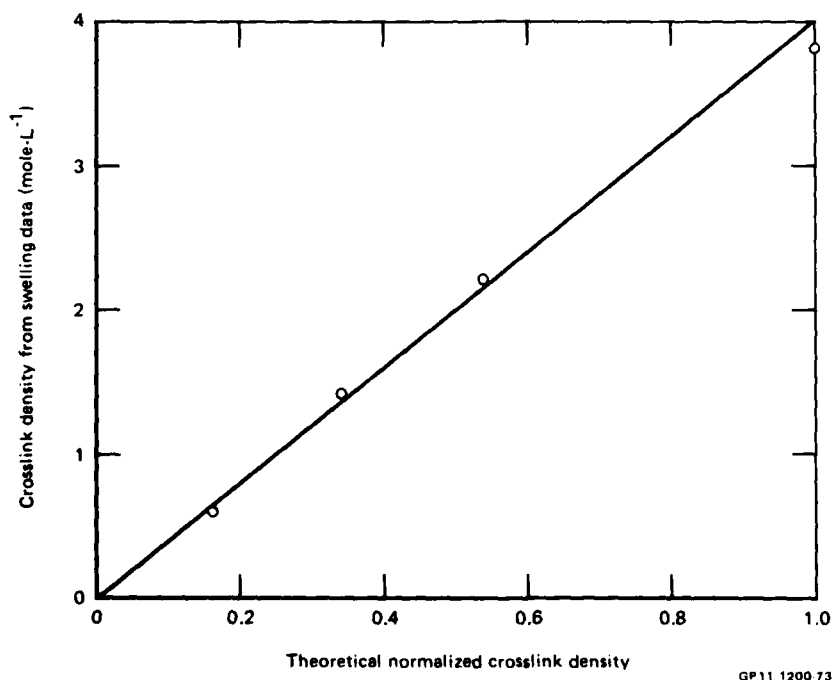


Figure 32. Least squares fit of experimental crosslink densities to theoretical normalized values. Variable parameter was χ . Best fit yields $\chi = 0.49$.

The following reasons are suggested for the reduction in swelling (i.e., weight loss) upon prolonged exposure to methylene chloride:

1. methylene chloride reacts with the amine to crosslink the sample, and this increased crosslinking leads to less swelling, and/or
2. there are unreacted epoxy and amine groups trapped in the rigid polymer matrix before swelling. After swelling and a plasticization of this matrix, these groups react with each other to increase the crosslinking which in turn leads to less swelling, and/or
3. unreacted amine and/or epoxy are leached from the samples by the methylene chloride.

Thus, the higher crosslink densities listed in Table 2b can correspond to an actual increase in crosslinking. On the other hand, there may be only an apparent increase in crosslink density resulting from less affinity of the epoxy sample for methylene chloride as low-molecular-weight material is leached out.

TABLE 2. CROSSLINK DENSITIES CALCULATED FOR AMINE-CURED DGEBA SAMPLES.

After 1 day in methylene chloride ($\chi = 0.52$)					
	Sample	% solvent	Volume fraction polymer	Crosslink density (mole·L ⁻¹)	Molecular wt between crosslinks
(a)	1:1 DDH:DGEBA	80	0.23	0.126	8850
	1:4:5 DAB:DDH:DGEBA	75.5	0.28	0.236	4750
	2:3:5 DAB:DDH:DGEBA	69.5	0.34	0.464	2450
	3:2:5 DAB:DDH:DGEBA	67.5	0.36	0.565	2020
	1:1 DAB:DGEBA	53	0.50	1.896	610
After 40 days in methylene chloride ($\chi = 0.49$)					
	Sample	% solvent	Volume fraction polymer	Crosslink density (mole·L ⁻¹)	Molecular wt between crosslinks
(b)	1:1 DDH:DGEBA	72.5	0.31	0.416	2680
	1:4:5 DAB:DDH:DGEBA	68.5	0.35	0.615	1830
	2:3:5 DAB:DDH:DGEBA	58.5	0.45	1.433	790
	3:2:5 DAB:DDH:DGEBA	52.5	0.51	2.209	520
	1:1 DAB:DGEBA	44	0.59	3.815	300

GP11 1200 79

Crosslink densities calculated from the benzene swelling data of Figure 30 agreed less favorably with the theoretical values than the methylene chloride data. This inconsistency also may be a consequence of the breakdown of applicability of the Flory-Rehner equation for the case of slightly swelled, highly crosslinked polymers.

Although benzene has the favorable property of being a nonreactive plasticizer, it appeared from the data in Figure 30 that the time to reach equilibrium swelling was inconveniently long (\sim days) for the EPR experiments. We therefore studied the EPR spectra of the spin probe TANOL in the epoxy samples having different average crosslink densities and containing different amounts of the solvent methylene chloride.

At low solvent contents (≤ 5 wt% methylene chloride), the EPR spectra of TANOL were only slightly modified from those of the dry samples by the presence of the solvent. At high solvent contents (≥ 30 wt% methylene chloride), only the narrow three-line spectrum was observed. At intermediate solvent contents (5 to 30 wt% methylene chloride), the observed spectra consisted of a superposition of a slow-phase spectrum differing little from that of the dry samples and a fast-phase spectrum characterized by a motional correlation time which was one-and-a-half orders of magnitude faster. Typical spectra observed on increasing the solvent contents of the samples are shown in Figures 33, 34, 35, and 36.

The spectra were digitized and stored on magnetic tapes using the data acquisition system (Varian E-900). The fractional amount of fast phase present in the composite spectrum was determined by removing the contribution of the slow-phase spectrum.⁹ This procedure was carried out by subtracting a scaled version of the dry-sample spectrum from the composite spectrum. The best criterion for the amount to be subtracted i.e., the scaling factor to be used, was found by displaying the resulting difference spectrum and obtaining the lineshape that appeared as the best fit to a fast-phase spectrum. Typical examples of the dry sample spectrum, the composite spectrum, and the difference spectrum for the fast phase are shown in Figure 37. The ratio of the areas under the absorption spectra (the first-integrals) of the difference spectrum and the composite spectrum was taken as the fast-phase fraction (i.e., the mobile fraction).

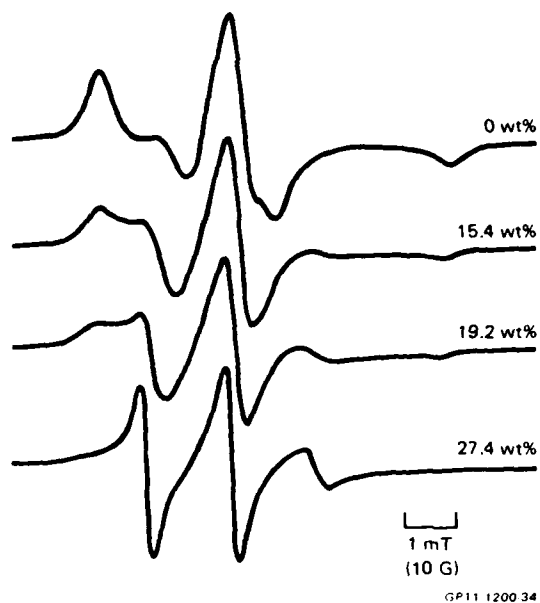


Figure 33. EPR spectra of TANOL in samples of DGEBA cured with DDH containing different amounts of methylene chloride.

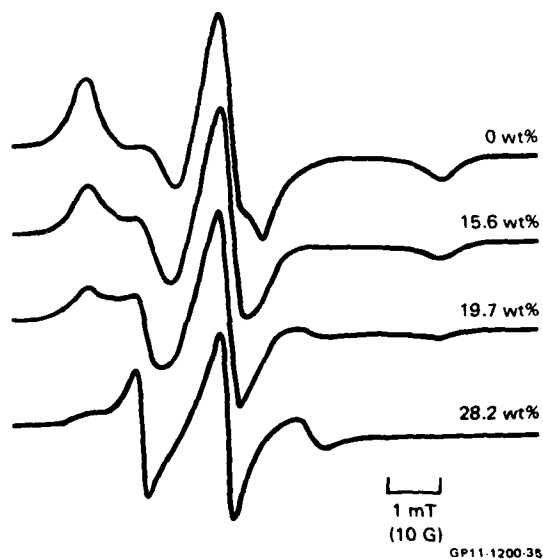


Figure 34. EPR spectra of TANOL in samples of DGEBA cured with DAB containing different amounts of methylene chloride.

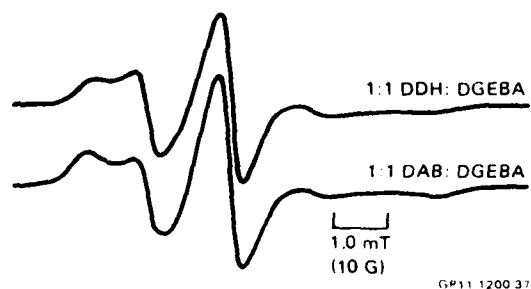


Figure 35. EPR spectra of TANOL in samples of DGEBA cured with DAB and DDH containing the same amounts of methylene chloride (19.5 wt%).

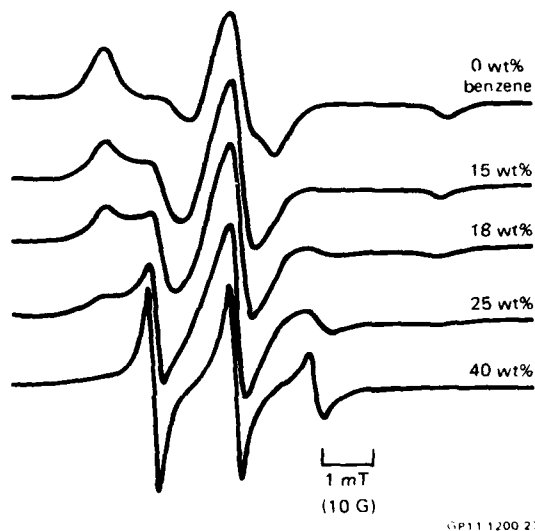


Figure 36. EPR lineshapes of TANOL in the 1:1 DDH/DGEBA sample as a function of benzene content.

The spectra of TANOL in the DGEBA samples cured with different crosslink densities show the same feature on increasing the solvent content, viz., the amount of fast phase increases with increasing solvent content.

The data plotted in Figure 38 show that for TANOL in all the amine-cured epoxy samples studied, the fractional amount of fast phase is linearly dependent on solvent content for 5 to 30 wt% solvent. At a given solvent content, the fast-phase fraction decreases slightly with crosslink density, but considering the uncertainty in the measurement this difference is small.

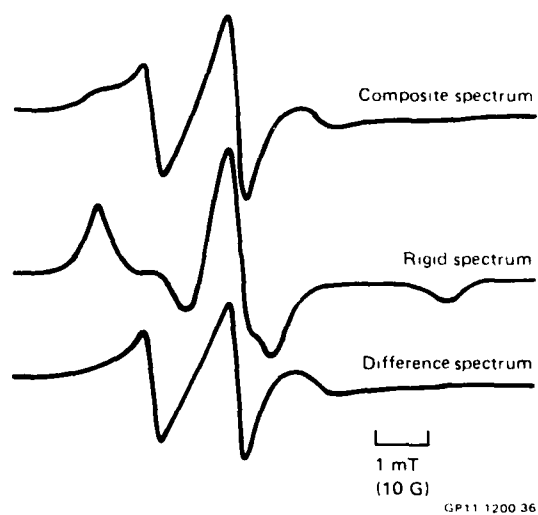


Figure 37. Typical examples of composite spectrum, unscaled rigid spectrum, and the resulting difference (mobile phase). Spectrum observed in the solvent plasticizing experiments.

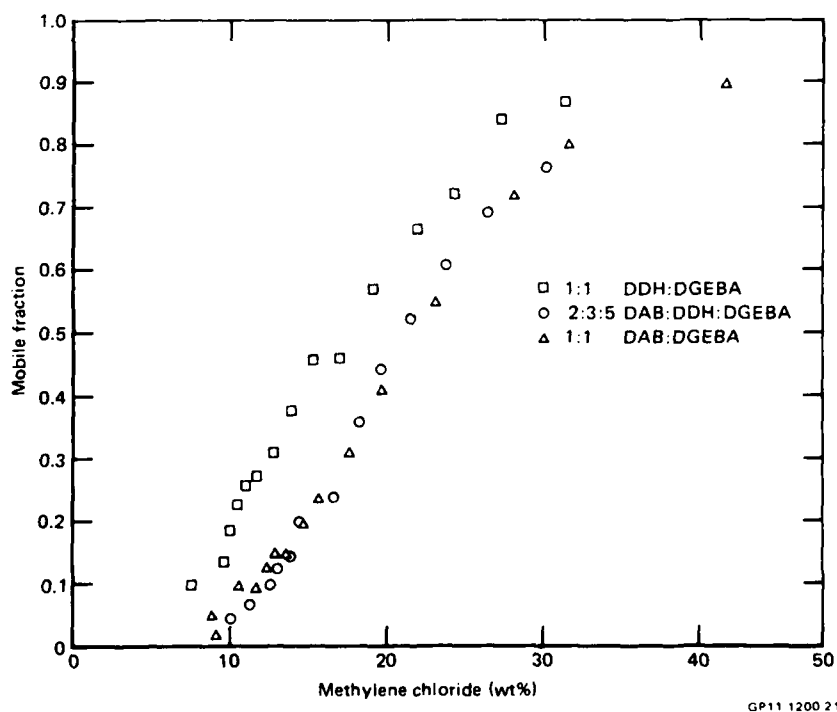


Figure 38. Plot of mobile fraction for TANOL in the amine-cured samples of DGEBA with the stoichiometries indicated.

2.3 Determination of the Number of Unreacted Epoxide Groups

In this task we devised the methodology of using the spin-probe/spin-label EPR technique to determine the number of unreacted epoxy groups in an amine-cured epoxy sample. The idea was to introduce nitroxide amine spin probes into a plasticized sample of the cured polymer for a long enough period to allow them to react with the unreacted epoxide rings and to bind into the polymer network. Unreacted nitroxide spin probe was then to be removed by successive washes of the sample. The spin count determined from the area under the EPR lineshape of the dry samples would then give the number of unreacted epoxide groups.

The epoxy system investigated was DGEBA cured with stoichiometric amounts of DDH, i.e., DGEBA:DDH = 1:1. Samples were immersed in a benzene solution of TAMIN for four weeks. The sample was then washed continuously with a Soxhlet extractor for several days. These procedures were repeated with identical DGEBA/DDH samples in solutions of METAMIN, DIMETAMIN, and TANOL in benzene (the sample containing METAMIN was rinsed only about 20 h). The number of unreacted epoxy groups found are shown in Table 3.

As expected, the nonreactive spin probe TANOL is removed completely from the washed epoxy, and the number of unreacted epoxy groups is approximately the same using either TAMIN or METAMIN. It is surprising, however, that DIMETAMIN should be so unreactive over a period of one month considering that it has been shown (Section 2.1) to have the same reactivity as METAMIN in the uncured DGEBA resin. This result suggests that the unreacted groups are trapped in regions of high crosslink density and the larger spin probe DIMETAMIN penetrates into these regions more slowly than TAMIN or METAMIN.

TABLE 3. AMOUNT OF UNREACTED EPOXY GROUPS IN A CURED SAMPLE WITH STOICHIOMETRY DGEBA:DDH = 1:1.

Nitroxide used	Amount of unreacted epoxy (%)
TANOL	0.001
TAMIN	0.16
METAMIN	0.11
DIMETAMIN	0.01

GP11 1200 80

Alternatively, since the epoxy groups are bound in the polymer lattice, the reactions with the nitroxide amines will have a heterogeneous nature. The rates for the different nitroxide amines then need not be the same.

The attractive feature of this method of using nitroxide amines to determine the number of unreacted epoxy groups in a cured epoxy sample is the inherent sensitivity. Thus, our estimates of the minimum detectable amount of unreacted epoxy groups is $10^{-3}\%$. The disadvantage of this method is the uncertainty of the nitroxide amine reacting with all unreacted epoxy groups in the sample. The latter is either a consequence of the slow diffusion rates of the nitroxide amines into the cured epoxy samples or the slow reaction rates of the nitroxide amines with the epoxy groups in the polymer.

2.4 Discussion of EPR Results

In many previous studies^{17,18} of amine-epoxy reactions, second-order kinetics were observed and details of the stereochemistry of the ring opening reactions were studied. The results indicated that an S_N2 mechanism was followed. In our studies of the reaction between nitroxide amines and DGEBA, pseudo-first-order reaction kinetics are obeyed because the amine concentrations are so low (< 0.1 wt%) that the DGEBA concentration effectively remains constant throughout the reaction (see Appendix A). It is surprising, however, that the rates for METAMIN and DIMETAMIN should have the same activation energy and frequency factor. One would expect these rates to differ if the difference between the nucleophilic character of these amines is large enough. Since basicity is a measure of nucleophilic character, the basicities of METAMIN and DIMETAMIN were measured from the pH values of their aqueous solutions. The results show that $K_b = 10^{-6}$ mole \cdot L $^{-1}$ for DIMETAMIN and $K_b = 3 \times 10^{-7}$ mole \cdot L $^{-1}$ for METAMIN. Thus, a factor of three difference in basicity is not large enough to effect an observable difference in the reaction rates.

It is well established^{17,19,20} that amine-epoxy reaction rates can be accelerated in solvents that can hydrogen bond with either the epoxy or the amine, e.g., water, alcohols, or acids. The rate-determining steps in such reactions involve transition states of the form shown in Figure 39. Our results support this contention in that the equality of the rate constants k_1 and k_2 implies that hydrogen displacement rates are fast and do not determine the overall rates of the reactions.

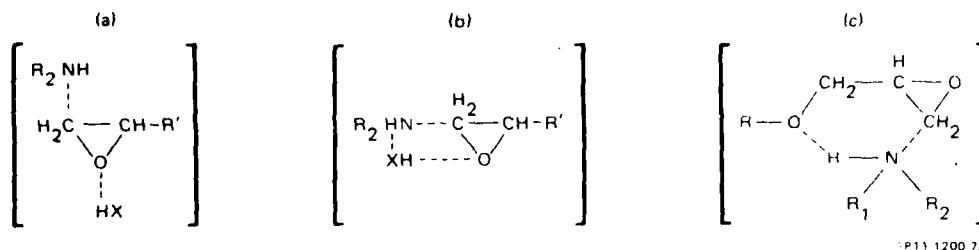


Figure 39. Proposed transition states involved in amine-epoxy curing reactions for the (a) Smith model, (b) Mika and Tanaka model, and (c) model proposed in Reference 21.

In the nitroxide amine reactions with DGEBA, the impurities in the DER 332 resin may play the role of the hydrogen-bond donors. Two such impurities can be present: water and a DGEBA dimer containing a hydroxyl group. Both nitroxides will form transition states of the type (a) shown in Figure 39, but only METAMIN can form the type (b) since DIMETAMIN is a tertiary amine and hence possesses no hydrogen-bond donors. Thus, if we are to account for the equality of the reaction rate constants k_1 and k_2 , we must conclude that only the transition states of the form (a) shown in Figure 39 are relevant.

The effect of hydrogen bonding to the oxygen in the oxirane ring is to weaken the C-O bonds. This weakening may be of paramount importance. It has even been suggested by some investigators^{19,20} that in the absence of hydrogen bonding as in the pure nonpolar solvents, the overall rates for amine-epoxy reactions are negligible.

The rate-determining step in the reactions of the nitroxide amines with DGEBA is the charge separation following the formation of the transition state of the form (a) in Figure 39.^{19,20} At this time the only explanation we offer for the equality of the rates of charge separation of the transition states involving DIMETAMIN and METAMIN is the following. Solvation effects of the surrounding DGEBA molecules reduce (1) the effects resulting from any difference in the steric factors which may exist in the transition state and also (2) the effects of the differences in the nucleophilic character of the nitroxide amines.

It has also been shown²¹ that the oxygen in the diglycidyl ether group can hydrogen bond to an amine hydrogen so that the amine is held in a suitable

position to attack the epoxide group (see Figure 39c). However, this effect should play no role in determining the value of the rate constant k_2 since DIMETAMIN possesses no hydrogen-bond donors.

Our investigations have shown that fast rotational nitroxide motions ($\tau_c < 3 \times 10^{-9}$ s) usually occur at temperatures above T_g of the host polymer. Moreover, we have found that in this fast-motion region, the motional correlation time for the nitroxide spin probe TANOL in several amine-cured epoxy samples obeys a modified form of the WLF equation.¹⁵ This agreement implies that the TANOL rotational motions depend on the free volume in the epoxy polymers. It is therefore not surprising to find, as shown in Figures 23 and 26, that the motional correlation times for TANOL depend on the average crosslink density since higher crosslink densities mean a higher value of T_g , which in turn means less free volume at any temperature above T_g .

At all temperatures, the EPR spectra of TANOL in these dry amine-cured epoxy samples can be characterized by one motional correlation time. Thus, the spectra give no indication of distributions in motional correlation time or crosslink density within a sample. In contrast, the solvent-dependent studies provide information on the distribution of crosslink density in a given sample. The mobile fractions in Figure 38 (given by the ratio of the areas under the fast-phase absorption spectra to those under the composite spectra) is considered to be a measure of the amount of rubbery regions present in the polymer. In a previous study,⁹ we concluded that the plasticizing solvent preferentially partitions into the low crosslink regions. As a result, the low crosslink regions having the greatest free volume in the dry polymer have even greater free volume content following addition of the solvent. The overall effect of the solvent plasticizer is to emphasize differences in rigidity and spin-probe rotational mobility so that microstructural differences in crosslink density will appear on varying the solvent content even when they are not observed in the dry samples on varying the temperature. Figure 38 also indicates that there is relatively little difference in the solvent dependence of the EPR spectra of TANOL in samples with different average crosslink densities.

3. NMR EXPERIMENTS ON EPOXY RESINS

3.1 Epoxy/Amine Reaction Kinetics

The purpose of this study was to perform epoxy/amine reactions and follow their progress through the gel stage using solid-state ^{13}C NMR with magic-angle spinning, cross-polarization, and high-power hydrogen decoupling.²²⁻²⁴ It was planned to follow the progress of the reaction quantitatively by measuring the decrease in the areas beneath the spectral lines of the reactants as they were consumed and measuring the increase in the areas beneath the spectral lines of the products as they were formed. As a basis for this study, simpler-solution NMR experiments were performed first to positively identify the spectral lines. These liquid studies proved to be complicated by the presence of small quantities of impurities (at first undetected) that strongly influenced the kinetics of the reaction. Therefore, model compounds were employed to reduce the number of possible reactions so that the kinetics studies of the DGEBA system could proceed more successfully with the knowledge gained from the simpler systems. The ^{13}C NMR measurements were performed on a spectrometer (JEOL FX-60QS) suitable for both liquid and solid-state studies.

3.1.1 Liquid Studies

The epoxy and amine used in this study were 1,2-epoxy-3-phenoxypropane (EPOP) (Eastman Kodak No. 6377) and N-methylbutylamine (MBA) (Aldrich Chemical No. 16, 212-4), as shown in Figure 40. Both of these were used without further purification. These materials are similar to the DGEBA and DDH used in the other parts of this study except that instead of being difunctional, they are monofunctional. This simplification prevented the production of a variety of large-molecular-weight products, which simplified analysis of the ^{13}C NMR spectra.

The kinetics of the epoxy/amine reaction were studied at 298 K. An excess of MBA was used because it was thought that this would produce a pseudo-first-order reaction, which would be simpler to analyze, and there would be less chance of competing epoxy/epoxy homopolymerization reactions complicating the analysis.

$$\text{CH}_2 - \text{CH} - \text{CH}_2 - \text{O} - \text{C}_6\text{H}_5$$

(EPOP)

$$\text{CH}_3-\text{CH}_2-\text{CH}_2-\text{CH}_2-\text{N} \begin{array}{l} \text{H} \\ \diagup \\ \text{CH}_3 \end{array}$$

(MBA)

JP11 1200 v7

The ^{13}C NMR spectrum of EPOP in CDCl_3 is shown in Figure 41(a). The intensity of the spectral line labeled g is small because the carbon atom producing this line is not adjacent to a hydrogen atom, which causes a reduced nuclear Overhauser enhancement (NOE) as well as an increased spin-lattice relaxation time, T_1 . The three small lines downfield of the line labeled c are solvent lines. The spectrum shown in Figure 41(b) was obtained 55 min after adding 0.386 g of EPOP to 2.327 g of MBA, a molar ratio of 1:9.97. In this spectrum, the lines from EPOP can be identified easily. Because MBA is undiluted, the spectra lines labeled α , β , γ , δ , and ϵ resulting from the MBA carbons are intense, and they have been truncated in all spectra shown in Figure 41. The spectral line downfield of line a, labeled i, is caused by an unidentified impurity in MBA. At 55 min, some product lines can be seen. Because the product lines can result from carbon atoms that have significantly different NOE's and T_1 's from the reactant carbons, the line intensities are not always reliable indicators of the extent of the reaction. In Figure 41(e) the product lines are identified.

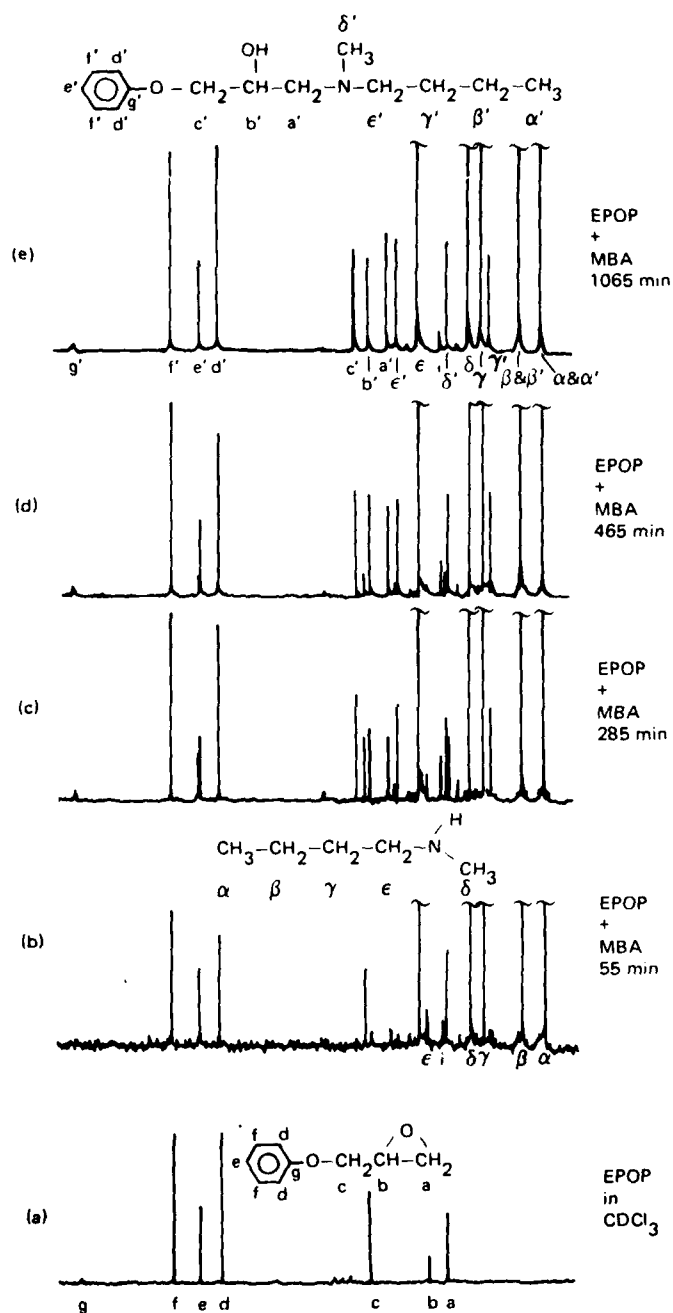


Figure 41. ^{13}C NMR spectra of the epoxy/amine reaction.

The line labeled e results from a carbon atom remote from the reaction site, yet it experienced a small but measureable upfield shift after the reaction. Because the relaxation time of this carbon was not expected to change significantly as a result of the reaction, it was used to determine the extent of the reaction. Figure 41(c), (d), and (e) shows spectral changes resulting from the reaction, and Figure 42(a)-(e) shows details of the spectral shift of the line labeled e. The lines labeled d and f also shift but to a lesser extent, and accurate intensity measurements were not always possible using these lines.

The reactant EPOP concentration (relative to its initial concentration) was determined by dividing the area beneath the downfield line e by the sum of areas of both the upfield and downfield lines e. The results for two similar experiments are shown in Figure 43, where the log of the relative reactant EPOP concentration is plotted as a function of time. In the figure, $[\text{EPOP}]_0$ and $[\text{MBA}]_0$ denote the initial concentrations of EPOP and MBA. The almost linear nature of the data suggests a pseudo-first-order reaction. A pseudo-first-order reaction might be expected for a tenfold excess of amine because if the reaction were actually second-order, then

$$\frac{d[\text{EPOP}]}{dt} = -k_2 [\text{EPOP}] [\text{MBA}] , \quad (8)$$

and if the MBA were in excess so that its concentration could be considered a constant equal to $[\text{MBA}]_0$, then

$$\frac{d[\text{EPOP}]}{dt} = -k_2 [\text{EPOP}] [\text{MBA}]_0 , \quad (9)$$

which is a pseudo-first-order reaction with a solution

$$[\text{EPOP}] = [\text{EPOP}]_0 e^{-k_2 [\text{MBA}]_0 t} . \quad (10)$$

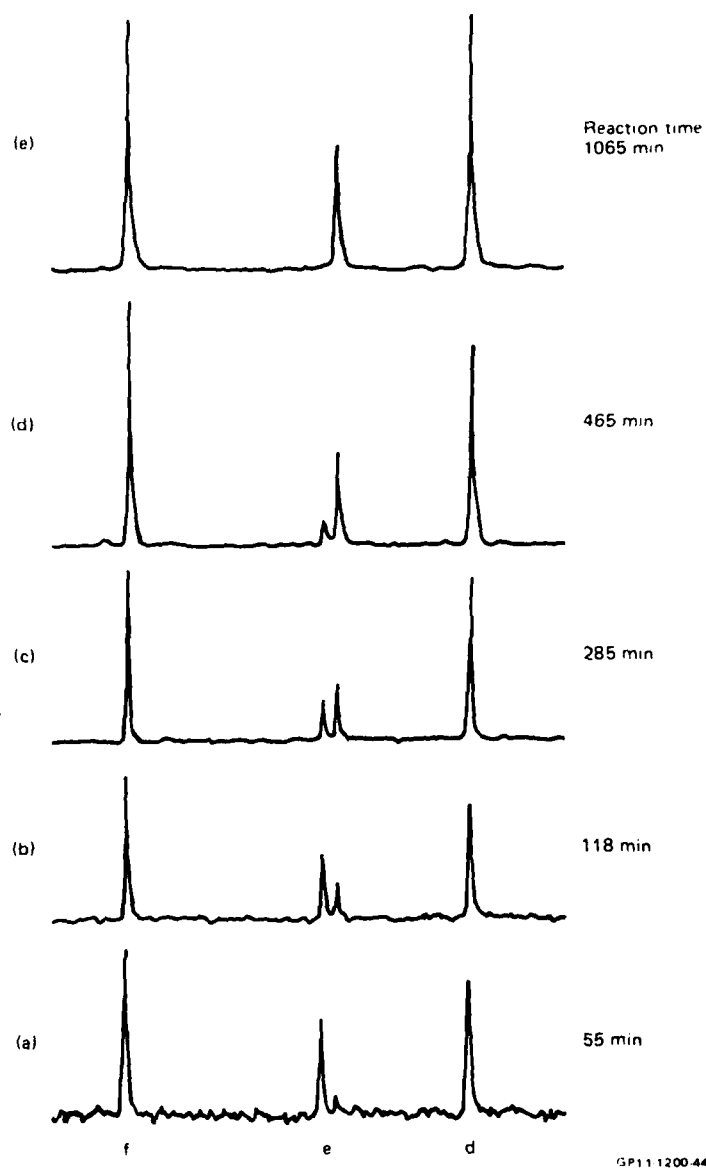


Figure 42. Aromatic ^{13}C spectra of epoxy/amine reaction.

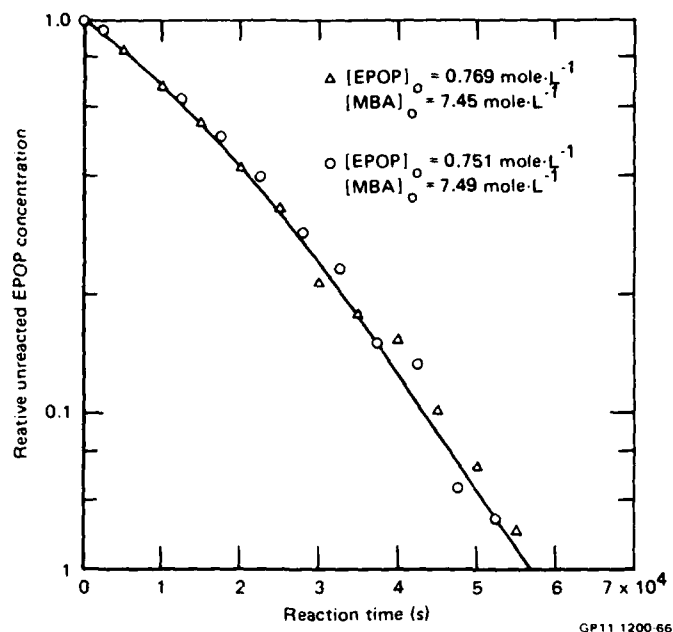


Figure 43. Kinetics for the reaction of approximately 1:9.8 mole mixtures of EPOP:MBA. The solid line is predicted using $k[\text{HX}]_0 = 4.2 \times 10^{-6} \text{ L} \cdot \text{mole}^{-1} \text{ s}^{-1}$ and $k' = 8 \times 10^{-6} \text{ L}^2 \cdot \text{mole}^{-2} \text{ s}^{-1}$.

Under these conditions the logarithm of the relative EPOP concentration plotted as a function of time would be linear with a slope of $-k_2[\text{MBA}]_0 \log e$. But the data points bend downward indicating a greater-than-expected reaction rate with an increase in time rather than a smaller-than-expected reaction rate as a result of the decrease in $[\text{MBA}]$ as the reaction proceeded. Even though there is scatter in the data, both experiments support the conclusion that the data points bend downward. This result indicates that the product in some way acts to increase the rate of reaction, i.e., the reaction is autocatalytic.

To understand the kinetics of this reaction, it was necessary to perform several experiments in which the initial conditions were varied to provide linearly independent data. Figure 44 shows the results of an experiment in which $[\text{EPOP}]_0$ was decreased by almost a factor of two from that shown in Figure 43, but $[\text{MBA}]_0$ was about the same. If Equations (8)-(10) were correct, the slope of the lines through the data points in Figures 43 and 44 would be the same, but they are different. If the difference is the result of an autocatalytic reaction, then before much of the product was formed, near $t = 0$, the slopes should be the same, but they are not. These results suggested the presence of another reactant participating in the reaction, perhaps an impurity.

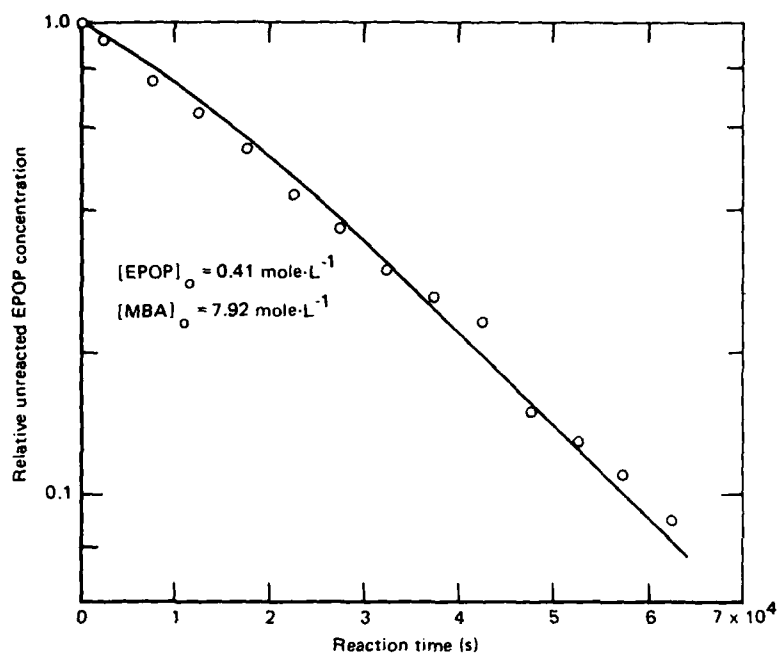
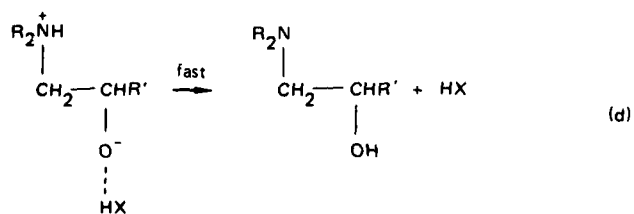
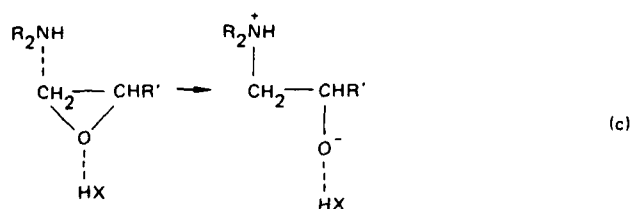
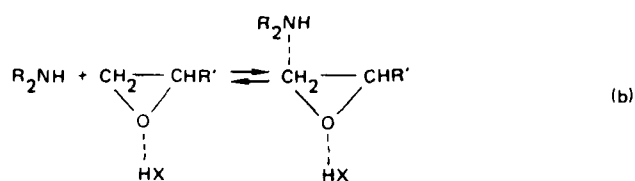
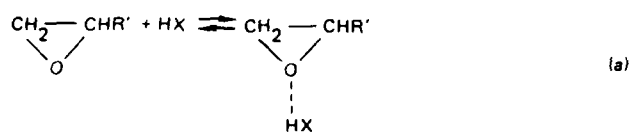


Figure 44. Kinetics for the reaction of a 1:19.3 mole mixture of EPOP:MBA. The solid line is predicted using $k[\text{HX}]_0 = 3.4 \times 10^{-6} \text{ L} \cdot \text{mole}^{-1} \text{ s}^{-1}$ and $k' = 8 \times 10^{-6} \text{ L}^2 \cdot \text{mole}^{-2} \text{ s}^{-1}$.

The kinetics equation that was able to describe these results, and the results that follow, is

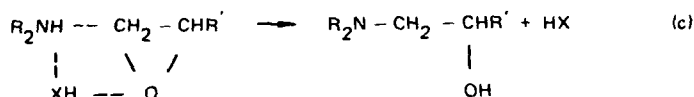
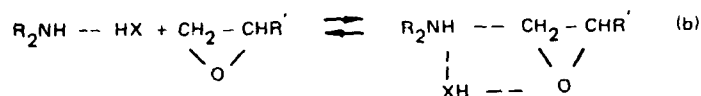
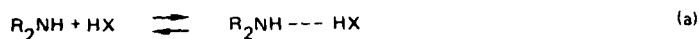
$$\frac{d[P]}{dt} = ([\text{EPOP}]_0 - [P]) ([\text{MBA}]_0 - [P]) (k[\text{HX}]_0 + k'[P]), \quad (11)$$

where $[\text{HX}]_0$ is the concentration of a hydrogen-bond donor (an impurity in EPOP and/or MBA), $[P]$ is the concentration of the product of the epoxy/amine reaction, which is also a hydrogen-bond donor because of the pendant OH on the product, and k and k' are the rate constants for the reactions involving the hydrogen-bond donor HX and the hydrogen-bond donor P, respectively. Equation (11) is applicable to two different mechanisms that have been proposed for the epoxy/amine reaction, provided the appropriate steps in the reaction mechanisms are rate controlling. The first mechanism, shown in Figure 45, was proposed by Smith,¹⁷ and the second mechanism, shown in Figure 46, was proposed by Tanaka and Mika.¹⁹



GP11-1200-82

Figure 45. Smith mechanism involving hydrogen bonding to the epoxy.



GP11 1200-63

Figure 46. Mika and Tanaka mechanism involving hydrogen bonding to the amine.

The solution to Equation (11) is given by¹⁷

$$\begin{aligned} \tau = & \frac{\ln \{ ([EPOP]_0 - [P]) / [EPOP]_0 \}}{(k[HX]_0 + k'[EPOP]_0)([EPOP]_0 - [MBA]_0)} \\ & - \frac{\ln \{ ([MBA]_0 - [P]) / [MBA]_0 \}}{(k[HX]_0 + k'[MBA]_0)([EPOP]_0 - [MBA]_0)} \\ & + \frac{k' \ln \{ (k[HX]_0 + k'[P]) / k[HX]_0 \}}{(k[HX]_0 + k'[EPOP]_0)(k[HX]_0 + k'[MBA]_0)} \quad (12) \end{aligned}$$

This equation was fit to the experimental results to determine $k[HX]_0$ and k' . The rate constant k' was expected to be the same for all experiments. Because $[HX]_0$ was not known, only the product $k[HX]_0$ could be determined, and because HX could be present in both EPOP and MBA in different concentrations, $k[HX]_0$ was not expected to be constant for all experiments.

The solid lines in Figures 43 and 44 are best fits of Equation (12) to the data using a value of $k' = 8 \times 10^{-6} \text{ L}^2 \text{ mole}^{-2} \text{ s}^{-1}$, which was used to fit all experimental data, more of which is shown in Figures 47-51. Figure 47

shows the reaction of a neat mixture containing more EPOP than used in the experiments shown in Figure 43 and 44. Since the product concentration in this experiment increased to larger values than it did for the experiments shown in Figures 43 and 44, the autocatalytic effect (the $k'[P]$ term in Equation (11)) is more pronounced, as shown by the greater downward curvature of the data.

Figures 48 and 49 show the reactions for two different concentrations of EPOP and MBA, but in both these cases, the MBA was dried before it was mixed with the EPOP by subjecting the MBA to a molecular sieve, (4A pore size, Davison Chemical). Comparing Figures 43 and 48, which present results of identical experiments except for drying the MBA, shows that the drying caused a reduction in the reaction rate with a resulting smaller value for $k[HX]_0$.

Figures 50 and 51 show the results of diluting the reactants in deuterated cyclohexane (C_6D_{12}). Because the concentrations of the reactants were reduced by dilution, the rates of the reactions were reduced significantly. The increased scatter in these data is a result of the smaller ^{13}C NMR signal in these dilute samples.

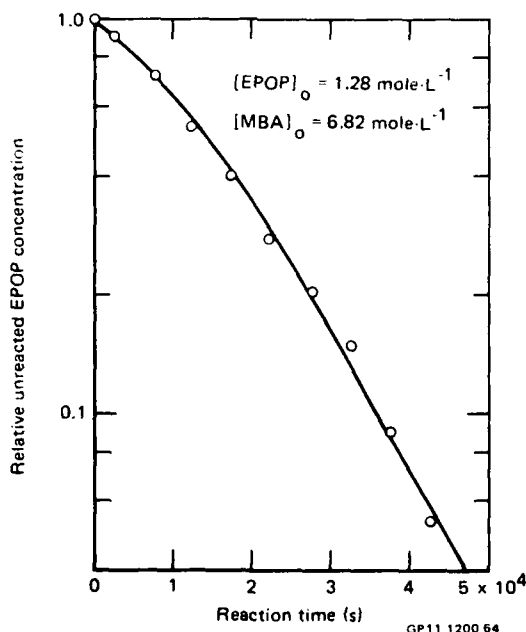


Figure 47. Kinetics for the reaction of a 1:5.3 mole neat mixture of EPOP:MBA. The solid line is predicted using $k[HX]_0 = 5 \times 10^{-6} \text{ L} \cdot \text{mole}^{-1} \text{ s}^{-1}$ and $k' = 8 \times 10^{-6} \text{ L}^2 \cdot \text{mole}^{-2} \text{ s}^{-1}$.

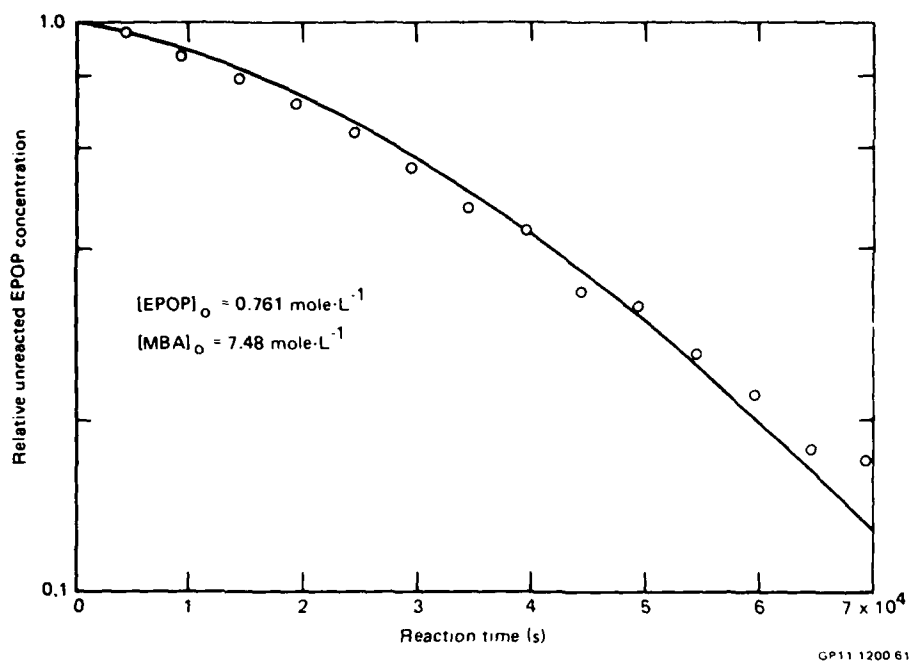


Figure 48. Kinetics for the reaction of a 1:9.8 mole mixture of EPOP:MBA. The MBA had been dried with molecular sieve 4A. The solid line is predicted using $k[\text{HX}]_0 = 1.3 \times 10^{-6} \text{ L}\cdot\text{mole}^{-1}\text{s}^{-1}$ and $k' = 8 \times 10^{-6} \text{ L}^2\cdot\text{mole}^{-2}\text{s}^{-1}$.

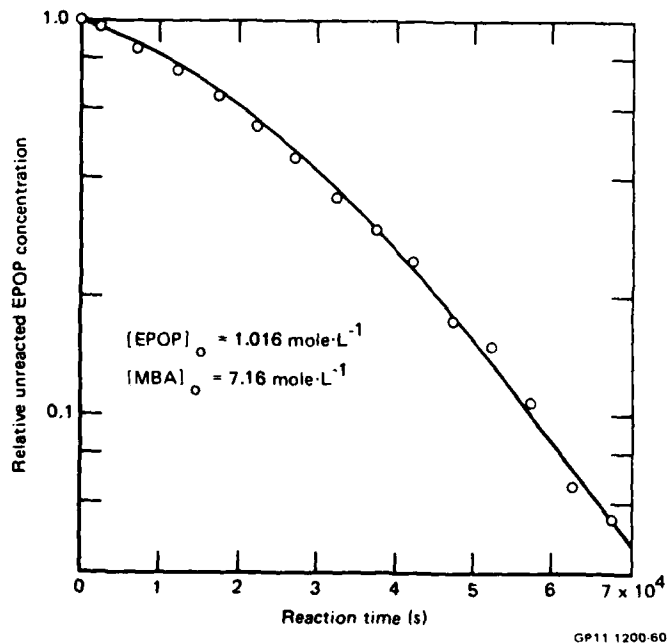


Figure 49. Kinetics for the reaction of a 1:7.04 mole mixture of EPOP:MBA. The MBA had been dried with molecular sieve 4A. The solid line is predicted using $k[\text{HX}]_0 = 2.0 \times 10^{-6} \text{ L}\cdot\text{mole}^{-1}\text{s}^{-1}$ and $k' = 8 \times 10^{-6} \text{ L}^2\cdot\text{mole}^{-2}\text{s}^{-1}$.

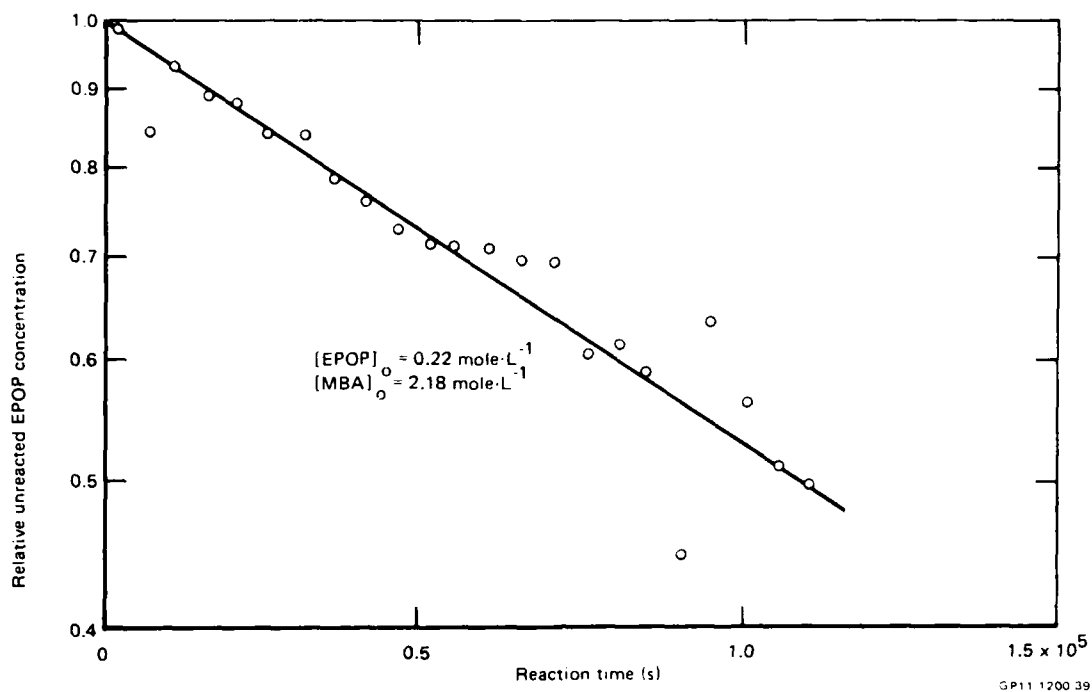


Figure 50. Kinetics for the reaction of a 1:9.9 mole mixture of EPOP:MBA diluted with C_6D_{12} to 0.29 of the neat concentration. The solid line is predicted using $k[HX]_0 = 2.4 \times 10^{-6} \text{ L} \cdot \text{mole}^{-1} \text{ s}^{-1}$ and $k' = 8 \times 10^{-6} \text{ L}^2 \cdot \text{mole}^{-2} \text{ s}^{-1}$.

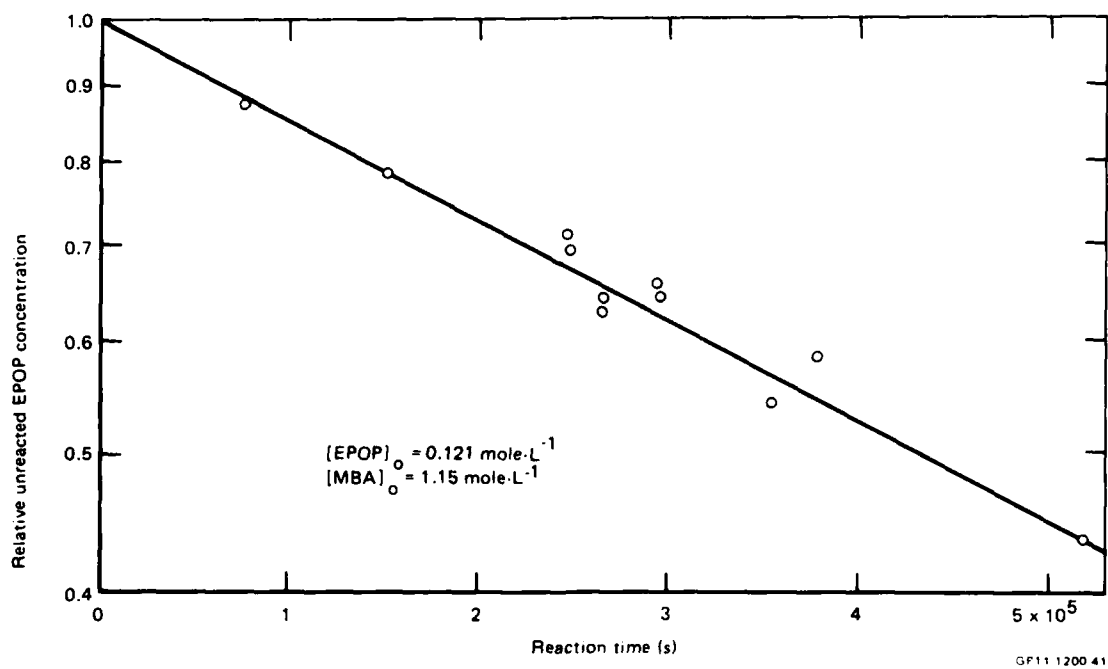


Figure 51. Kinetics for the reaction of a 1:9.5 mole mixture of EPOP:MBA diluted with C_6D_{12} to 0.15 of the neat concentration. The solid line is predicted using $k[HX]_0 = 1.2 \times 10^{-6} \text{ L} \cdot \text{mole}^{-1} \text{ s}^{-1}$ and $k' = 8 \times 10^{-6} \text{ L}^2 \cdot \text{mole}^{-2} \text{ s}^{-1}$.

In an effort to determine the source of the hydrogen-bond donor HX leading to the term $k[\text{HX}]_0$, it was assumed that both the EPOP and MBA contained HX impurities. As a result, it was assumed that $k[\text{HX}]_0$ could be given by a linear combination of the initial EPOP and MBA concentrations, viz.,

$$k[\text{HX}]_0 = A[\text{MBA}]_0 + B[\text{EPOP}]_0. \quad (13)$$

This equation is rewritten in the form $y = ax + b$ by dividing both sides by $[\text{EPOP}]_0$ to yield

$$\frac{k[\text{HX}]_0}{[\text{EPOP}]_0} = A \frac{[\text{MBA}]_0}{[\text{EPOP}]_0} + B. \quad (14)$$

The experimental data, tabulated in Table 4, are plotted in Figure 52 in the form of Equation (14) to determine A and B. The nine points in Figure 52 do not fall on a straight line, but this discrepancy is easily explained. The three points denoted by squares are for experiments in which the MBA was dried; thus, if the molecular sieve removed the water or low-molecular-weight hydrogen-bond donor in the MBA, the MBA for these three experiments would not have contributed to $k[\text{HX}]_0$. This lack of contribution to $k[\text{HX}]_0$ for these three experiments requires setting the $A[\text{MBA}]_0/[\text{EPOP}]_0$ term in Equation (14) to zero, or equivalently shifting the three square points in Figure 52 horizontally left to $[\text{MBA}]_0/[\text{EPOP}]_0 = 0$. The result of this shift can be visualized to fall close to the straight line drawn through the four other points denoted by triangles. The two points denoted by circles are for the mixtures diluted with C_6D_{12} and do not correctly belong to this analysis because the C_6D_{12} may also contain HX, or the C_6D_{12} may alter the reaction mechanisms slightly; therefore these two points are neglected. The straight line shown in Figure 52 is a least-squares fit to the data with the three square points shifted to the left. The least-squares fit yielded $A = 0.34 \times 10^{-6} \text{ L}^2 \text{ mole}^{-1} \text{ s}^{-1}$ and $B = 1.97 \times 10^{-6} \text{ L}^2 \text{ mole}^{-1} \text{ s}^{-1}$. Table 4 compares the values of $k[\text{HX}]_0$ determined from the experiments with those determined using these values of A and B in Equation (14). The agreement for the neat mixtures is excellent and shows that the source of the hydrogen-bond donors HX has been quantitatively determined from these experiments.

TABLE 4. VERIFICATION OF THE SOURCE OF THE HYDROGEN-BOND DONORS CONTRIBUTING TO THE TERM $k[\text{HX}]_0$.

Type of mixture	$[\text{MBA}]_0$ (mole·L ⁻¹)	$[\text{EPOP}]_0$ (mole·L ⁻¹)	$\frac{[\text{MBA}]_0}{[\text{EPOP}]_0}$	Calculated contribution to $k[\text{HX}]_0$ ($\mu\text{L}\cdot\text{mole}^{-1}\cdot\text{s}^{-1}$) [*]			Experimentally determined $k[\text{HX}]_0$ ($\mu\text{L}\cdot\text{mole}^{-1}\cdot\text{s}^{-1}$)
				$A[\text{MBA}]_0$	$B[\text{EPOP}]_0$	$A[\text{MBA}]_0 + B[\text{EPOP}]_0$	
Neat	6.82	1.280	5.33	2.32	2.52	4.82	5.0
Neat	7.45	0.769	9.69	2.53	1.52	4.05	4.2
Neat	7.49	0.751	9.97	2.55	1.48	4.03	4.2
Neat	7.92	0.410	19.32	2.69	0.81	3.50	3.4
Neat, dry MBA	7.16	1.016	7.04	2.43**	2.00	2.00***	2.0
Neat, dry MBA	7.48	0.761	9.83	2.54**	1.50	1.50***	1.3
Neat, dry MBA	7.52	0.724	10.39	2.56**	1.40	1.40***	1.4
C ₆ D ₁₂ solution	2.18	0.220	9.91	0.74	0.43	1.17	2.4
C ₆ D ₁₂ solution	1.15	0.121	9.50	0.39	0.24	0.63	1.2

^{*} $A = 0.340 \times 10^6 \text{ L}^2 \text{ mole}^{-1} \text{ s}^{-1}$ and $B = 1.97 \times 10^6 \text{ L}^2 \text{ mole}^{-2} \text{ s}^{-1}$

^{**} Should be replaced by zero if the molecular sieve removed the hydrogen-bond donors, HX.

^{***} Excludes contribution from dry MBA.

GP11 1200 85

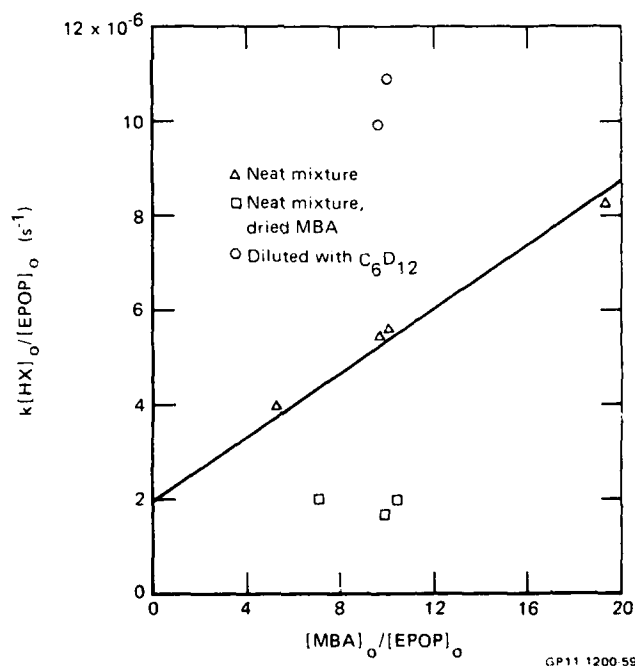


Figure 52. Identification of the sources of the hydrogen-bond donors contributing to the term $k[\text{HX}]_0$. The solid line is the least squares fit to the data for the neat mixtures after moving the three \square points left to the ordinate; see text.

3.1.2 Solid Studies

Solid-state ^{13}C NMR using magic-angle spinning, cross-polarization, and high-power decoupling was used to obtain high-resolution spectra of epoxy/amine samples undergoing reactions past the gel stage. Because of the large amount of time consumed in the liquid studies, the solid studies were not pursued past the preliminary experiment stage. Figure 53 is included as an example of the high-resolution ^{13}C NMR spectrum of a 5:0:5 DAB:DDH:DGEBA sample that was obtained in the preliminary experiments to determine optimum spectrometer parameters.

3.2 Crosslink Structure Studies

In previous NMR studies of crosslinked epoxy polymers,^{9,10} it was observed that as the temperature was increased, the hydrogen spin-spin relaxation time, T_2 , increased only slightly until a certain temperature region was reached where T_2 increased to a significantly larger value, denoted as the high-temperature plateau value of T_2 . The temperature at which the increase occurred was related to the glass-transition temperature, and the value of T_2 at the high-temperature plateau appeared to be related to the crosslink density of the epoxy; smaller values of T_2 at the plateau occurred for epoxies suspected of being more highly crosslinked. These results were tentatively explained as the result of less complete averaging of spin-spin interactions caused by the larger number of crosslinks, which prevented complete isotropic

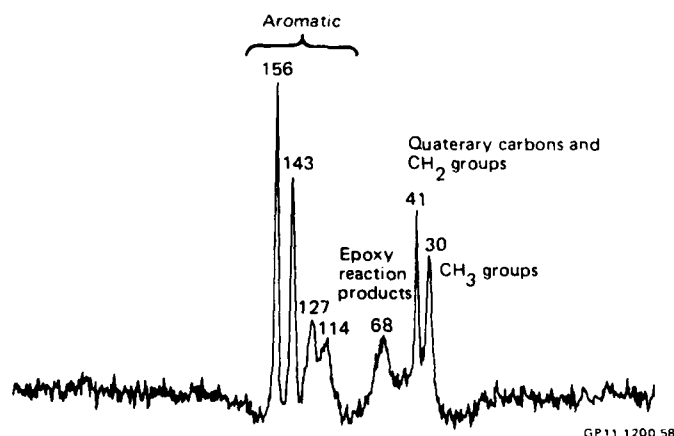


Figure 53. ^{13}C NMR spectrum of a solid 5:0:5 DAB:DDH:DGEBA sample. The resonances are identified in ppm relative to TMS, assuming the methyl resonance is at 30 ppm.

molecular motion. Similarly, it had been observed^{9,10} that sorbed solvents in crosslinked epoxy polymers produced increased molecular motion with an attending increase in the spin-spin relaxation time T_2 , and the increase in T_2 appeared to be less for those epoxies suspected of being more highly crosslinked.

The purpose of this study was to prepare a variety of epoxy polymers having quantifiably different crosslink densities and subject them to temperature-dependent and solvent-dependent NMR measurements to determine how T_2 is related to crosslink density.

3.2.1 NMR Sample Preparation

Samples of DGEBA were room-temperature cured with stoichiometric amounts of six different mixtures of a tetrafunctional amine, 1,4-diaminobutane (DAB) and a difunctional amine, N,N-dimethyl-1,6-diaminohexane (DDH), as shown in Figure 1. These samples are denoted as X:Y:Z where X refers to the equivalents of DAB, Y refers to the equivalents of DDH, and Z refers to the equivalents of DGEBA used in the mixture. In these experiments all samples were made from stoichiometric mixtures of amines and epoxy, so that $X + Y = Z$. The DAB:DDH:DGEBA samples studied were 0:5:5, 1:4:5, 2:3:5, 3:2:5, 4:1:5, and 5:0:5. Because of the functionalities of the amines, the 0:5:5 sample had the lowest crosslink density, and the 5:0:5 sample had the largest crosslink density.

3.2.2 NMR Measurements

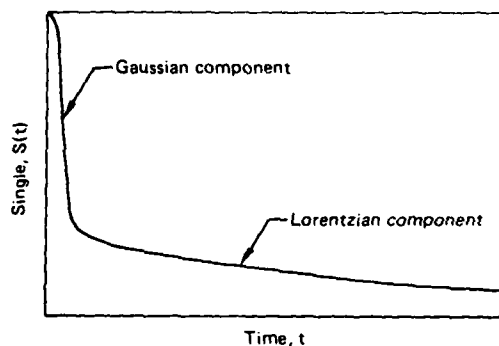
Pulsed hydrogen NMR measurements were performed on a variable-temperature single-coil spectrometer operating at 100 MHz. The signal from an external fluorine sample at 94 MHz was used to stabilize the magnetic field so that small signals could be signal-averaged without the attendant drift. A transient recorder (Biomotion 826) was used to collect the data, and a micro-computer (Digital Equipment Corporation MINC) was used to perform signal averaging, data storage, and analysis.

Three different types of pulsed NMR experiments were performed: 1) a single 90° pulse experiment to determine the relative amounts of rigid and mobile phases and their spin-spin relaxation times T_2 ,²⁵ 2) a 180° , τ , 90° pulse experiment to determine the spin-lattice relaxation times T_1 ,²⁵ and 3) a

90° , τ , 180° pulse experiment to more accurately measure long spin-spin relaxation times T_2 .²⁵

3.2.3 Characteristics of NMR Signals from Crosslinked Epoxies

The free-induction decay signal from a crosslinked epoxy sample contains two components, as shown in Figure 54. The computer performs a least-squares fit to the free-induction decay signal to determine five parameters A_G , T_{2G} , n , A_L , and T_{2L} . Unplasticized epoxy resins at room temperature generally contain a true Gaussian component, i.e., $n = 2$. In general the Gaussian component results from hydrogen in molecules that are rigid, and the Lorentzian component results from hydrogen in molecules that are undergoing extensive, liquid-like motion. Thus, the Gaussian component results from the rigid polymer below its glass transition temperature, and the Lorentzian component results from sorbed solvents, plasticized polymer, or polymer above its glass transition temperature. The Gaussian amplitude, A_G , and the Lorentzian amplitude, A_L , are proportional to the number of hydrogens in the rigid and mobile portions of the polymer, respectively.



$$\text{Signal} = \text{Gaussian component (rigid)} + \text{Lorentzian component (mobile)}$$

$$S(t) = A_G \exp \left\{ - (t/T_{2G})^n \right\} + A_L \exp \left\{ - t/T_{2L} \right\}$$

GP11-1200-86

Figure 54. Hydrogen NMR free-induction decay signal.

3.2.4 Temperature-Dependent Studies

Temperature-dependent NMR studies were performed on the six different DAB:DDH:DGEBA samples from 295 K to 510 K. The temperature dependence of the Lorentzian and Gaussian spin-spin relaxation times T_{2L} and T_{2G} and the Lorentzian fraction F_L ($F_L = A_L/(A_L + A_G)$) of the six samples are shown in Figures 55, 56, and 57 respectively. In Figure 56 the dominant T_{2L} is plotted instead of T_{2G} for those temperatures at which the signal is totally Lorentzian (although it may contain two Lorentzian components). The increase in the T_2 's and F_L 's with increasing temperature is explained as follows. The spin-spin relaxation time T_2 is governed by magnetic dipole-dipole interactions between neighboring hydrogen spins, and the sign and magnitude of this magnetic dipole-dipole interaction is dependent upon the relative positions of the hydrogens and the relative directions in which the spins are aligned. In the absence of significant motion, this dipolar interaction causes the NMR

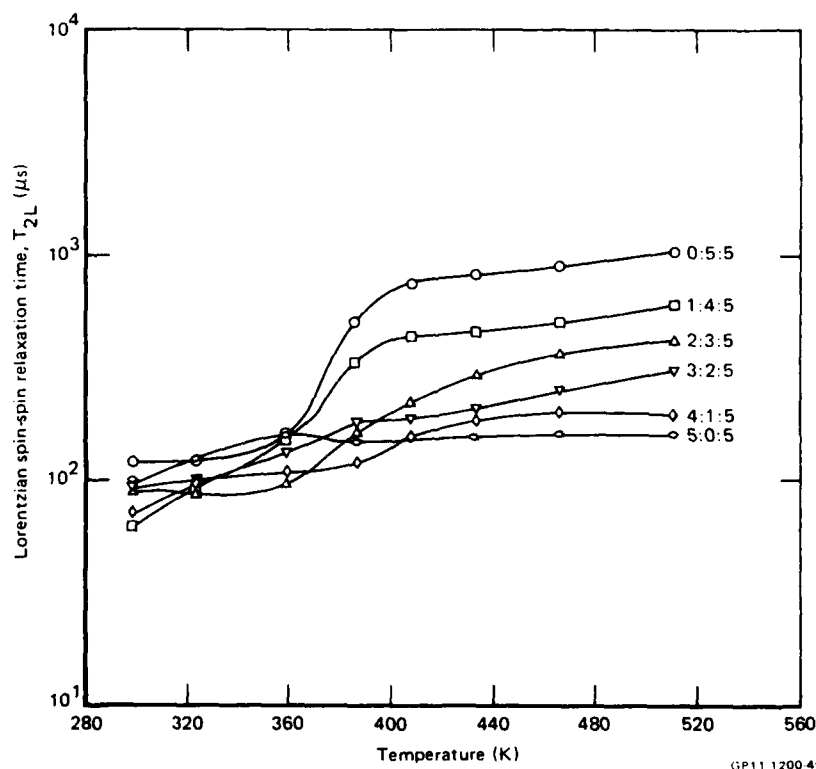


Figure 55. Temperature dependence of Lorentzian spin-spin relaxation time for DAB:DDH:DGEBA samples.

signal to be Gaussian. If one hydrogen moves isotropically relative to another within a time period that is short compared with the time required for the two hydrogen spins to interact (this time is approximately equal to the spin-spin relaxation time T_2 in the absence of motion), then the coupling fluctuates in sign and magnitude so that its average value is reduced and T_2 increases. Thus, an increase in T_2 with increasing temperature is an indication of the onset of a molecular motion with a correlation time about equal to the value of T_2 just before the onset of the molecular motion. If this motion is not completely isotropic, as a result of steric effects, chain entanglements, or crosslinks, or if only a few molecular groups in the polymer participate in the motion, the increase in T_2 will cease and a plateau will be reached. At higher temperatures other molecular groups may experience an onset of rapid motion, or the molecular groups already in motion may become less restricted and experience a more isotropic motion, thus producing a series of increases and plateaus in the temperature dependence of T_2 .

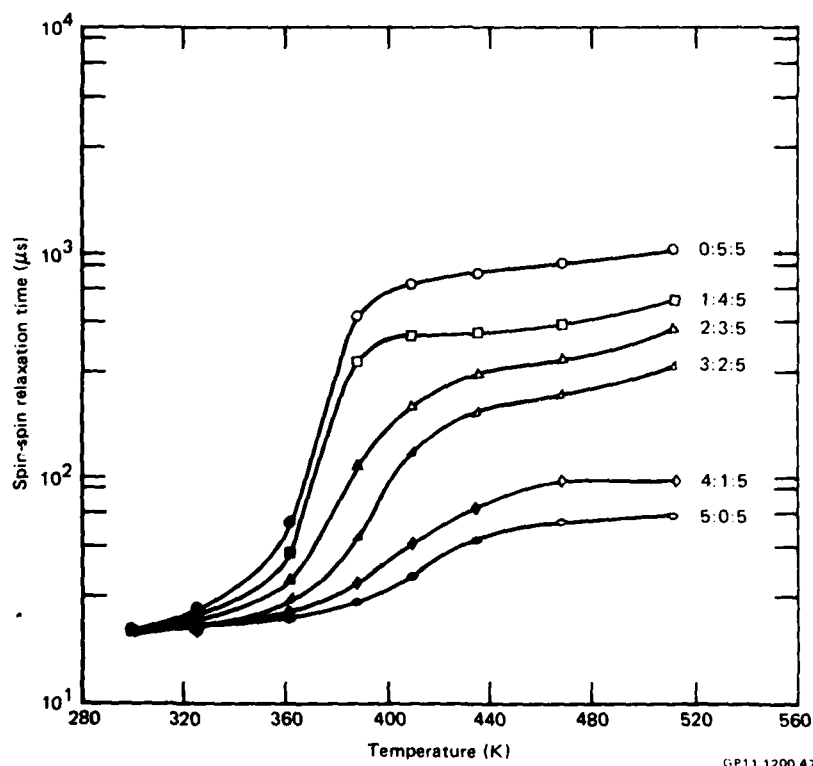


Figure 56. Temperature dependence of spin-spin relaxation times for DAB:DDH:DGEBA samples. The solid symbols are the Gaussian values, and the open symbols are the Lorentzian values.

In these crosslinked epoxies the motion is restricted by relatively permanent chemical bonds, and the first plateau value was not significantly exceeded with increasing temperature. Within these inhomogeneous crosslinked epoxies, it was possible to have some molecular groups in nearly isotropic motion and others in anisotropic motion, which produced NMR signals with both Lorentzian and Gaussian components. The network structure in these epoxies also permitted two or more types of nearly isotropic motion at high temperatures, which produced NMR signals with two or more Lorentzian components. When the NMR signal contained more than two components, it was not possible to uniquely decompose the signal into its components. Thus, only two components were considered in the analysis, which produced errors in the results that were considered acceptable at the stage of this study.

The T_2 data show that at high temperatures, the plateau values of T_2 increase with decreasing crosslink density. The Lorentzian T_2 's at ~ 300 K are about 100 μ s; from Figure 57 it is seen that the Lorentzian signal is at

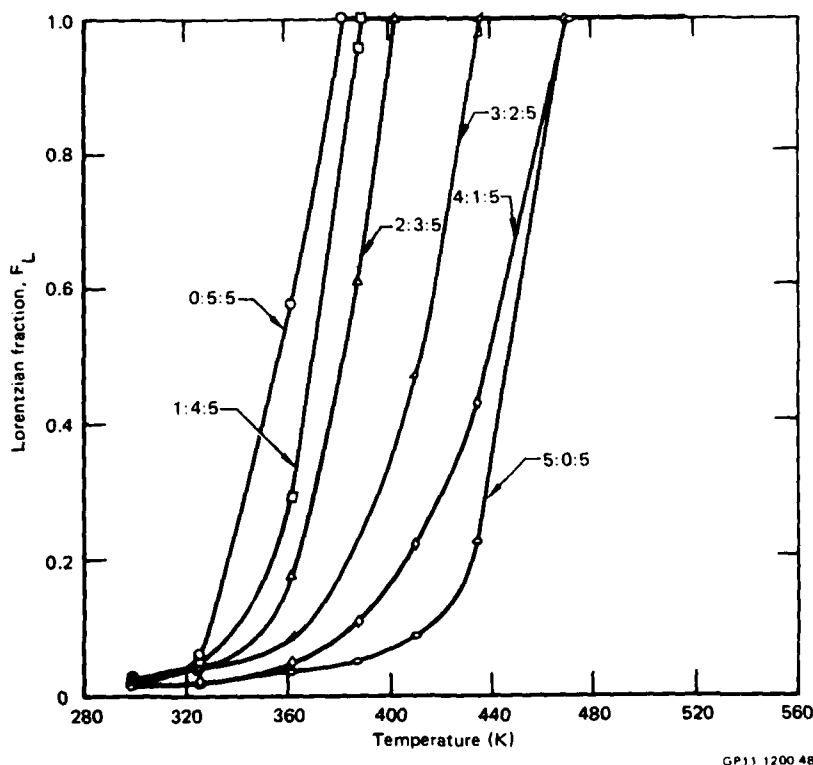


Figure 57. Temperature dependence of the Lorentzian fraction for DAB:DDH:DGEBA samples.

most 2% of the total signal, so it is possible that this Lorentzian signal resulted from sorbed water obtained from the ambient air. The Lorentzian-fraction temperature dependence shown in Figure 57 illustrates the wide range of glass transition temperatures for these samples. The glass transition temperatures of these samples as determined from dynamic mechanical measurements are compared with the Lorentzian-fraction transition temperature (where $F_L = 0.5$) and the spin-spin relaxation transition temperatures (where T_{2G} increases most rapidly) in Table 5. The agreement between the mechanically determined glass transition temperature, sensitive to motion having a frequency ≈ 10 Hz, and the temperature of the F_L transition, sensitive to motion having a frequency $\approx 10\,000$ Hz, is good if one subtracts 36 K from the F_L transition temperature. This result compares well with a 7 K increase in temperature for a factor of ten increase in frequency typically found in polymers.²⁶

Because the T_2 's were determined from the free-induction decays, they tend to underestimate the true value when $T_2 \gtrsim 500$ μ s. This error is caused by hydrogens with different chemical shifts becoming out of phase with each other (because of their different resonance frequencies) before the dipolar T_2 mechanisms produce the dephasing. In many previous studies of epoxies, the T_2 's rarely exceeded 400 μ s; hence this method of determining T_2 was routinely used. After realizing the seriousness of the errors in these measurements, the pulse-echo method (90° , τ , 180° , τ echo) was used to determine the correct value of T_{2L} on the high-temperature plateau. These values of T_{2L} for the major and minor Lorentzian components are given in Table 6.

TABLE 5. COMPARISON BETWEEN DIFFERENT TRANSITION TEMPERATURES.

Sample	Transition temperature (K)		
	Dynamic mechanical, $\tan \delta$	Gaussian spin-spin relaxation time, T_{2G}	Lorentzian fraction, F_L
0.5:5	329	372	357
1.4:5	—	374	368
2.3:5	348	382	380
3.2:5	364	394	411
4.1:5	—	416	438
5.0:5	408	424	446

GP11 1200 81

TABLE 6. HIGH-TEMPERATURE PLATEAU VALUES OF THE LORENTZIAN SPIN-SPIN RELAXATION TIMES DETERMINED USING PULSE-ECHO METHOD.

Sample	Major component		Minor component	
	Relative amplitude	T_{2L} (μ s)	Relative amplitude	T_{2L} (μ s)
0.5:5	1.00	10 900	-	-
1:4:5	0.78	2 500 - 3 800	0.22	30 000
2:3:5	0.81	440 - 700	0.19	38 000
3:2:5	0.83	310 - 670	0.17	3 600
4:1:5	0.90	100 - 350	0.10	2 000
5:0:5	0.95	70 - 160	0.05	2 000

GP11 1200 82

The temperature dependence of the spin-lattice relaxation times T_1 are plotted in Figure 58 for the six DAB:DDH:DGEBA samples. In general the spin-lattice relaxation time passes through a minimum when molecular motion in the sample has a correlation time, $\tau_c \sim 0.1/f_0$ where f_0 is the spectrometer frequency.²⁷ Thus, at the minimum, a particular molecular group has a correlation time of 10^{-9} s. The motion responsible for the minimum shown in Figure 58 is probably the methylene group motion in the DAB and DDH.

Assignment of the minimum in T_1 to the methylene group motion is based primarily on two previous studies. In the first study of the DGEBA:DETA system,¹⁰ a minimum above 400 K was suspected, and as the stoichiometry was varied the rate of spin-lattice relaxation T_1^{-1} was in direct proportion to the number of methylene groups in the DETA. In the second study of the MY720:DDH system,⁹ a minimum in T_1 occurred between 420 K and 500 K, depending upon the stoichiometry, and as in the DGEBA:DETA system, the rate of spin-lattice relaxation T_1^{-1} was in direct proportion to the number of methylene groups in the DDH. In these two previous studies, the minima occurred at lower temperatures as the crosslink density decreased, as it does here, as shown in Figure 58. The lower-temperature minimum of the DDH-rich samples shows that the greater length of the chains between crosslinks in these samples causes the methylene group motion to begin at a lower temperature than in the DAB-rich samples. The value of T_1 at the minimum is smaller for the DDH-rich samples than for the DAB-rich samples because DDH contains six methylene groups while DAB contains only four methylene groups. Also, the broader minimum for the highly crosslinked DAB-rich sample suggests that a broader

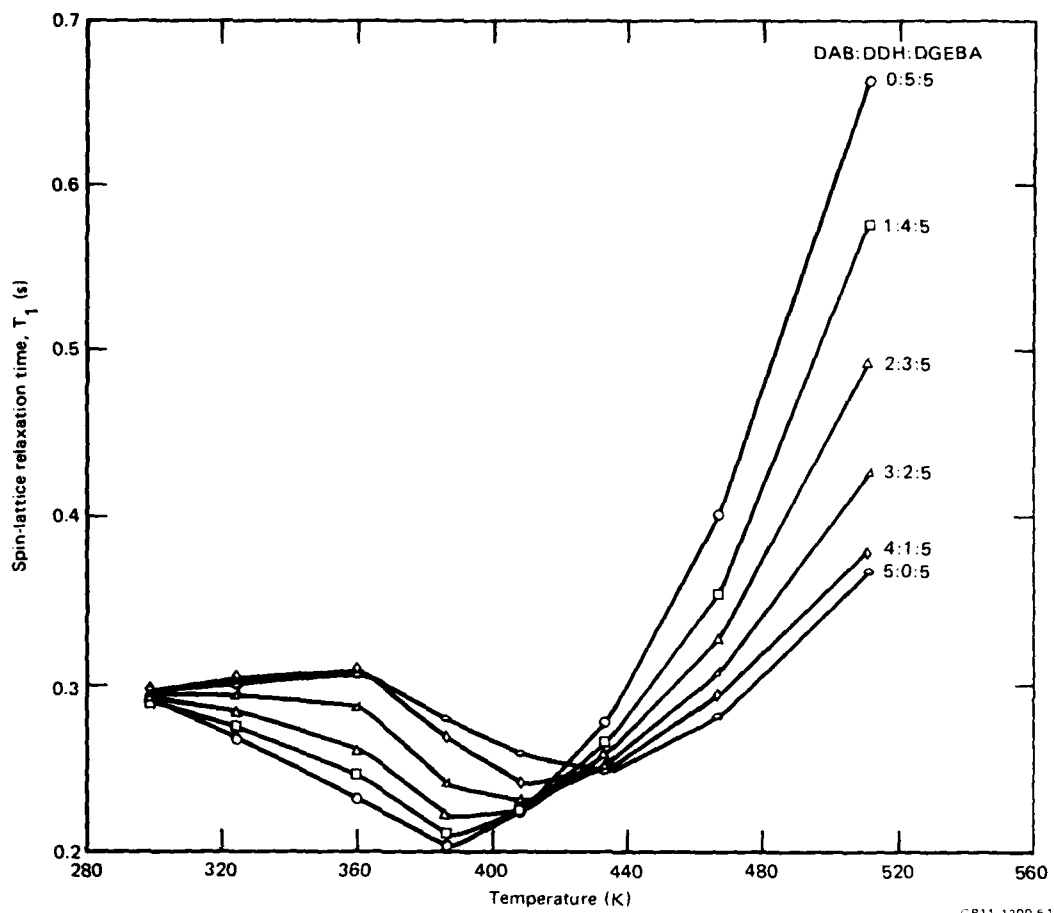


Figure 58. Temperature dependence of the spin-lattice relaxation time for DAB:DDH:DGEBA samples.

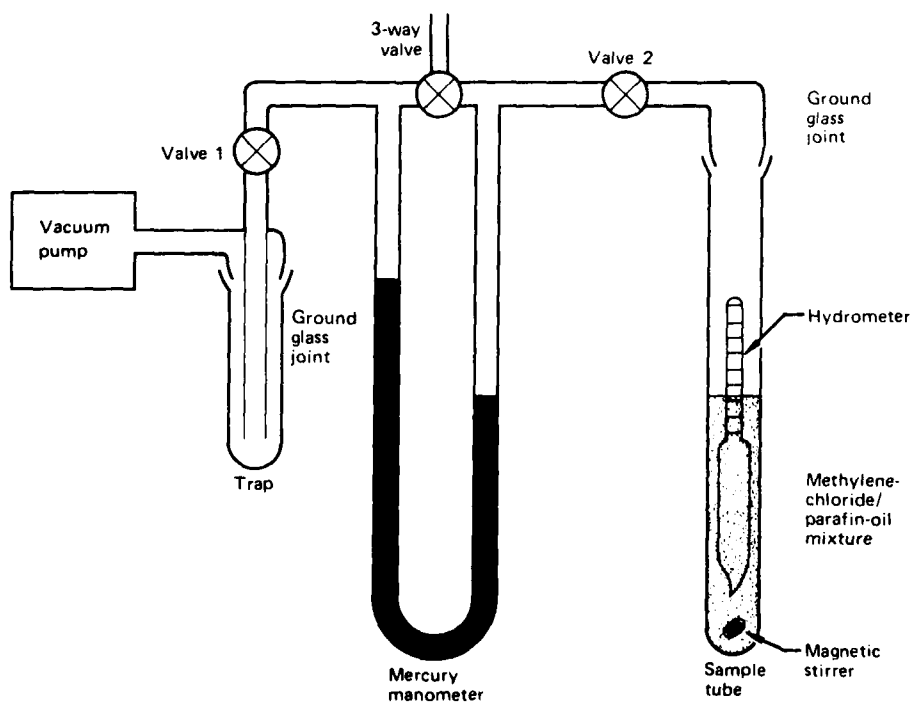
range of motional correlation times exists in the DAB-rich sample than in the DDH-rich sample.

3.2.5 Solvent-Dependent Studies

In previous hydrogen NMR studies^{9,28,29} it was observed that the sizes of the mobile regions in crosslinked epoxy samples containing large amounts of sorbed chloroform were larger than those in samples containing smaller amounts of sorbed water. It was suspected that the swelling caused by sorbing large quantities of chloroform caused bond rupture which produced larger-sized mobile regions. As a result, rather than immersing the samples in solvent and performing a series of measurements as various amounts of sorbed solvent were

removed, it was decided to subject the sample to increasing vapor pressures of the solvent. In this way it might be possible to determine if the sizes of the mobile region remain constant for small amounts of sorbed solvent, and then increase as molecular bonds rupture as more solvent is sorbed. The experimental procedures that had to be developed and perfected for this study were difficult and time consuming, and measurements of the sizes of the mobile regions was not performed. However, a complete series of solvent-dependent measurements was performed to compare with the temperature-dependent measurements.

The vapor pressure of the methylene chloride used in the study was controlled by dissolving methylene chloride (Fisher D-37) in paraffin oil (Fisher O-1109). Solutions of known concentrations were used at first, but it later became evident that the concentration changed with time as the methylene chloride was consumed or inadvertently lost through evaporation. As a result, the methylene chloride vapor pressures were determined and monitored using density measurements. The apparatus in Figure 59 was used to determine the



GP11 1200 71

Figure 59. Apparatus for determining the relation between the methylene chloride vapor pressure and the density of the methylene-chloride/paraffin-oil mixture.

relation between the methylene chloride vapor pressure and the density of the methylene-chloride/paraffin-oil mixture. The procedure consisted of first filling the sample tube with a mixture rich in methylene chloride and then evacuating the entire system for a short time. During this evacuation, sorbed gases were removed from the mixture as the mixture boiled; the magnetic stirrer was agitated during evacuation to prevent violent boiling. Valve 2 was then closed, and the rest of the system was pumped to a low pressure, (< 133 Pa). The three-way valve was closed, and valve 2 was opened. After waiting for the temperature of the mixture to reach room temperature, the vapor pressure and density were recorded. Then the three-way valve was opened to volatilize more methylene chloride from the mixture so that another vapor pressure and density pair could be measured. This procedure was repeated several times, and the resulting data are shown in Figure 60. The vapor pressure P shown in Figure 60 is normalized by dividing by the room-temperature (297 K) vapor pressure P_0 ($= 54.7$ kPa) of the pure methylene chloride solution. The solid line in Figure 60 is a best fit to the data assuming validity of Raoult's law and the additivity of the volumes in the mixture, viz.,

$$\frac{P}{P_0} = 1 - \left(\frac{1 - \rho/\rho_M}{1 - \rho/\rho_P} \frac{M_M}{M_P} \right)^{-1}, \quad (15)$$

where ρ , ρ_M ($= 1.317$ g/cm³), and ρ_P ($= 0.847$ g/cm³) are the densities of the mixture, methylene chloride, and paraffin oil, respectively, and M_M ($= 84.9$) and M_P ($= ?$) are the molecular weights of the methylene chloride and paraffin oil, respectively. The best fit to the data yielded an effective molecular weight M_P of 500 for the paraffin oil. During the solvent-dependent measurements, the density of the methylene chloride/paraffin oil mixture was measured, and then Equation (15) was used to determine P/P_0 .

The epoxy samples were cut into small pieces so they could quickly sorb the methylene chloride vapor. About 40 mg of the shavings were loosely packed into a 5 mm o.d. NMR tube that was fully open at the top and had a 0.5 mm diameter hole in the bottom. About 5 mg of quartz wool (which did not sorb significant quantities of methylene chloride) were placed at each end of the epoxy shavings to hold them in place in the NMR tube. Vapor pumps were devised for rapidly introducing the methylene chloride vapors to the epoxy

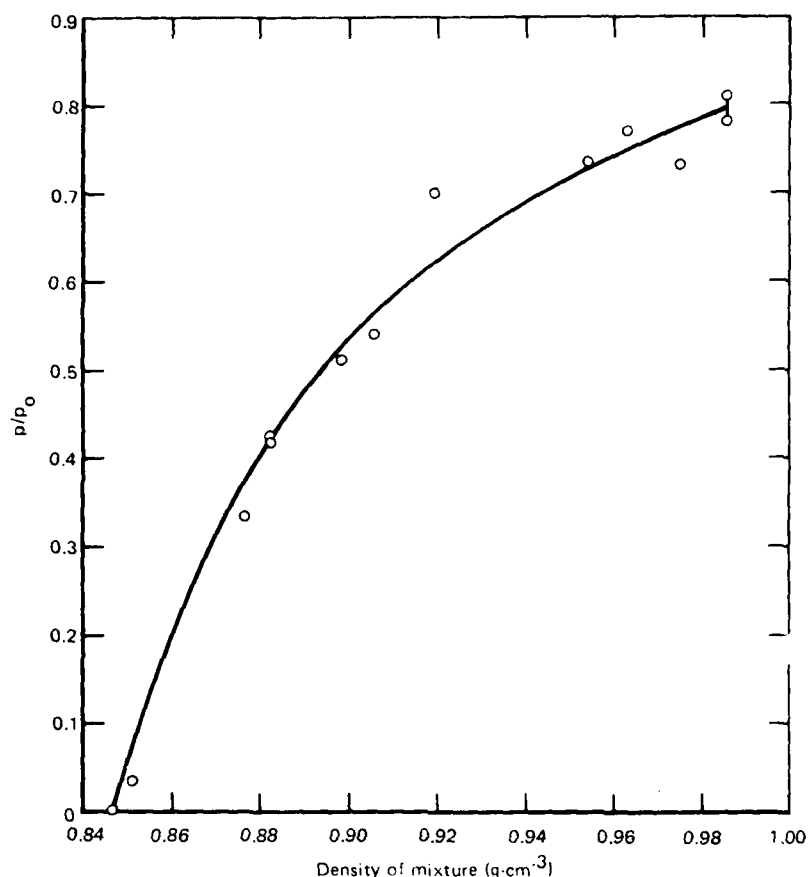
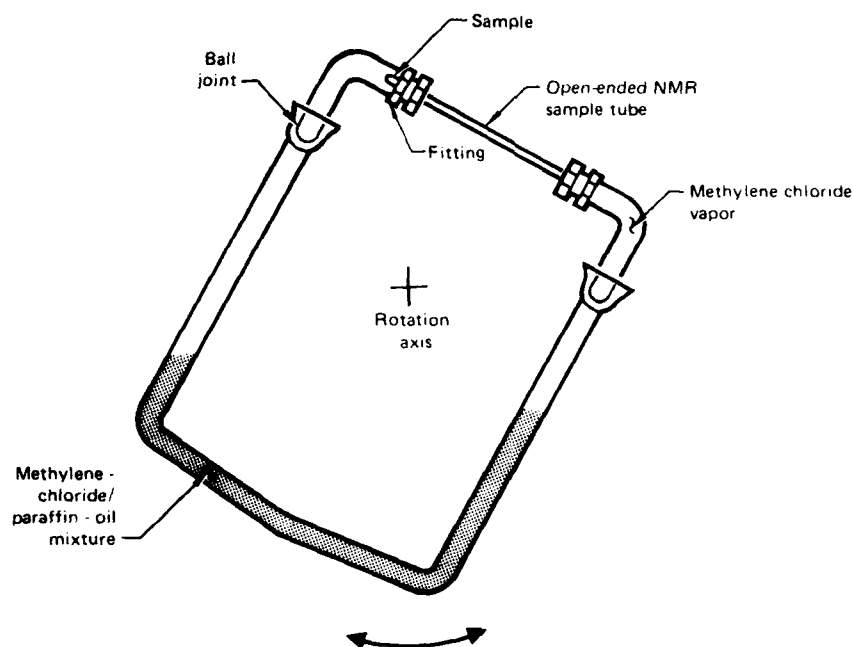


Figure 60. Normalized pressure of methylene chloride vapor in equilibrium with a methylene-chloride/paraffin-oil mixture. The solid line is a fit to the data using Raoult's law.

samples, as shown in Figure 61. The NMR tube was held in place by air-tight fittings over the top of a U-tube containing the methylene-chloride/paraffin-oil mixture. The entire apparatus was rotated back and forth about the axis indicated in the figure. As the fluid moved up and down in both arms of the U-tube, it forced the methylene chloride vapor back and forth past the epoxy sample in the NMR tube. The angle of rotation was about $\pm 40^\circ$ and the frequency of the rotation was about four times a minute. With no rotation it took over 48 h for the sample to come into equilibrium with the vapor, but with rotation it took about 1.5 h to reach equilibrium. However, 4 h or more were used to assure equilibrium.



SP11 1200 46

Figure 61. Vapor pump for rapidly introducing methylene chloride vapor to the epoxy sample.

Two of each of the six different DAB:DDH:DGEBA epoxy samples were prepared and weighed for the solvent-dependent measurements. At the start of this experiment, four samples were placed on the four vapor pumps containing only paraffin oil, and the systems were evacuated for at least 4 h. After evacuation, a sample was removed and capped at both ends, and the density of the mixture was measured. A new sample was placed on the pump, and NMR measurements were performed (the bottom cap was removed during this time ≈ 15 min). The NMR tube was then weighed after flushing with 40 cm^3 of air to remove methylene chloride vapors (which could increase the weight by as much as 4 mg, or 10% of the original sample weight). After all 12 samples had been processed in this manner, a small amount of methylene-chloride was added to the vapor pumps and the process was repeated. This process was repeated several times to obtain the solvent-dependent data.

Figure 62 shows the room-temperature sorption isotherms that were generated as a result of the weight measurements during the course of the solvent-dependent NMR study. Lack of time prevented measurements between $P/P_0 = 0.8$ and 1.0. The open and solid data points represent data from the pairs of like samples. The vertical scale is defined so that equal weights of methylene

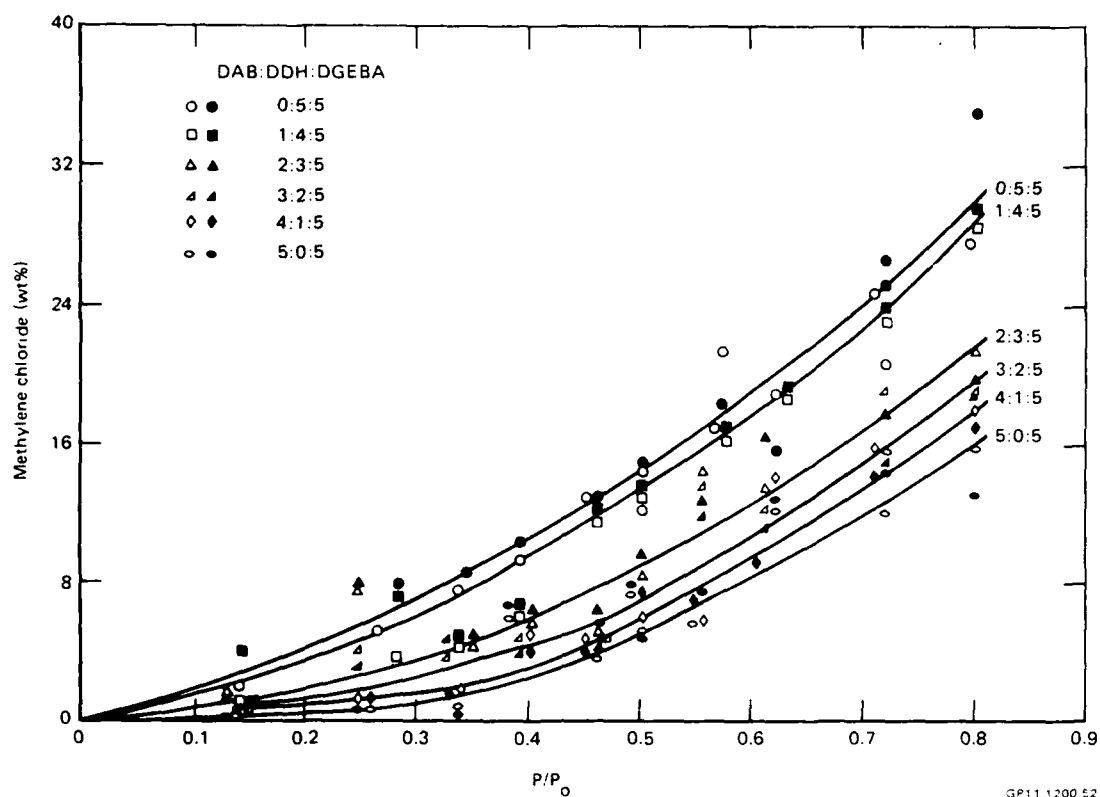


Figure 62. Room-temperature sorption isotherms for DAB:DDH:DGEBA samples exposed to methylene chloride.

chloride and epoxy are at 50% on the scale. The scatter in these data is larger than anticipated and is probably caused by variable weight losses between the time of removing the sample from the vapor pump and the time of measuring the sample weight. Even with the scatter, it is obvious that the epoxies having the smallest crosslink density sorb the largest amounts of methylene chloride. The relation between the crosslink density and the amount of sorbed methylene chloride will be quantitatively discussed in Section 3.2.6.

The solvent-dependent NMR measurements are similar to the temperature-dependent NMR measurements, and the data are presented in the same manner except that instead of temperature being the independent variable, the methylene chloride content (wt%) or normalized methylene chloride vapor pressure is the independent variable.

In previous hydrogen NMR studies^{9,10} of highly crosslinked epoxy resins containing sorbed water, the Lorentzian fraction F_L could be quantitatively accounted for by the hydrogen contained in the sorbed water plus the hydrogens contained in deliberately added non-stoichiometric excess amine. In stoichiometric epoxies few if any hydrogens contained in the polymer contributed to the Lorentzian component when plasticized with water. In this study of stoichiometrically cured DAB:DDH:DGEBA epoxy polymers, which contain no excess amine, the hydrogens in the polymer were observed to contribute to the Lorentzian component when plasticized with methylene chloride. This result is shown in Figure 63, where the dotted line shows the predicted Lorentzian fraction if only the hydrogens in the methylene chloride contributed to the Lorentzian component. The data for the 5:0:5 sample, which is the most highly crosslinked of these samples, lie along the predicted curve (except near 0 wt%

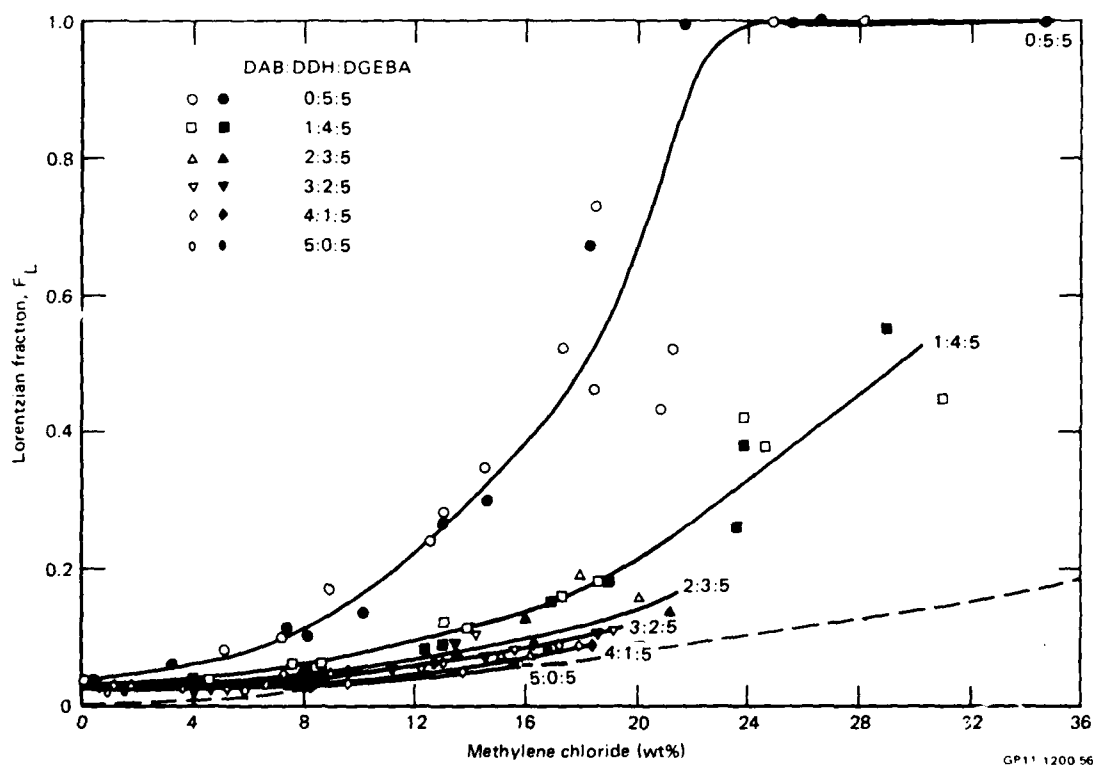


Figure 63. Lorentzian fraction of DAB:DDH:DGEBA samples as a function of sorbed methylene chloride. The dashed line is predicted if only the hydrogens in the methylene chloride produced the Lorentzian component.

methylene chloride, where sorbed water from the ambient air causes a larger than expected Lorentzian fraction). This result is similar to that obtained in the earlier studies.^{9,10} The data for the 4:1:5 sample lie perceptibly above the predicted curve, which indicates sufficient plasticization to cause some of the polymer to undergo extensive molecular motion. The other curves show that as the crosslink density decreases, the ability of the solvent to cause the polymer to undergo extensive molecular motion increases.

Figures 64 and 65 show the dependence of the Gaussian spin-spin relaxation time on the methylene chloride normalized vapor pressure P/P_0 and solvent content, respectively. When plotted against P/P_0 , large differences between the samples are observed; the differences are enhanced in this plot because the differences are primarily caused by differences in sorbed solvent content. In Figure 65 the differences between the samples are less pronounced. The highly crosslinked samples, 5:0:5, 4:1:5, 3:2:5, and even the 2:3:5, exhibit

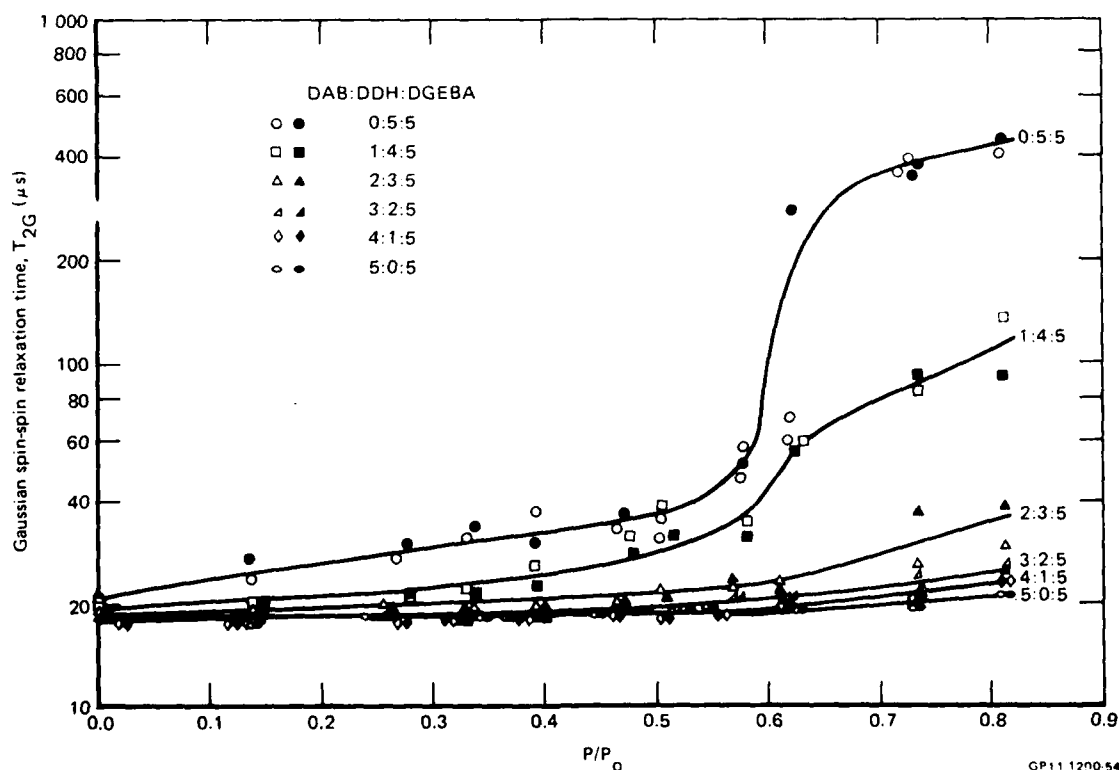


Figure 64. Gaussian spin-spin relaxation times of DAB:DDH:DGEBA samples exposed to methylene chloride vapor.

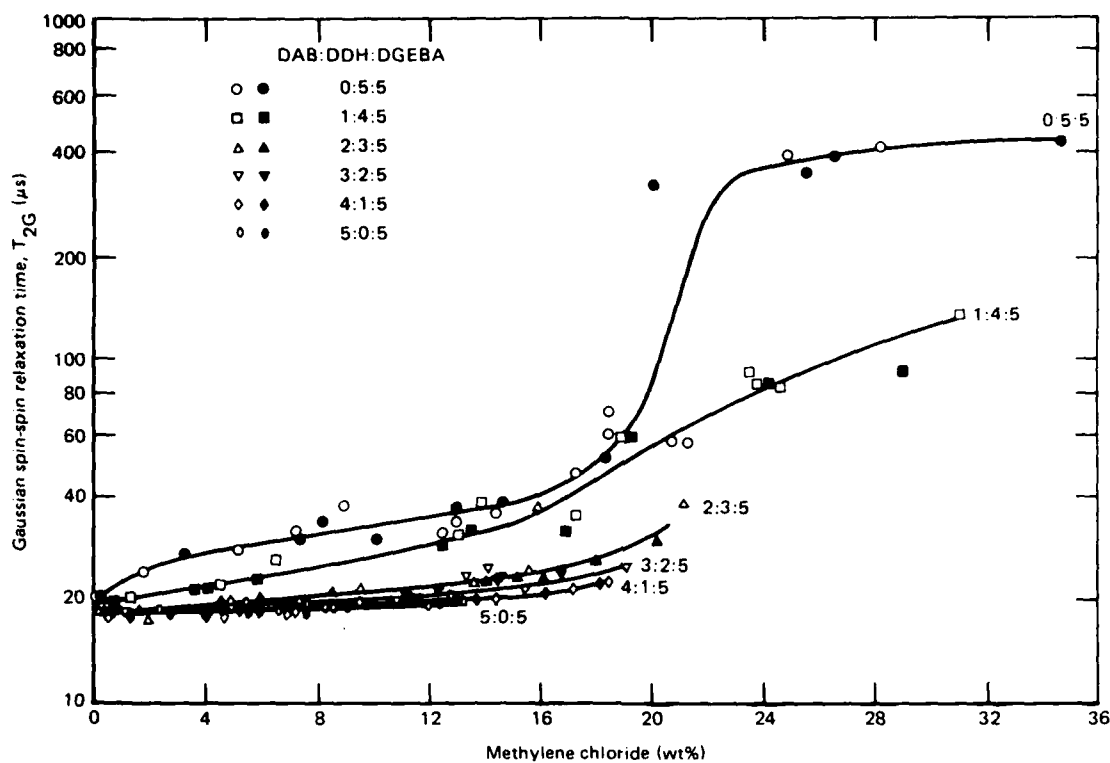
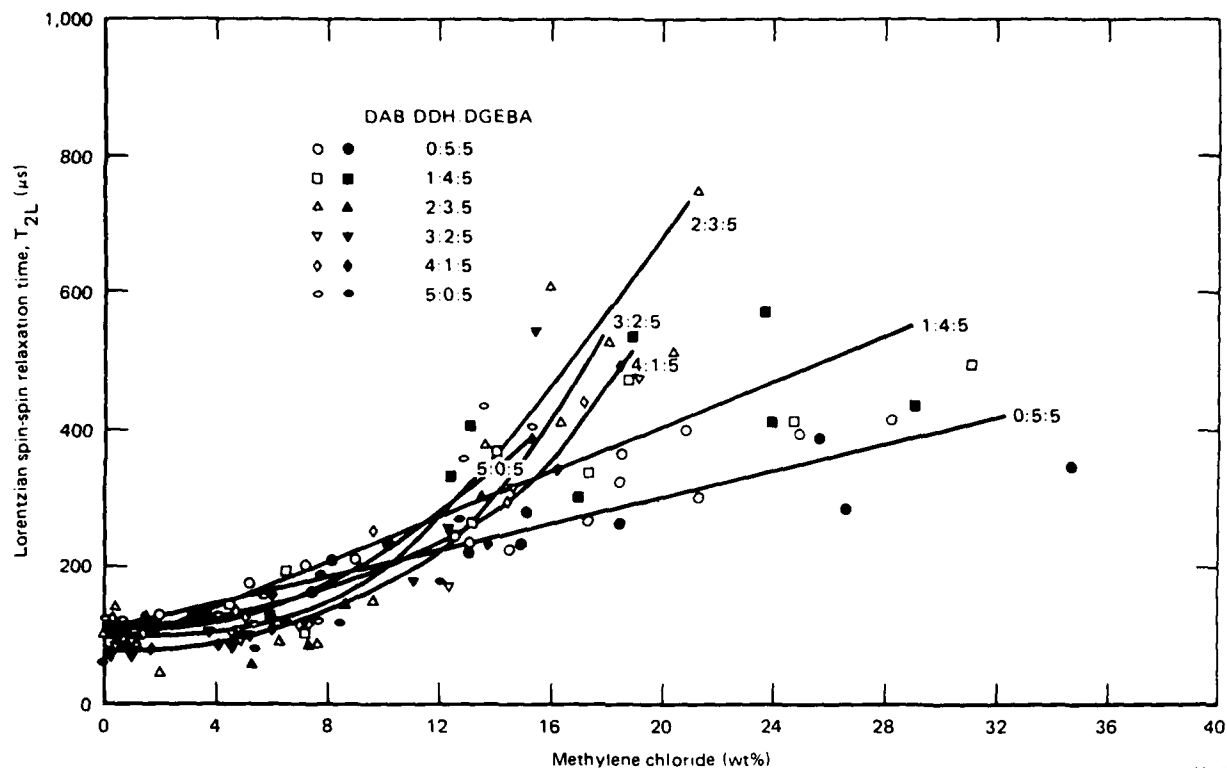


Figure 65. Gaussian spin-spin relaxation times of DAB:DDH:DGEBA samples as a function of sorbed methylene chloride.

similar increases in T_{2G} with increasing solvent content. Only the lightly crosslinked samples 0:5:5 and 1:4:5 exhibit what can be regarded as distinctly different behavior.

Figure 66 shows the dependence of the Lorentzian spin-spin relaxation time on methylene chloride content. These results are subject to many errors, and conclusions derived from them are only tentative. The errors were caused by nonunique decomposition of the free-induction decay into two components, especially when the amplitude of the Lorentzian component being measured was small (see Figure 63), and failure to use the spin-echo method for determining the T_2 's when they became large. This last error was not present in a separate set of experiments in which NMR measurements were made on samples that had been exposed to pure methylene chloride vapor ($P/P_0 = 1$). These results are shown in Table 7, where it is seen that two Lorentzian components were observed in all samples. Because no Gaussian components were observed, it is



GP11 1200 51

Figure 66. Lorentzian spin-spin relaxation times of DAB:DDH:DGEBA samples as a function of sorbed methylene chloride.

TABLE 7. LORENTZIAN SPIN-SPIN RELAXATION TIMES OF SAMPLES SATURATED WITH METHYLENE CHLORIDE VAPOR ($P/P_0 = 1$) DETERMINED USING THE PULSE-ECHO METHOD.

Sample	Methylene chloride content (wt%)	Major Lorentzian component		Minor Lorentzian component		Fraction of the hydrogens contained in methylene chloride
		Relative amplitude	T_{2L} (μs)	Relative amplitude	T_{2L} (μs)	
0:5:5	78	~ 0.7	10 600	~ 0.3	~ 5 000	0.48
1:4:5	60	0.72	4 400	0.28	15 000	0.29
2:3:5	42	0.82	530	0.18	24 000	0.17
3:2:5	34	0.85	290	0.15	9 900	0.13
4:1:5	32	0.85	205	0.15	6 700	0.12
5:0:5	26	0.87	200	0.13	7 800	0.10

GP11 1200 83

concluded that the molecular motion was nearly isotropic, even for the highly crosslinked sample 5:0:5. However, the fact that the T_2 's for the highly crosslinked samples were smaller than those for the lightly crosslinked samples does indicate more anisotropic (restricted) motion in the highly crosslinked samples.

In Table 7 there is reasonably good agreement between the fraction of hydrogens contained in the methylene chloride and the relative amplitude of the minor Lorentzian component (except for sample 0:5:5). This agreement suggests that the minor Lorentzian component is caused almost totally by the methylene chloride hydrogens. The fact that the methylene chloride hydrogens contributed a separate NMR component with distinctly different spin-spin relaxation times T_{2L} implies that the motion of the methylene chloride is distinctly different from that of the polymer, even though the Lorentzian character of the NMR component assigned to the polymer implies nearly isotropic polymer motion. Table 7 shows different results for the 0:5:5 sample. Here, for this lightly crosslinked sample, the solvent and a large portion of the polymer exhibit similar motions; in this case the minor Lorentzian component represents the less mobile portions of polymer.

Returning to Figure 66, it is necessary to explain why the T_{2L} 's for the more highly crosslinked samples can be greater than those for the more lightly crosslinked samples for equal solvent contents. It is also necessary to explain the large value of T_{2L} of the minor Lorentzian component shown in Table 7 for sample 2:3:5. These results are tentatively explained in terms of the inhomogeneities suspected in crosslinked epoxy polymers as a result of a nonuniform distribution of crosslinks. If the solvent were to selectively reside in the lightly crosslinked regions of a highly inhomogeneous polymer, the molecular motion that the solvent would produce could easily be greater than the motion it would produce if it were uniformly distributed throughout a more homogeneous polymer. If this explanation is correct, then the 2:3:5 sample is the most inhomogeneous of the samples (contains the largest sized mobile regions). Unfortunately, lack of time prevented the NMR determination of the sizes of the mobile regions for these samples.

The solvent dependence of the spin-lattice relaxation time T_1 is shown in Figure 67, which should be compared with the temperature dependence of the spin-lattice relaxation time shown in Figure 58. As either solvent content or

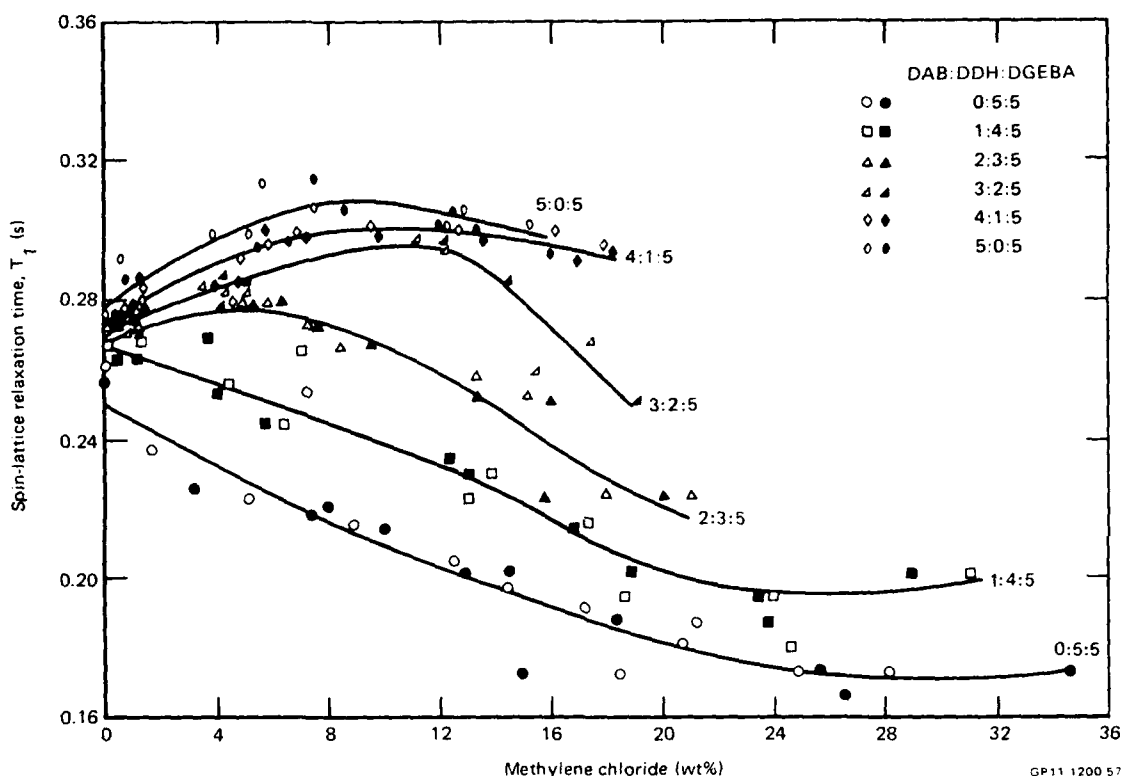


Figure 67. Spin-lattice relaxation times of DAB:DDH:DGEBA samples as a function of sorbed methylene chloride.

temperature was increased, the T_1 for sample 5:0:5 increased and then later decreased. Likewise the T_1 for sample 0:5:5 decreased to a minimum. Because of the limited solvent data, it is not possible to determine a detailed relation between the solvent and temperature effects.

3.2.6 Crosslink Density Determinations

Although the crosslink densities of the DAB:DDH:DGEBA samples are not necessarily given by their composition because of the variety of competing chemical reactions that occur during curing, these values were calculated for comparison with those determined from experimental results. In these calculations it was assumed that the DAB molecule contained two trifunctional crosslink points connected by the methylene groups rather than assuming a tetrafunctional crosslink point. In a polymer that has n -functional crosslink points, there are n -chains connecting crosslink points for every two crosslink

points. In addition to computing the molecular weight between crosslink points, for later calculations it is necessary to know the number of chemical bonds along the backbone of the polymer chain between crosslink points (actually, the number of statistically independent segments is required, but this value is related to the number of bonds along the backbone). For this purpose it was assumed that DAB had five backbone bonds and a molecular weight of 88, DDH had seven backbone bonds and a molecular weight of 144, and DGEBA had ten backbone bonds and a molecular weight of 340. Thus, the 3:2:5 polymer, where 3/4 moles of DAB and 2/2 moles of DDH were added to 5/2 moles of DGEBA, on a per mole basis: 1) the DAB contributed (3/4) x 5 backbone bonds, (3/4) x 2 crosslink points, and (3/4) x 88 g weight, 2) the DDH contributed (2/2) x 7 backbone bonds, no crosslink points, and (2/2) x 144 g weight, and 3) the DGEBA contributed (5/2) x 10 backbone bonds, no crosslink points, and (5/2) x 340 g weight. The totals are 37.75 backbone bonds, 1.5 crosslink points, and 1060 g weight. Since there are three chains per two crosslink points, there are 2.25 chains, giving an average of 15.9 (= 37.75/2.25) backbone bonds per chain and an average weight M_C of 471 g (= 1060/2.25) between crosslink points. Table 8 shows the calculated crosslink parameters for the DAB:DDH:DGEBA samples.

The molecular weight between crosslinks M_C was determined from the sorption data using the relation^{14,16,30}

$$\ln a = \ln(1 - v_2) + v_2 + \chi_1 v_2^2 + \frac{M_s}{\rho_s} \frac{\rho_p}{M_C} \left(v_2^{1/3} - 2v_2/f \right), \quad (16)$$

TABLE 8. CALCULATED CROSSLINK PARAMETERS FOR THE DAB:DDH:DGEBA SAMPLES.

Sample	Average molecular weight between crosslinks M_C (g)	Average number of bonds between crosslinks
0:5:5	∞	∞
1:4:5	1547	53.7
2:3:5	740	25.3
3:2:5	471	15.9
4:1:5	337	11.2
5:0:5	256	8.3

GP11 1200 84

where a is the activity of the solvent, assumed equal to P/P_0 , M_S and ρ_S are the molecular weight and density of the solvent, ρ_P is the density of the unswollen polymer, v_2 is the volume fraction of the swollen polymer, χ_1 is the dimensionless Flory-Huggins interaction parameter, and f is the functionality of the crosslink. This equation was used assuming equality of the solvent volume fraction ($1 - v_2$) and solvent weight fraction. The value for χ_1 was found to be equal to 0.59 by fitting Equation (16) to the methylene chloride weight fraction data at $P/P_0 = 1$ for the 0:5:5 sample assuming $M_C = \infty$. This value of χ_1 is in reasonable agreement with the value of 0.49 that was determined independently by another method in Section 2.2. Using this value of χ_1 in Equation (16), the values of M_C for the other samples were determined from the measured methylene chloride content data given in Table 7 for $P/P_0 = 1$. Then using these values of χ_1 and M_C in Equation (16), the sorption isotherm data were calculated and plotted in Figure 68 along with the smoothed experimental data from Figure 62 and Table 7. The fits of Equation (16) to the data are good for the lightly crosslinked samples, 0:5:5 and 1:4:5, but deviate significantly for the more heavily crosslinked samples, which is not unexpected because Equation (16) is best suited for lightly crosslinked systems.

The values of M_C determined using Equation (16) are compared with the calculated values of M_C in Figure 69. The experimentally determined values underestimate the predicted values for all samples except the 1:4:5 sample. Since Equation (16) is applicable for large molecular weights ($M_C \gtrsim 3000$) between crosslinks, it is not unexpected that the values of M_C determined using Equation (16) underestimate the predicted value. However, it is unexpected that the determined value of M_C for the 1:4:5 sample is larger than calculated.

The correlation between the high-temperature and high-solvent content values of the spin-spin relaxation time T_2 and the crosslink density are now examined. Figure 70 shows these values of T_2 plotted as a function of the calculated molecular weight between crosslinks. The solid lines are predicted on the basis of a statistical analysis of the range of angles over which neighboring hydrogen spins can possibly be oriented, assuming a particular number of independently rotatable segments along the chain.³¹ The results of this analysis indicate that the limiting, or plateau, value of T_2 is given by

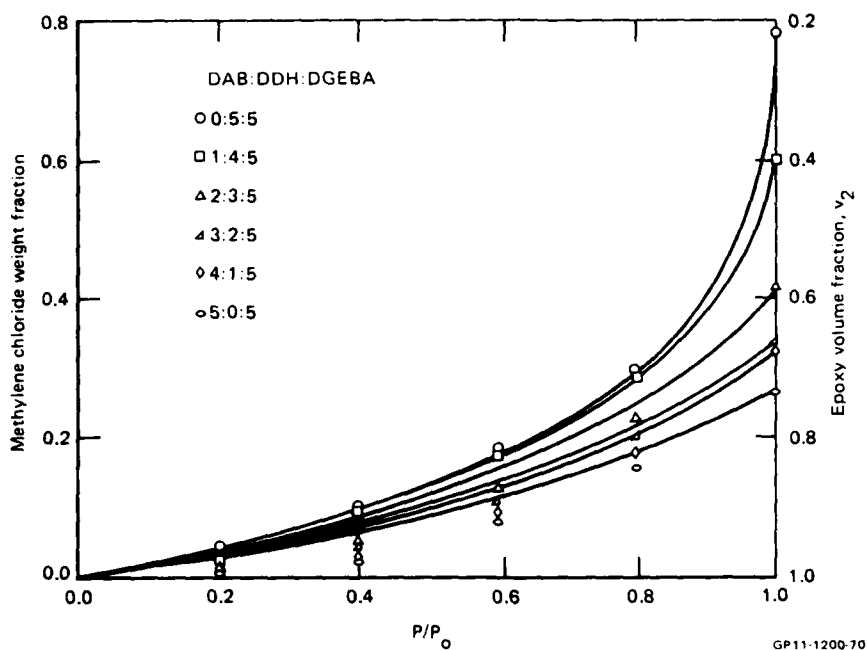


Figure 68. Calculated equilibrium epoxy volume fractions as a function of methylene chloride vapor pressure compared with the measured methylene chloride weight fractions. Agreement is good for low crosslink density epoxies at all pressures, but is poor for high crosslink density epoxies at low pressures.

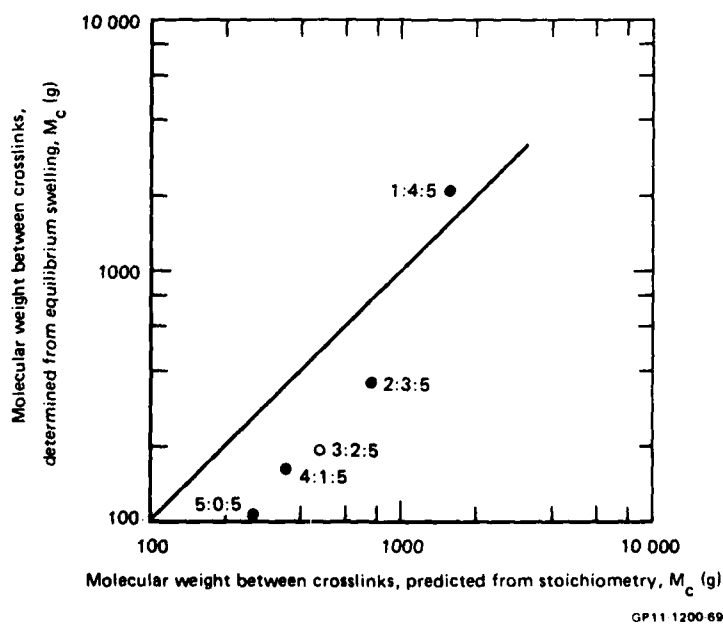
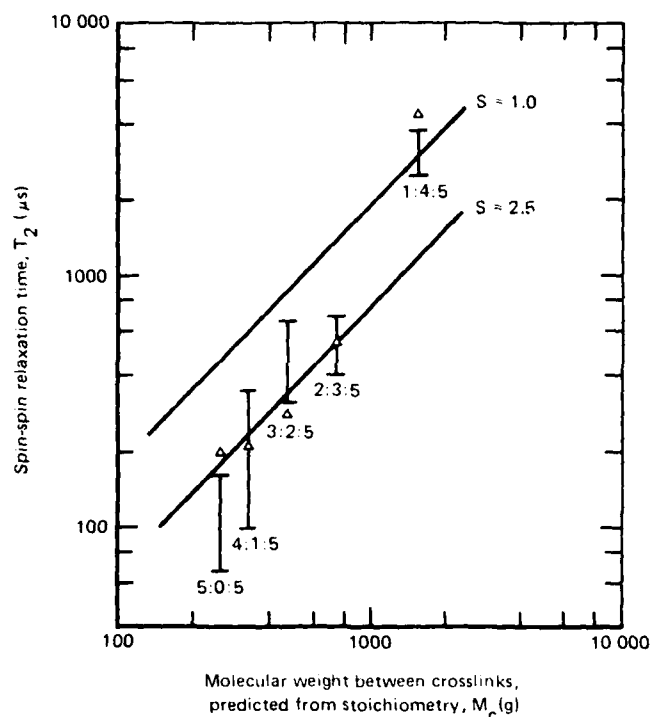


Figure 69. Comparison of molecular weight between crosslinks of DAB:DDH:DER epoxy samples as predicted from stoichiometry and as determined from swelling measurements. The solid line identifies perfect agreement.



GP11 1200 68

Figure 70. Plateau values of spin-spin relaxation times of DAB:DDH:DER epoxy samples at high temperature (vertical bars) or saturated with methylene chloride (Δ). The solid lines are predicted assuming S backbone bonds are per statistical segment.

$$T_2 \approx \frac{5.6 Z}{\gamma [(\Delta H_0)^2]^{1/2}}, \quad (17)$$

where Z is the number of statistical segments along the chain between crosslinks, γ is the gyromagnetic ratio of the hydrogen nucleus ($= 2.67 \times 10^8 \text{ rad} \cdot \text{s}^{-1} \text{ T}^{-1}$), and $(\Delta H_0)^2$ is the second moment of the rigid lattice ($\approx 1.6 \times 10^{-7} \text{ T}^2$). This equation clearly states that the larger the number of statistical segments Z along the chain, the easier the chain can move isotropically and hence the larger will be T_2 . The two lines drawn in Figure 70 were obtained from Equation (17) assuming Z equal to the average number of backbone bonds along the chain between crosslinks, as tabulated in Table 8, and assuming Z reduced by a factor of 2.5, i.e., there were 2.5 backbone bonds per statistical segment. The agreement for the latter line is good. Hence

the NMR data, like the sorption data shown in Figure 69, show an anomaly with the 1:4:5 sample. Either the analyses of both sets of data show this discrepancy because they fail at large crosslink densities and not at small crosslink densities, or sample 1:4:5 has a smaller crosslink density than predicted on the basis of the stoichiometry.

4. SUMMARY OF CONCLUSIONS

4.1 EPR Conclusions

- The reaction rates for the initial step in the reactions of a secondary amine and tertiary amine nitroxide with DGEBA obey pseudo-first-order kinetics at low nitroxide concentrations.
- The temperature dependence of both reaction rates is given by $k_{1,2} = k_0 \exp - \Delta E/RT$, where $k_0 = 7.8 \times 10^2 \text{ s}^{-1}$ and $\Delta E = 41.5 \text{ kJ} \cdot \text{mole}^{-1}$.
- The spectra of the spin probe TANOL in amine-cured samples with different average crosslink densities can be characterized by one motional correlation time at each temperature, thus giving no indication of any distribution of correlation times.
- The motional correlation time for TANOL in these amine-cured samples above T_g obeys the WLF equation.
- The logarithm of the motional correlation time for TANOL in these amine-cured epoxy samples is linearly dependent on the crosslink density over the range of crosslink densities studied.
- The spectra of TANOL in these amine-cured epoxy samples plasticized with methylene chloride can be characterized by a bimodal distribution of motional correlation times at some solvent contents.
- The bimodal spectrum provides information on the extent and amount of crosslink density variations within a given sample.
- The mobile fraction evaluated from the area under the fast-phase spectrum in plasticized epoxy samples is approximately linearly dependent on the solvent weight fraction.
- The behavior of the spectra of TANOL in the plasticized amine-cured epoxy samples varies only slightly with average crosslink density.

- Fast-phase spectra ($\tau_c < 3 \times 10^{-9}$ s) for nitroxides in dry or plasticized epoxy samples are always observed when the host region for the nitroxide is above its T_g value.
- Reasonable crosslink densities for amine-cured epoxy can be calculated from dynamic mechanical analysis data.
- Amine-nitroxides which are diffused into cured epoxy samples covalently bind to unreacted epoxy groups in the polymer.

4.2 NMR Conclusions

- The kinetics of the epoxy/amine reaction can be monitored using ^{13}C NMR.
- The rate of the EPOP/MBA reaction is dependent upon hydrogen-bond donors in the mixture; thus it is a third-order reaction.
- The hydrogen-bond donors are present as impurities in the EPOP and the MBA and also are created by the reaction.
- The room-temperature rate constant for the third-order reaction of EPOP and MBA involving the hydrogen-bond donor created during the reaction was $8 \times 10^{-6} \text{ L}^2 \text{ mole}^{-2} \text{ s}^{-1}$.
- The sources of the hydrogen-bond donors present as impurities of the starting materials were quantitatively identified using ^{13}C NMR.
- The hydrogen spin-spin relaxation times of DAB:DDH:DGEBA polymers at high temperature or saturated with methylene chloride are related to the crosslink density.
- The relation between the hydrogen spin-spin relaxation time and the crosslink density is in agreement with the predictions of Gotlib et al.³¹

- Crosslinked DAB:DDH:DGEBA polymers saturated with sorbed methylene chloride display a free-induction decay signal containing two Lorentzian components, and within experimental error, one component can be identified as originating from the polymer and the second component can be identified as originating from the methylene chloride.
- At low methylene chloride contents (< 20 wt%), the free-induction decay signal from the highly crosslinked 5:0:5 DAB:DDH:DGEBA sample contained Gaussian and Lorentzian components, and the Lorentzian component was due totally to the sorbed methylene chloride. For DAB:DDH:DGEBA samples having smaller crosslink densities, the Lorentzian component was larger and was due to plasticized polymer as well as methylene chloride.

AD-A116 542

MCDONNELL DOUGLAS RESEARCH LABS ST LOUIS MO

F/6 7/4

MAGNETIC RESONANCE DETERMINATIONS OF STRUCTURE AND REACTION KIN--ETC(U)

DEC 81 I M BROWN, A C LIND, T C SANDRECZKI

N00019-80-C-0552

NL

UNCLASSIFIED

MDC-00759

2 OF 2

AD-A
116542



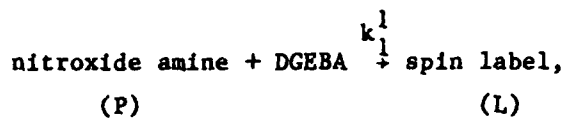
END

DATE
FILMED

08-82
DTIC

APPENDIX A: Pseudo-first-order reaction rates in
spin-label formation

In the reaction



the rate of disappearance of P can be written:

$$\frac{dP}{dt} = -k_1 [\text{DGEBA}] [P] .$$

If the concentration of P is always small, [DGEBA] should remain effectively constant throughout the reaction:

$$\frac{dP}{dt} = -k_1 [P] ,$$

so that

$$\frac{P}{P_0} = \exp(-k_1 t) ,$$

where P_0 is the value of P at $t = 0$, or

$$\left(1 - \frac{L}{P_0}\right) = \exp(-k_1 t)$$

since $P_0 = L + P$.

REFERENCES

1. A. S. Kenyon and L. E. Nielson, Characterization of Network Structure of Epoxy Resins by Dynamic Mechanical and Liquid Swelling Tests, *J. Macromol. Sci.* A3, 275 (1976).
2. R. E. Cuthrell, Macrostructure and Environment Influenced Surface Layer in Epoxy Polymers, *J. Appl. Polymer Sci.* 11, 949 (1967).
3. J. L. Racich and J. A. Koutsky, Nodular Structure in Epoxy Resins, *J. Appl. Polymer Sci.* 20, 2111 (1976).
4. J. S. Mijovic and J. A. Koutsky, The Effect of Postcure Time on the Fracture Properties and Nodular Morphology of an Epoxy Resin, *J. Appl. Polymer Sci.* 23, 1037 (1979).
5. J. Mijovic and J. A. Koutsky, Correlation Between Nodular Morphology and Fracture Properties of Cured Epoxy Resins, *Polymer* 20, 1095 (1979).
6. R. J. Maty, D. R. Uhlmann, and J. A. Koutsky, Structure of Glassy Polymers, Small Angle X-Ray Scattering from Epoxy Resins, *J. Polymer Sci.* 18, 1053 (1980).
7. R. J. Morgan and J. E. O'Neal, The Microscopic Failure Processes and Their Relation to Structure of Amine-Cured Bisphenol A Diglycidyl Ether Epoxies, *J. Mater. Sci.* 12, 1966 (1977).
8. L. J. Berliner, Ed., Spin Labeling: Theory and Applications (Academic Press, New York, 1976).
9. I. M. Brown, A. C. Lind, and T. C. Sandreczki, Magnetic Resonance Studies of Epoxy Resins, Technical Report MDC Q0721 (7 December 1980) Final Report, Naval Air Systems Command Contract N00019-79-C-0414.
10. I. M. Brown, A. C. Lind, and T. C. Sandreczki, Magnetic Resonance Studies of Epoxy Resins and Polyurethanes, Technical Report MDC Q0673 (3 May 1979) Final Report, Naval Air Systems Command Contract N00019-78-C-0031.
11. I. M. Brown, and T. C. Sandreczki, Nitroxide Spin Label Studies in an Epoxy Resin, *Chem. Phys. Letters* 64, 85 (1979).
12. D. Kivelson, Theory of ESR Linewidths of Free Radicals, *J. Chem. Phys.* 33, 1094 (1960).
13. D. Katz, and A. V. Tobolsky, Rubber Elasticity in a Highly Crosslinked Epoxy System, *Polymer* 4, 417 (1963).

14. P. J. Flory and J. Rehner, Statistical Mechanics of Crosslinked Polymer Networks I, J. Chem. Phys. 11, 512 (1943).
15. J. D. Ferry, Viscoelastic Properties of Polymers, (John Wiley, New York, 1980).
16. P. J. Flory and J. Rehner, Statistical Mechanics of Crosslinked Polymer Networks II Swelling, J. Chem. Phys. 11, 521 (1943).
17. I. T. Smith, The Mechanism of the Crosslinking of Epoxide Resins by Amines, Polymer 2, 95 (1961).
18. N. S. Isaacs and R. E. Parker, Mechanisms of Epoxide Reactions, Chem. Rev. 59, 737 (1959).
19. Y. Tanaka and T. F. Mika, Epoxide-Curing Reactions, Epoxy Resins, C. May and Y. Tanaka, Ed., (Marcel Dekker, Inc., New York, 1973).
20. J. J. King and J. P. Bell, Reactions in a Typical Epoxy-Aliphatic Diamine System, Epoxy Resin Chemistry (American Chemical Society Symposium Series Number 114, Washington, D.C., 1979).
21. S. A. Reines, J. R. Griffith and J. G. O'Rear, Effects of Fluorine Substitution upon Glycidyl Ether-Dibutylamine Reaction Rates, J. Org. Chem. 35, 2772 (1970).
22. Jacob Schaefer, E. O. Stejskal, and R. Buchdahl, High-Resolution Carbon-13 Nuclear Magnetic Resonance Study of Some Solid, Glassy Polymers, Macromolecules 8, 291 (1975).
23. A. Pines, M. G. Gibby, and J. S. Waugh, Proton Enhanced NMR of Dilute Spins in Solids, J. Chem. Phys. 59, 569 (1973).
24. S. R. Hartmann and E. L. Hahn, Nuclear Double Resonance in the Rotating Frame, Phys. Rev. 128, 2042 (1962).
25. David W. McCall, Nuclear Magnetic Resonance Studies of Molecular Relaxation Mechanisms in Polymers, Acc. Chem. Res. 4, 223 (1971).
26. L. E. Nielsen, Mechanical Properties of Polymers and Composites, (Marcel Dekker, Inc., New York, NY, 1974), Vol. I, p. 145.
27. N. Bloembergen, E. M. Purcell, and R. V. Pound, Relaxation Effects in Nuclear Magnetic Resonance Absorption, Phys. Rev. 73, 679 (1948).
28. A. C. Lind, An NMR Study of Inhomogeneities in Epoxy Resins, Polymer Preprints 21, No. 2, 241 (1980).
29. A. C. Lind, NMR Study of Inhomogeneities in Amine-Cured Epoxies, Polymer Preprints 22, No. 2, 333 (1981).

30. P. J. Flory, Principles of Polymer Chemistry, (Cornell University Press, Ithaca, NY, 1953), p. 578.
31. Yu. Ya., Gotlib, M. I. Lifshits, V. A. Shevelev, I. S. Lishanskii, and I. V. Balanina, The Influence of the Chemical Crosslinking Network on the Spin-Spin Relaxation of Crosslinked and Swelling Polymer Systems, Polymer Sci. USSR 18, 2630 (1976).

DISTRIBUTION

	Copies		Copies
Commander Naval Air Systems Command Department of the Navy ATTN: Code AIR-5304C2 Washington, DC 20361	8	Commander Naval Air Systems Command Department of the Navy ATTN: Code AIR-320A Washington, DC 20361	1
Commander Naval Air Systems Command Department of the Navy ATTN: Code AIR-954 (DDC) Washington, DC 20361	12	Director Naval Research Laboratory ATTN: Code 6110 (1 copy) Code 6120 (1 copy) Code 6170 (1 copy) Washington, DC 20375	3
Commander Naval Surface Weapons Center ATTN: Code WR-31 White Oak Silver Spring, MD 20910	2	Commanding Officer Naval Ship R&D Center Annapolis Laboratory Annapolis, MD 21402	1
Commander Naval Air Development Center ATTN: Code 606 Warminster, PA 18974	2	Commander Naval Weapons Center ATTN: Code 385 China Lake, CA 93555	1
Office of Naval Research ATTN: Code 472 800 N. Quincy St. Arlington, VA 22217	1	Office of Naval Research Boston Branch Office ATTN: L. H. Peebles 495 Summer St. Boston, MA 02210	1
Army Materials & Mechanics Research Center ATTN: Dr. George Thomas Watertown, MA 02172	2	U.S. Army Research Office ATTN: Dr. John Hurt Box CM, Duke Station Durham, NC 27706	1

	Copies		Copies
Director Air Force Materials Laboratory ATTN: Codes AFWAL/MLBE (1 copy) AFWAL/MLXE (1 copy) AFWAL/MLBC (1 copy) AFWAL/MLBP (1 copy) Wright-Patterson AFB, OH 45433	4	Air Force Office of Scientific Research ATTN: D. R. Ulrich Bolling Air Force Base Washington, DC 20332	1
NASA Headquarters Materials & Project Office ATTN: Mr. Charles F. Bersch 600 Independence Ave., S.W. Washington, DC 20546	1	NASA Langley Research Center ATTN: Dr. N. Johnston Head, Polymer Group Hampton, VA 23665	1
NASA Lewis Research Center ATTN: R. W. Lauver Cleveland, OH 44135	1	National Bureau of Standards Institute for Materials Research ATTN: Dr. Leslie Smith Washington, DC 20234	1
Plastics Technical Evaluation Center Picatinny Arsenal ATTN: Code DRDARSCM-O Dover, NJ 07801	1	Acurex/Aerotherm ATTN: Mr. Robert Washburn 485 Clyde Avenue Mountain View, CA 94042	1
Fred A. Keimel, President Adhesive & Sealants Newsletter P.O. Box 72 Berkeley Heights, NJ 07922	1	Aerospace Corporation ATTN: W. J. Versino P.O. Box 92957 Los Angeles, CA 90009	1
Battelle Columbus Laboratories 505 King Avenue Columbus, OH 43201	1	The Boeing Company Aerospace Group ATTN: Mr. Clyde H. Sheppert P.O. Box 3999 Seattle, WA 98124	1
CIBA-GEIGY Corporation Plastics & Additives Division ATTN: Raymond Seltzer Ardsley, NY 10502	1	General Dynamics Corp Convair Division ATTN: Mr. Ed Harrison San Diego, CA 92128	1

	Copies		Copies
General Electric R&D Center P.O. Box 8 Schenectady, NY 12301	1	Goodyear Aerospace Corporation ATTN: Hugh Boyd Akron, OH 44315	1
Grumman Aerospace Corp. ATTN: Mr. H. Borstell Bethpage, LI., NY 11714	1	Hercules, Inc. ATTN: Dr. R. E. Hoffman P.O. Box 98 Magna, UT 84044	1
ITT Research Institute 10 W. 35th Street Chicago, IL 60616	1	University of California Lawrence Livermore Laboratory ATTN: T. T. Chiao P.O. Box 808 Livermore, CA 94550	1
Lockheed California Co. Dept. 74-54, Bldg. 63 ATTN: Mr. J. H. Wooley Box 551 Burbank, CA 91503	1	Lockheed Missile & Space Company, Inc. ATTN: Clayton A. May P.O. Box 504 Sunnyvale, CA 94088	1
University of Maryland ATTN: Dr. W. J. Bailey College Park, MD 20742	1	Polymer Research Institute University of Massachusetts Amherst, MA 01002	1
McDonnell Douglas Corp. ATTN: Dr. James Carpenter P.O. Box 516 St. Louis, MO 63166	1	McDonnell Douglas Research Laboratories P.O. Box 516 St. Louis, MO 63166	1
New York University Dept. of Applied Science ATTN: Dr. Walter Brenner Barney Building 26-36 Stuyvesant St. New York, NY 10003	1	Northrop Corporation ATTN: D. Crabtree (Nonmetallic Research Dept.) 3901 W. Broadway Hawthorne, CA 90250	1

	Copies		Copies
Northwestern University Dept. of Materials Science & Engineering ATTN: Dr. J. O. Brittain Evanston, IL 60201	1	Columbus Aircraft Division Rockwell International ATTN: J. Fasold 4300 E. Fifth Avenue Columbus, OH 43216	1
Southwest Research Institute ATTN: W. E. Woolam 1150 Connecticut Ave., Suite 613 Washington, DC 20036	1	Stanford Research Institute 333 Ravenswood Avenue Menlo Park, CA 94025	1
University of Tennessee Polymer Science & Engineering Program ATTN: Prof. John F. Fellers 419 Dougherty Engineering Bldg. Knoxville, TN 37916	1	TRW ATTN: R. W. Vaughn One Space Park Rodundo Beach, CA 90278	1
United Technologies Research Center ATTN: Dr. Dan Scola East Hartford, CT 06108	1	Vought Corporation Advanced Technology Center P.O. Box 6144 Dallas, TX 75222	1
Vought Corporation Aeronautics Division ATTN: A. Hohman P.O. Box 5907 Dallas, TX 75222	1	Westinghouse Corporation R&D Center ATTN: Z. N. Sanjana 1310 Beulah Road Pittsburgh, PA 15235	1

FILMED
8-8